AD_____

GRANT NUMBER DAMD17-97-1-7229

TITLE: Novel Combinatorial Chemistry-Derived Inhibitors of Oncogenic Phosphatases

PRINCIPAL INVESTIGATOR: John S. Lazo, Ph.D.

CONTRACTING ORGANIZATION: University of Pittsburgh
Pittsburgh, Pennsylvania 15260

REPORT DATE: August 1998

TYPE OF REPORT: Annual

PREPARED FOR: U.S. Army Medical Research and Materiel Command
Fort Detrick, Maryland 21702-5012

REPORT DOCUMENTATION PAGE

Form Approved
OMB No. 0704-0188

1. AGENCY USE ONLY *(Leave blank)*	2. REPORT DATE	3. REPORT TYPE AND DATES COVERED
	August 1998	Annual (15 Jul 97 - 14 Jul 98)

4. TITLE AND SUBTITLE

Novel Combinatorial Chemistry-Derived Inhibitors of Oncogenic Phosphatases

5. FUNDING NUMBERS

DAMD17-97-1-7229

6. AUTHOR(S)

John S. Lazo, Ph.D.

7. PERFORMING ORGANIZATION NAME(S) AND ADDRESS(ES)

University of Pittsburgh
Pittsburgh, Pennsylvania 15260

8. PERFORMING ORGANIZATION REPORT NUMBER

9. SPONSORING / MONITORING AGENCY NAME(S) AND ADDRESS(ES)

U.S. Army Medical Research And Materiel Command
ATTN: MCMR-RMI-S
504 Scott Street
Fort Detrick, Maryland 21702-5012

10. SPONSORING / MONITORING AGENCY REPORT NUMBER

11. SUPPLEMENTARY NOTES

12a. DISTRIBUTION / AVAILABILITY STATEMENT

Approved for public release; distribution unlimited

12b. DISTRIBUTION CODE

13. ABSTRACT *(Maximum 200 words)*

Our overall goal of this US Army Breast Cancer Grant entitled "Novel Combinatorial Chemistry-Derived Inhibitors of Oncogenic Phosphatases" is to identify and develop novel therapeutic agents for human breast cancer. During the past year we synthesized a novel second generation, small molecule library designed on our previous natural product pharmacophore that was targeted against oncogenes implicated in human breast cancer, namely the dual specificity phosphatases (DSP) Cdc25. The new library maintains unique, rigid backbone structures that should provide more structural information about the active site of DSP. Several of the new compounds are potent competitive inhibitors of Cdc25. In addition we have identified the first selective VHR inhibitor, namely FY2-α009. This compound should facilitate our studies of the biological function of VHR, which are currently unknown. We continued our studies of the prototype member of the first combinatorial library with the best antiCdc25 activity, namely SC-ααδ9. We have determined that SC-ααδ9 is selectively cytotoxic to cells, which overexpress Cdc25B due to transformation with SV-40 large T antigen. We have also discovered that SC-ααδ9 disrupts a key mitogenic and antiapoptotic pathway, insulin-like growth factor-1 (IGF-1), and downregulates Cdc2 expression. SC--ααδ9 also blocks human breast cancer (MDA-MB-231) and other cells at G2/M consistent with Cdc25B or C inhibition. Thus, our combinatorial approach for selective DSP inhibitors remains very promising.

14. SUBJECT TERMS	15. NUMBER OF PAGES
Breast Cancer	117
	16. PRICE CODE

17. SECURITY CLASSIFICATION OF REPORT	18. SECURITY CLASSIFICATION OF THIS PAGE	19. SECURITY CLASSIFICATION OF ABSTRACT	20. LIMITATION OF ABSTRACT
Unclassified	Unclassified	Unclassified	Unlimited

FOREWORD

Opinions, interpretations, conclusions and recommendations are those of the author and are not necessarily endorsed by the U.S. Army.

____ Where copyrighted material is quoted, permission has been obtained to use such material.

____ Where material from documents designated for limited distribution is quoted, permission has been obtained to use the material.

___ Citations of commercial organizations and trade names in this report do not constitute an official Department of Army endorsement or approval of the products or services of these organizations.

___ In conducting research using animals, the investigator(s) adhered to the "Guide for the Care and Use of Laboratory Animals," prepared by the Committee on Care and use of Laboratory Animals of the Institute of Laboratory Resources, national Research Council (NIH Publication No. 86-23, Revised 1985).

___ For the protection of human subjects, the investigator(s) adhered to policies of applicable Federal Law 45 CFR 46.

___ In conducting research utilizing recombinant DNA technology, the investigator(s) adhered to current guidelines promulgated by the National Institutes of Health.

___ In the conduct of research utilizing recombinant DNA, the investigator(s) adhered to the NIH Guidelines for Research Involving Recombinant DNA Molecules.

___ In the conduct of research involving hazardous organisms, the investigator(s) adhered to the CDC-NIH Guide for Biosafety in Microbiological and Biomedical Laboratories.

7/15/98

PI - Signature Date

D. TABLE OF CONTENTS

E. INTRODUCTION

DSPases are a recently described novel class of protein phosphatases. Some are stress activated, some control cell entry into mitosis and others are oncogenic. CDC25 in fission yeast drives entry into mitosis by dephosphorylating and activating the key mitotic inducer CDC2, a cyclin-dependent protein kinase (CDK) (1-3). This CDC25 function has been conserved through evolution and in human cells is performed by the Cdc25C protein. Distinct human proteins termed Cdc25A and Cdc25B (or Cdc25Hu2 and Hu3) (4, 5) share with Cdc25C the ability to substitute for the loss of CdcC25 in fission yeast cells. In mammalian cells Cdc25A has a role in the G_1 phase of the cell cycle, where it may be responsible for removing inhibitory phosphate from T17 of CDK4. After DNA damage, this inhibitory phosphorylation is important in the checkpoint pathway that delays cell cycle progression in G1 and promotes DNA repair. Human Cdc25B may control early G_2/M transition and possibly regulate apoptosis. Consistent with their proposed roles as positive modulators of cell proliferation or inhibitors of apoptosis, Cdc25A and Cdc25B behave as oncogenes, cooperating with Ha-RAS or loss of RB to transform primary fibroblasts, and Cdc25B is overexpressed in several human tumor cells, notably breast cancer cells (5, 6). The few known inhibitors of the human Cdc25 protein family are not potent, are natural products that are not readily available, and may not have any specificity (7, 8). The only widely used inhibitor of DSPase is vanadate. The overall goal of this application is to synthesize more potent inhibitors of Cdc25A, B and C and to evaluate their potential as drugs for the treatment of breast cancer.

Hypothesis/Purpose

Our hypothesis is that DSPases, specifically Cdc25A and B, are key oncogenes in many human breast cancers and inhibition of their threonine/tyrosine phosphatase activity will produce an agent that is useful for the treatment of breast cancer. A secondary working hypothesis is that selective inhibitors of Cdc25A, B and C can be developed using a combinatorial chemistry approach with the basic pharmacophore of a threonine phosphatase inhibitor.

Technical Objectives

Our technical objectives are to: (1) synthesize 3,000 novel compounds based on the calyculin A pharmacophore, (2) investigate the ability of the new synthesized compounds to inhibit Cdc25A, Cdc25B, Cdc25C DSPases, (3) determine the specificity of phosphatase inhibition by examining the ability of the compounds to inhibit the DSPases CL100 and PTEN, the protein serine/threonine phosphatase PP2A, and the protein tyrosine phosphatase PTP1B, (4) test the newly synthesized compounds to inhibit the growth or cause apoptosis in human breast cancer cells and (5) to examine the specificity of the agents using mouse embryonic cells (MEC) transfected with SV-40 large T antigen or H-RAS^{G12V} and Cdc25A or Cdc25B and in MEC that are null for Cdc25A or B.

F. PROPOSAL BODY

The following manuscripts and abstracts have been published or are in press and were supported by this grant. All manuscripts are found in the Appendix.

Peer-Reviewed Manuscripts

Wipf, P., Cunningham, A., Rice, R.L. and Lazo, J.S. Combinatorial synthesis and biological evaluation of a library of small-molecule ser/thr-protein phosphatase inhibitors. Bioorg. Med. Chem. 5:165-177, 1997.

Rice, R. L., Rusnak, J.M., Yokokawa, F., Yokokawa, S., Messner, D.J., Boynton, A.L., Wipf, P. and Lazo, J.S. A targeted library of small molecule, tyrosine and dual specificity phosphatase inhibitors derived from a rational core design and random side chain variation. Biochemistry 36:15965-15974, 1997.

Vogt, A., Rice, R.L., Settineri, C.E., Yokokawa, F., Yokokawa, S., Wipf, P. and Lazo, J.S. Disruption of IGF-1 signaling and downregulation of Cdc2 by SC-ααδ9, a novel small molecule antisignaling agent identified in a targeted array library. J. Pharmacol. Exper. Therap. In Press

Rice, R.L., Bernardi, R.J., Rusnak, J.M., Yokokawa, F., Yokokawa, S., Wipf, P. and Lazo, J.S. Identification of a selective inhibitor of VHR phosphatase in a novel, targeted small molecule library. Biochemistry, Submitted.

Abstracts

Rice, R.L., Rusnak, J.M., Yokokawa, F., Wipf, P. and Lazo, J.S. Oncogenic dual specificity phosphatase inhibitors identified in a novel combinatorial library. Proc. Amer. Assoc. Cancer Res. 38:3156, 1997.

Rice, R.L., Vogt, A., Johnson, C.S., Yokokawa, F., Yokokawa, S., Wipf, P. and Lazo, J.S. Antiproliferative and antitumor activity of targeted combinatorial library members modeled from natural product phosphatase inhibitors. Proc. Amer. Assoc. Cancer Res. 39:1208, 1998.

Vogt, A., Rice, R.L., Yokokawa, F., Yokokawa, S., Wipf, P. and Lazo, J.S. Selective toxicity of the Cdc25 inhibitor SC-ααδ9 is associated with disruption of the IGF-1 receptor signaling pathway. Proc. Amer. Assoc. Cancer Res. 39:2160, 1998.

Carr, B.I., Wang, Z., Kar, S., Wang, M., Rice, R.L. and Lazo, J.S. Novel K vitamins inhibit EGF-mediated hepatocyte DNA-synthesis (DNA-S) and induce selective protein tyrosine phosphorylation. Amer. Assoc. Study Liver Dis. In Press.

Specific Aim 1. Development of combinatorial chemical libraries

To assess the importance of stereoisomers of our most promising compound in the initial library, namely SC--ααδ9, we have synthesized both the R and S enantiomers by traditional solution chemistry (Rice et al., manuscript submitted; see Appendix). We have also increased the complexity of the R_4 groups of our initial pharmacophore to reduce hydrophobicity (8). Additionally, we have expanded the diversity of our initial library by altering the ethyldiamine central core with a variety of rigid diamines, namely piperazine, diamine cyclohexane and benzene structures; this has increased our fundamental pharmacophore core ten-fold (Figure 1). We are now easily in a position to generate the several thousand combinatorial compounds required for the advance stages of the other Specific Aims. Several of the new compounds of the FY series have shown interesting and quite potent (< 1 μM) inhibition of DSPases (see below). Moreover, we have recently purchased the instrumentation to permit rapid synthesis of our proposed compounds by solid phase chemistry. The recent publication of the crystal structure of Cdc25A and the availability of the crystal structure coordinates now permits us to more rationally design inhibitors. Two manuscripts (Rice et al., manuscript submitted and Vogt et al. In Press; see Appendix) have been appended that detail our synthetic advances further.

Specific Aim 2. AntiDSPase activity assays

We have evaluated the antiDSPase activity the new members of the library, which now numbers more than 50 compounds. An additional 50 compounds have not yet been systematically evaluated. Enantimers of SC-ααδ9 showed no difference in their ability to act as competitive inhibitors of Cdc25. This encouraged us to explore other more rigid pharmacophores. We identified two compounds in the new more rigid library, namely FY7-αα09 and FY8-αα09, which acted as competitive inhibitors of $Cdc25B_2$ with a K_{is} of 4 μM (Figures 2 and 3). Although we have not examined their activity against other Cdc25 isoforms, these two compounds are more potent *in vitro* inhibitors of Cdc25 than members of the previous library. We have been interested in determining the importance of hydrophobicity especially in the R4 position and have been examining this by modifying the R4 position. Our results reveal an absolute requirement for the hydrophobic R4 position for inhibition of both tyrosine and DSPases. Presumably this reflects a proximal hydrophobic pocket in the active site. Two manuscripts (Rice et al., submitted, and Vogt et al., In Press) have been appended that detail our studies further.

Specific Aim 3. Counter assays for antiphosphatase specificity

An important but often overlooked aspect of drug discovery is the identification of compounds that are highly selective for the molecular target. Thus, we have adopted several counter assays that should decrease significantly the concern about nonspecific inhibition of protein phosphatases. Specifically we have examined the inhibitory activity of our new compounds against PTP1B, PP1 and VHR. We believe VHR is an important phosphatase in these assays, because it has the same catalytic activity as the other

DSPases but it has no known function. Within our new library we have found the most selective and potent inhibitor of the DSPase VHR ever reported, namely the cyclohexyldiamine-containing congener FY2-ααα09 (Figure 2). FY2-ααα09 displayed a competitive kinetic profile against VHR phosphatase with a K_{is} of 4 ± 1 μM. While we are uncertain of the therapeutic importance of this discovery, we believe the resulting compounds will be tremendously usefulness in our efforts to understand the biological function of this enzyme. Among the other members of the second generation library we found several potent (K_i ~1 μM) competitive inhibitors of PTP1B. The exquisite and distinct sensitivities of VHR, Cdc25 and PTP1B to structural modifications of our lead pharmacophore document that selective inhibition of DSPase and protein tyrosine phosphatases is feasible.

We have begun to use our Silicon Graphics modeling system and Flexidock software to determine the physical properties that dictate inhibition of DSPases. We have also used the new structural information from the x-ray crystal structure of the recombinant catalytic region of Cdc25A (9) for our next generation chemical library. We have also begun a collaboration with John Cogswell at Glaxo-Wellcome to cocrystalize SC-ααδ9 with the catalytic domain of human Cdc25A using their previously described methods (9). Our experimental results suggest we have a unique inhibitor of the catalytic domain of the Cdc25 type domain that should be tractable for further modification. We have also begun to test other chemical structures based on vitamin K with Prof. Craig Wilcox from the University of Pittsburgh and this new information will be added to our data base.

Specific Aim 4. Cell culture assays

We have examined the cellular activity of compounds of our library. Two compounds exhibited antiproliferative activity against the human breast cancer cell line MDA-MB-231 cells (10). The IC_{50} values for AC-ααδ9 and AC-αα6β were approximately 100 and 20 μM, respectively. Unfortunately AC-αα6β caused no additional growth inhibition below 50% and further studies with it were abandoned. Thus, we focused our efforts on ACααδ9, which was also synthesized by solution method to form SC-ααδ9 and the IC_{50} for growth inhibition (continuous exposure) was 30 μM. We found AC-ααδ9 and SC-ααδ9 cause a prominent G1 arrest consistent with an inhibition of Cdc25A (10). We have also examined the murine SCCVII cells, which grows both in mice and in culture, for *in vivo* studies because our initial results with the poor commercial antibodies to Cdc25 A and B suggested these cells overexpressed Cdc25B. SC-ααδ9 had an IC50 of approximately 60 μM in these cells (Figure 3). Our initial studies with this tumor and an excision colony formation model suggests a single dose of 30 mg/kg caused a 50% decrease in tumor cell number *in vivo*. These experiments, however, need to be repeated and will require additional compound to be synthesized.

We have made several attempts to examine the MDA-MB-231 cells for induction of apoptosis and for evidence of either G2/M blockage. Unfortunately, with asynchronous cells we can not see apoptosis or a prominent G2/M arrest with concentrations of SC-ααδ9 that are low enough for the compound to remain in solution. Thus, we for most of

our cellular studies we have turned to other cell types: namely mouse embryonic cells (MEC) and a temperature sensitive mouse cell line that has an altered cdc2, tsFT210 (see Specific Aim 5 below). We have, however, examined MDA-MB-231 cells for proteins associated with cell cycle checkpoints. The retinoblastoma protein (Rb), Cdk2 and Cdk4 proteins are essential G1 cell cycle checkpoints, which were studied by Western blotting. We found treatment of MDA-MB-231 cells with 100 μM SC-ααδ9 continuously for 48 h resulted in an increase in hypophosphorylated Rb and an overall loss of Rb, Cdk2 and Cdk4 protein (Figures 4 & 5). We found no alteration in cyclin D1 levels, which is important in G1 progression. Cyclin B1 and p34cdc2 protein, which are involved in G2 progression, were also lost in a concentration-dependent manner in MDA-MB-231 cells treated with CD-ααδ9. A loss of phosphorylation of ERK2 is often associated with growth arrest in cells and ERK2 in MDA-MB-231 cells treated with 100 μM SC-ααδ9 was dephosphorylated. Because of loss Rb phosphorylation and cdc2 protein, we considered the status of Rb and p34cdc2 in SCCVII and MEC cells. After treatment with SC-ααδ9, both SCVII and MEF lost hyperphosphorylated Rb and gained phosphorylated Rb as shown by Western blot with no discernible loss of Rb protein (Figure 6 and Vogt et al., In Press; Appendix). Cdc2 protein levels were also depleted in the SCCVI and MEF cells in a concentration-dependent manner after extended treatment with SC-ααδ9. The phosphorylation status of Cdc2 can be detected by its electrophoretic mobility if the protein is present. We reasoned that changes in phosphorylation could be cell cycle-dependent and, thus, obscured in asynchronized cell populations. To probe alterations in Cdc2 phosphorylation further, we used the temperature sensitive tsFT210 cells, which permit easy cell cycle synchronization (see Specific Aim 5). Treatment of tsFT210 cells with 50 μM SC-ααδ9 increased the hyperphosphorylated (upper band) form of Cdc2 compared to control cells (Figure 7). These results were consistent with an inhibition of Cdc25B and Cdc25C within the tsFT210 cells.

Specific Aim 5. Cellular selectivity assays

To develop a basic model of transformed and nontransformed cells for analyses of tumor specificity, we have transformed MEC with DNA encoding SV40 large T antigen. The details of this approach and our results are found in Vogt et al. (Appendix) and will only briefly be summarized here. MEC were isolated from fetuses of 14.5 day pregnant mice. Primary cultures of MEC were transformed with DNA from SV40 large T antigen under the control of its own promoter by means of cationic lipid. Clones were identified and expanded. Primary MEC of <15 passages were used a "normal" or wildtype cells. Overexpression of Cdc25B but not Cdc25A or Cdc25C was detected (Vogt et al. In Press). Using both a clonogenic and an MTT assay, we found SC-ααδ9 was selectively toxic to the transformed cells, which overexpressed Cdc25B (Figure 8). Okadaic acid or vanadate were not selectively toxic to the transformed cells.

We have also begun a collaboration with Dr. Peter Donovan, Thomas Jefferson University Cancer Center, who has generated Cdc25B null mice. We have used our above mentioned method to generate MEC from the Cdc25B null mice and have begun to characterize the cells. Their cell cycle time and morphology was indistinguishable

from the wildtype. Response to cytotoxic anticancer agents is indistinguishable from wildtype cells. The cells do not overexpress Cdc25A or Cdc25C compared to wildtype. Our initial studies suggest the null cells do not response selectively to SC-ααδ9, which may indicate the target for this agent is Cdc25A or Cdc25C. These cells should be extremely useful for our future planned studies with the new agents.

We have used the tsFT210 carcinoma cells to examine further the actions of SC-ααδ9. These cells represent a unique cell system for the study of cell cycle effects of compounds because they possess a temperature sensitive $p34^{cdc2}$ protein. Upon shift from the permissive temperature of 32°C to the non-permissive temperature of 39.4°C, p34cdc2 protein is lost and cells arrest in the G2 phase of the cell cycle. When cells are again released to the permissive temperature, p34cdc2 protein levels recover within an hour and the cells proceed through mitosis and resume normal proliferation. This system provides a way to easily synchronize cells and to examine specific effects of compounds on precise phases of the cell cycle with a minimum of variables.

The effects of SC-ααδ9 were first investigated with asynchronous growing tsFT210 cells to determine what phases of the cell cycle were most likely to be effected by the compound. When cells were treated with the known G2 inhibitor nocodazole (1 μM) for 17 h, we observed a complete G2/M arrest by flow cytometry consistent with a cell cycle time of <17 h (Figure 8). When tsF210 cells were treated with 50 μM SC-ααδ9 for 17 h, there was a prominent increase in the g1 phase of the cell cycle with an equal decrease in the S phase and no change in the percentage of cells in the G2/M phase (Figure 8). This is consistent with what we previously observed with the human breast cancer MDA-MB-231 cells. If the compound had only caused a G1 arrest, then we would have expected a decrease in the G2/M phase. Because this was not observed, we tested the hypothesis that SC-ααδ9 caused a G2/M arrest. We synchronized tsFT210 cells in G2 by incubating them at the non-permissive temperature for 17 h and releasing the cells in the absence or presence of compound or vehicle. Treatment with vehicle alone for ~6-7 h permitted a majority of cells to progress to the G1 phase (Figure 8). No decrease in cell viability was detected with either vehicle or nocodazole. Treatment with 50 μM SC-ααδ9 , however, caused a complete G2 arrest (Figure 8). Furthermore, we found a concentration-dependent arrest of tsFT210 cells in G2 and a concentration and time-dependent decrease in viability with SC-ααδ9; there was 50% and 75% loss in viability after a 6.5 h treatment with SC-ααδ9.

G. CONCLUSIONS

These results suggest our combinatorial approach will lead to the identification of novel and selective inhibitors of Cdc25, which will be potential therapeutic agents. The chemical composition of these compounds, namely molecular weight below 800daltons and pI 1-3, are important attributes that are frequently associated with therapeutically active agents. With the availability of a crystal structure for the catalytic domain of human Cdc25A, we are in an unusually exciting time for compound design and analysis. The cellular results with MDA-MB-231, MEC (SV40 large T antigen transformed and Cdc25B-/-), and tsFT210 cells are consistent with intracellular inhibition of Cdc25. We have achieved all of the major goals outline in the proposal for the first year.

H. REFERENCES

1. Nurse, P. Ordering s phase and m phase in the cell cycle. *Cell* **79:**547-550 (1994).
2. Norbury, C., and P. Nurse. Animal cell cycles and their control. *Ann. Rev. Biochem.* **61:**441-470 (1992).
3. Gautier, J., M. J. Solomon, R. N. Booher, J. F. Bazan, and M. W. Kirschner. Cdc25 is a specific tyrosine phosphatase that directly actiates $p34^{cdc2}$. *Cell* **67:**197-211 (1991).
4. Nagata, A., M. Igarashi, S. Jinno, K. Suto, and H. Okayama. An additional homolog of the fission yeast cdc25+ gene occurs in humans and is highly expressed in some cancer cells. *New Biologist* **3:**959-968 (1991).
5. Okayama, H., A. Nagata, M. Igarashi, K. Suto, and S. Jinno. *Mammalian G2 regulatory genes and their possible involvement in genetic instability in cancer.* CRC Press, Boca Rotan, FL (1992).
6. Galaktionov, K., A. K. Lee, J. Eckstein, G. Draetta, J. Meckler, M. Loda, and D. Beach. CDC25 phophatases as potential human oncogenes. *Science* **269:**1575-1577. (1995).
7. Takashi, H., K. Nishi, S. Hakoda, S. Tanida, A. Nagata, and H. Okayama. Dnacin A1 and dnacin B1 are antitumor antibiotics that inhibit cdc25B phosphatase activity. *Biochemical Pharmacol.* **48:**2139-2141 (1994).
8. Rice, R. L., J. M. Rusnak, F. Yokokawa, S. Yokokawa, D. J. Messner, A. L. Boynton, P. Wipf, and J. S. Lazo. A targeted library of small molecule, tyrosine and dual specificity phosphatase inhibitors derived from a rational core design and random side chain variation. *Biochemistry* (36):15965-15974 (1997).
9. Fauman, E. B., J. P. Cogswell, B. Lovejoy, W. J. Rocque, W. Holmes, V. G. Montana, H. Piwnica-Worms, M. J. Rink, and M. A. Saper. Crystal structure of the catalytic domain of the human cell cycle control phosphatase, Cdc25A. *Cell* **93:**617-625 (1998).
10. Wipf, P., A. Cunningham, R. L. Rice, and J. S. Lazo. Combinatorial synthesis and biological evaluation of a library of small-molecule Ser/Thr protein phosphatase inhibitors. *Bioorg. Med. Chem.* **5:**165-177 (1997).

Figure Legends

Figure 1. Chemical Structure of Basic and Modified Pharmacophores.

Figure 2. Chemical Structures of Selected Library Compounds.

Figure 3. Growth Inhibition of Murine SCCVI Cells in Culture after Continuous Exposure to SC-ααδ9. Cell numbers determined by colorimetric (MTT) assay. See (10) for additional details about the assay.

Figure 4. Expression of Rb, Cyclin D1, Cyclin B1, $p34^{cdc2}$ and ERK2 in MDA-MB-231 cells treated continuously for 48 h with 100 μM SC-ααδ9. Panel A. MDA-MB-213 whole cell lysate separated on an 8% Novex Tris-Glycine gel and blotted with an antibody against Rb (G3-245). Panel MDA-MB-213 whole cell lysate separated on an 14% Novex Tris-Glycine gel and blotted with an antibody against cyclin D1. Panel C. MDA-MB-213 whole cell lysate separated on an 14% Novex Tris-Glycine gel and blotted with an antibody against human $p34^{cdc2}$. Panel E. MDA-MB-213 whole cell lysate blotted with an antibody against ERK2.

Figure 5. Expression of Cdk4 and Cdk2 in MDA-MB-231 Cells Treated for 48 h with SC-ααδ9. Panel A. MDA-MB-231 whole cell lysate separated on a 10% Novex Tris-Glycine gel and blotted with an antibody against mouse cdk2. Panel B. MDA-MB-231 whole cell lysate separated on a 10% Novex Tris-Glycine gel and blotted with an antibody against mouse cdk4.

Figure 6. Expression of Rb and $p34^{cdc2}$ in SCCVII cells treated for 24 h with SC-ααδ9. Panel A. SCCVII whose lysate run on a 12% Novex Tris-Glycine gel and blotted with an antibody against mouse $p34^{cdc2}$. Panel B. SCCVII whole lysate run on an 8% Novex Tris-Glycine gel and blotted with an antibody against Rb (C-15). N=2 independent experiments.

Figure 7. Expression of $p34^{cdc2}$ in G2 synchronized tsFT210 cells treated for 6.5 h with 50 μM SC-ααδ9 after release from G2 block. MDA-MB-231 whole cell lysate separated on a 10% Novex Tris-Glycine gel and blotted with an antibody against mouse $p34^{cdc2}$.

Figure 8. Cell cycle distribution of asynchronous tsFT210 cells after 17 h treatment determined by flow cytometry. Panel A. Flow cytometry analysis of tsFT210 cells a 0 h after release from G2 block. Panel B. Flow cytometry analysis 6.5 h after release from G2 block with vehicle exposure alone. Panel C. Flow cytometry analysis 6.5 h after release from G2 block with 50 μM SC-ααδ9 exposure. Panel D. Flow cytometry analysis 6.5 h after release from G2 block with 100 μM SC-ααδ9 exposure. Panel E. Flow cytometry analysis 6.5 h after release from G2 block with 1 μM nocodazole exposure. Fluorescence channel measures intracellular propidium iodide concentration, an index of DNA content.

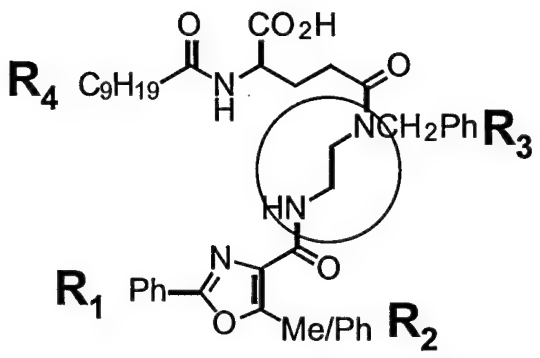

SC–α1δ9/**SC**–ααδ9

SC-αα09/SC-α109

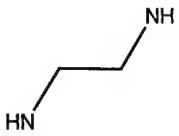

FY5-αα09/FY5-α109

FY2-αα09/FY2-α109

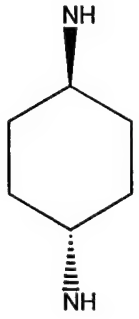

FY7-αα09/FY7-α109

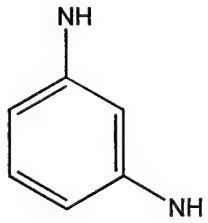

FY3-αα09/FY3-α109

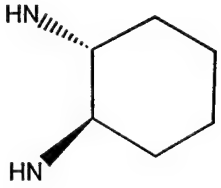

FY8-αα09/FY8-α109

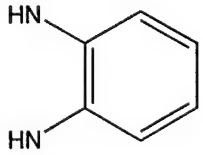

FY4-αα09/FY4-α109

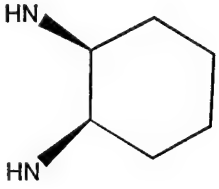

FY9-αα09/FY9-α109

FY10-αα09/FY10-α109

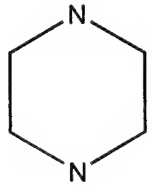

Figure 1

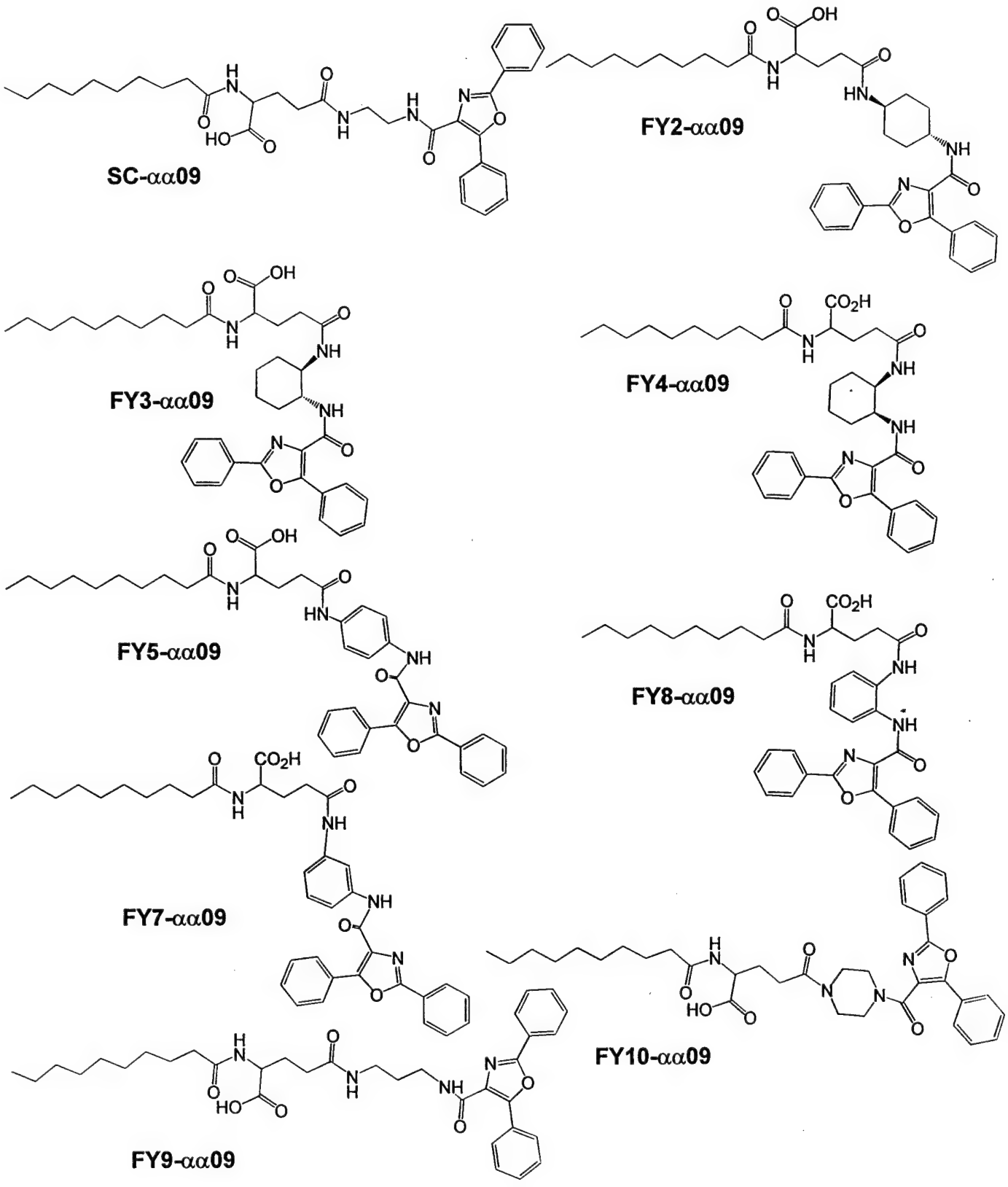
SC-αα09
FY2-αα09
FY3-αα09
FY4-αα09
FY5-αα09
FY8-αα09
FY7-αα09
FY10-αα09
FY9-αα09

Figure 2

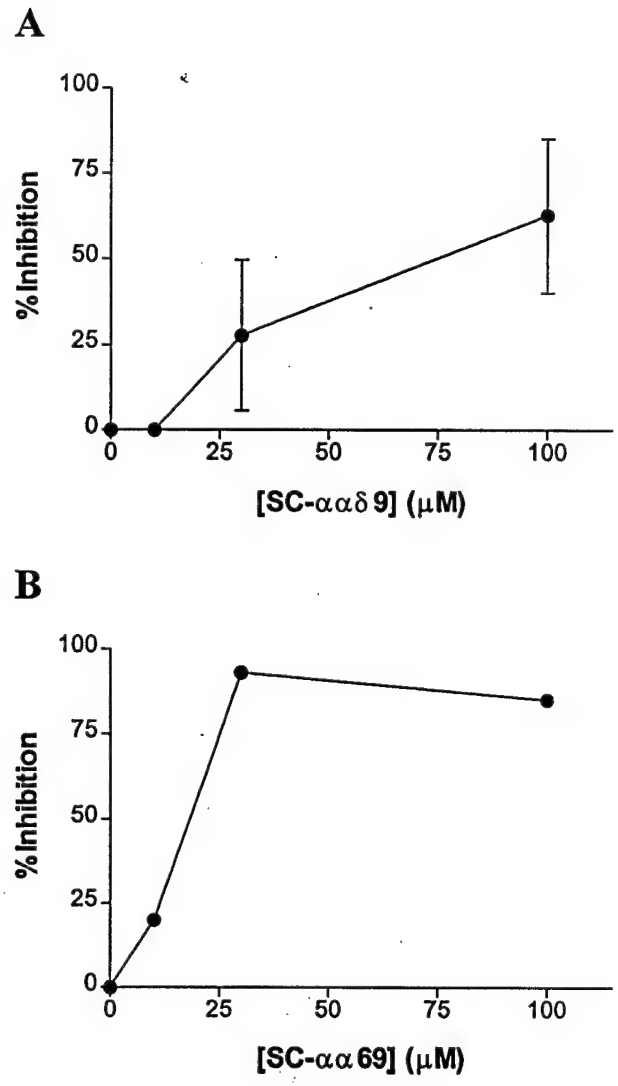
A
100
75
50
25
0
% Inhibition
0
25
50
75
100
[SC-ααδ9] (μM)
B
100
75
50
25
0
% Inhibition
0
25
50
75
100
[SC-αα69] (μM)

Figure 3

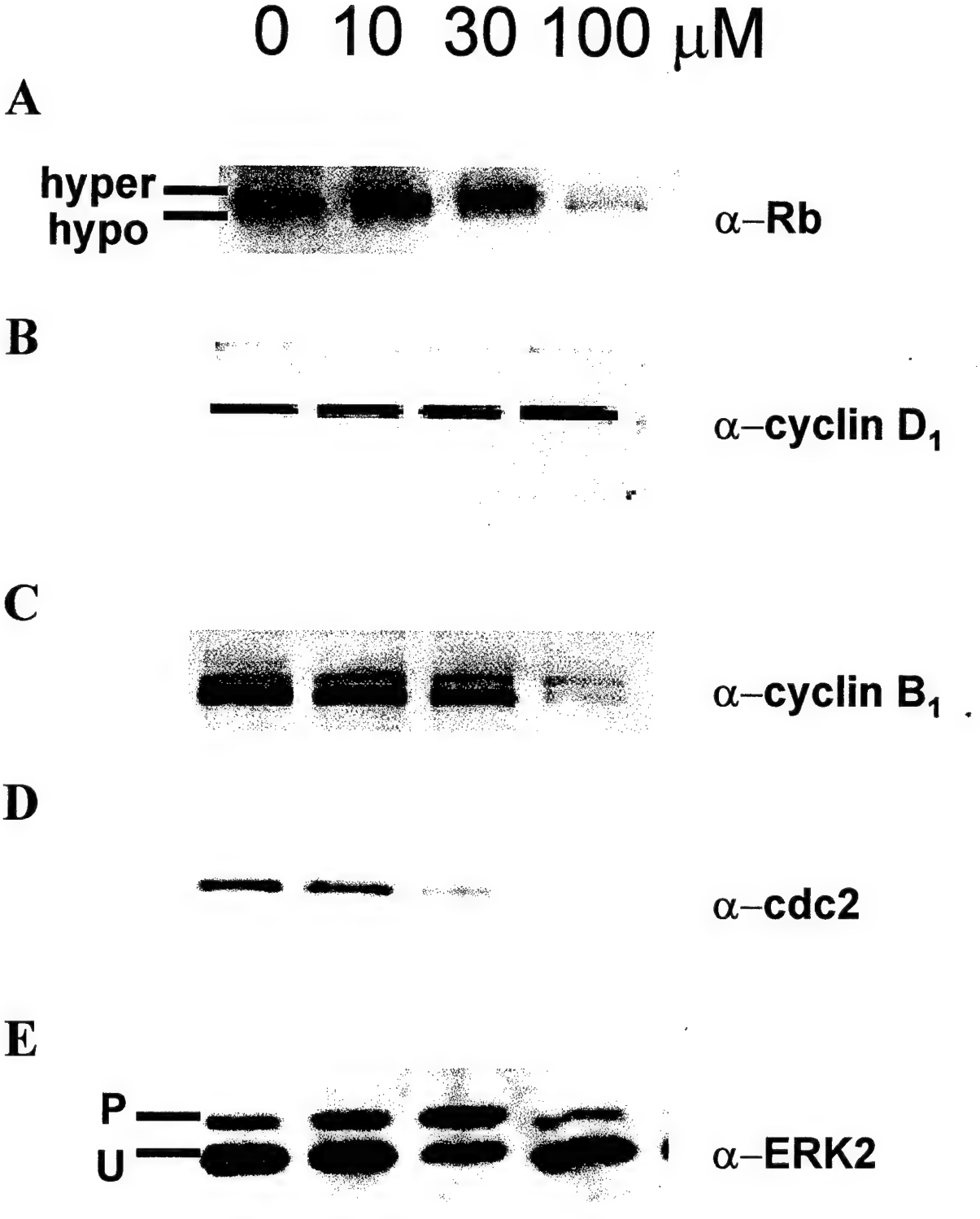
0 10 30 100 μM
A
hyper
hypo
α–Rb
B
α–cyclin D1
C
α–cyclin B1
D
α–cdc2
E
P
U
α–ERK2

Figure 4

Figure 5

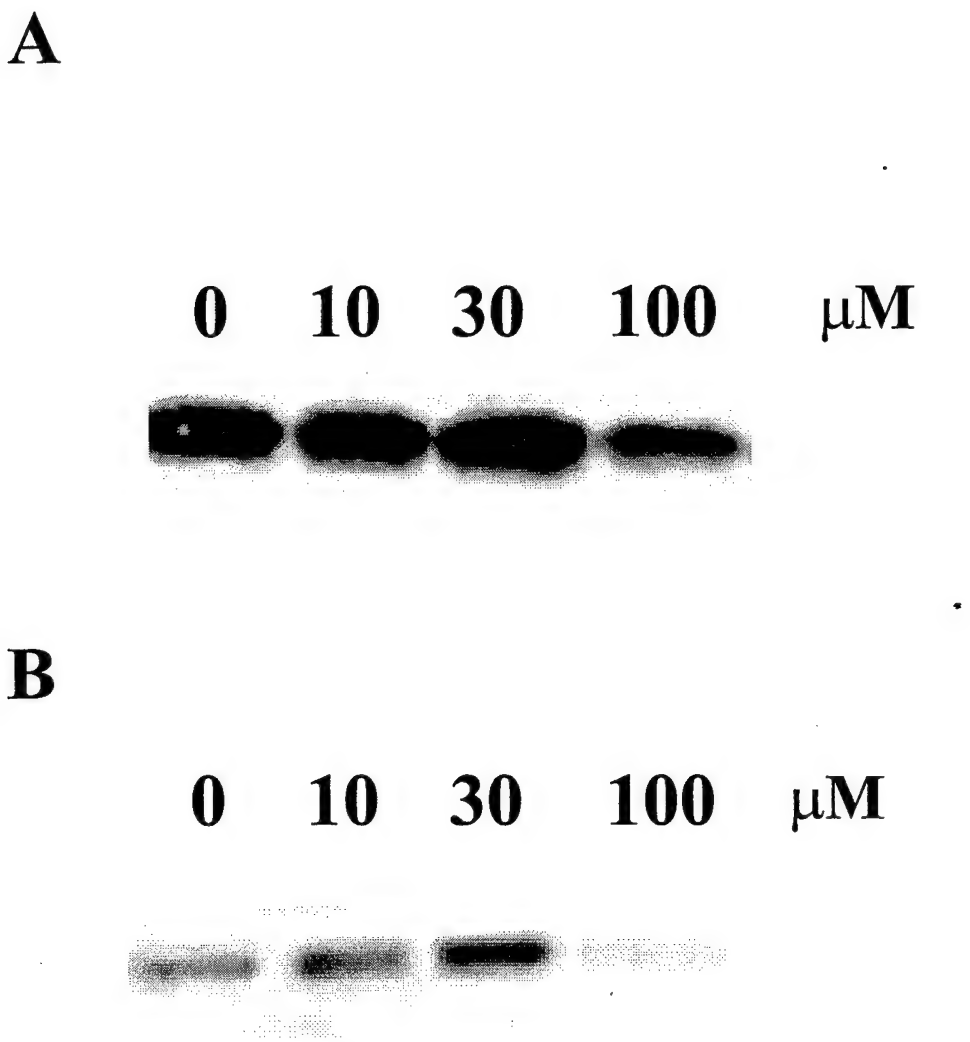

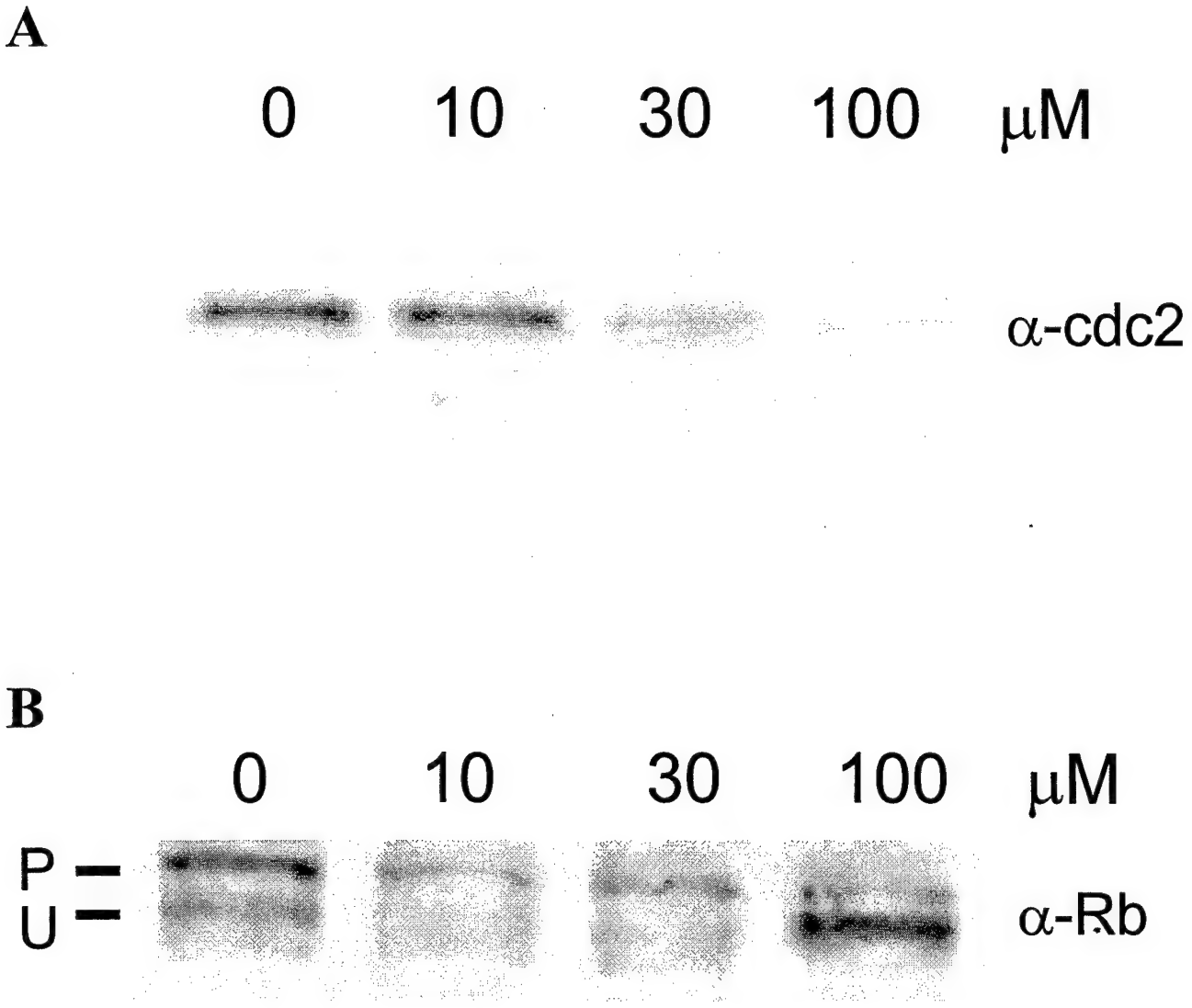

Figure 6

Figure 7

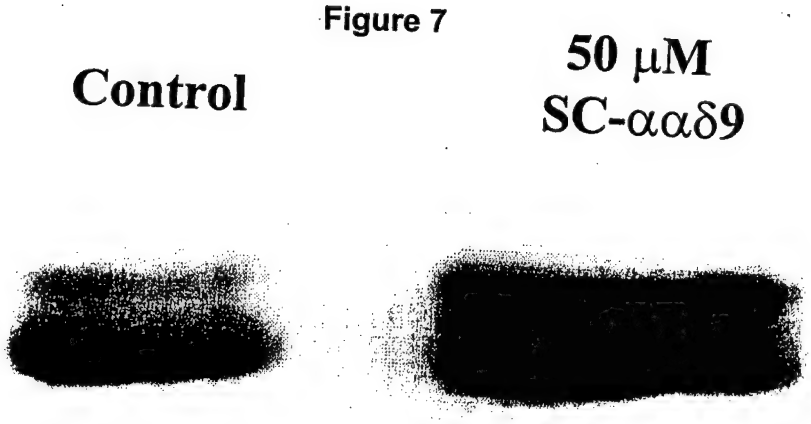

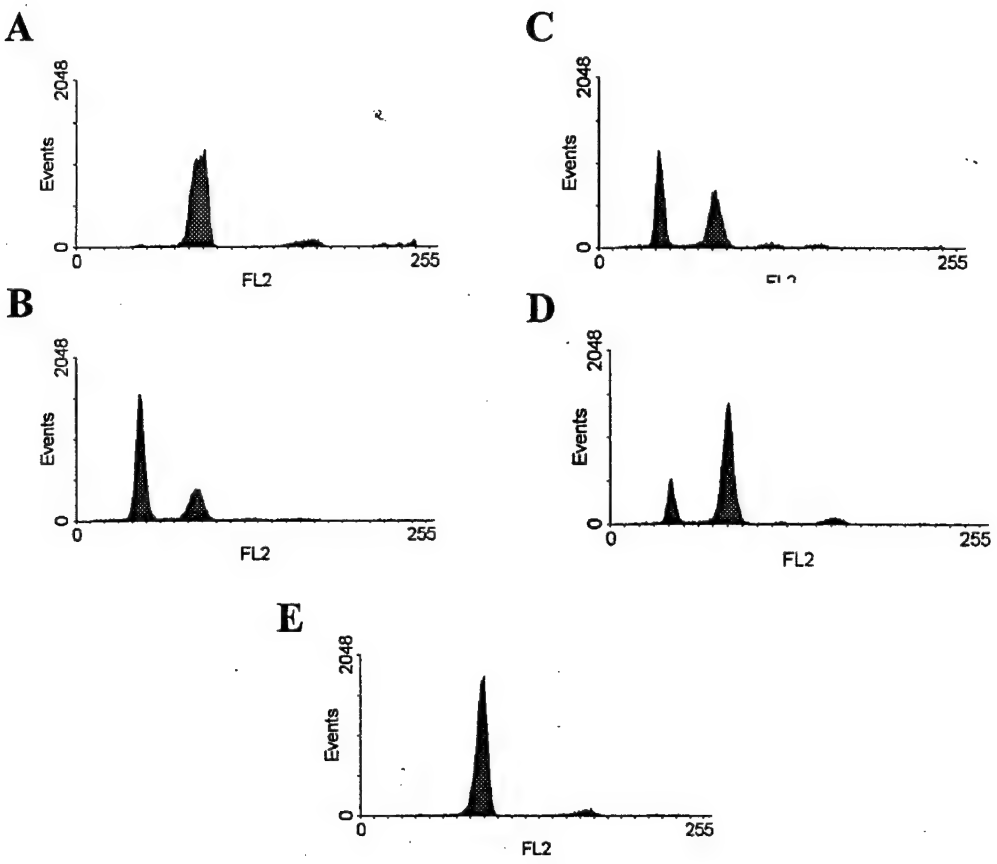
A
2048
Events
0
0
255
FL2
C
2048
Events
0
0
255
B
2048
Events
0
0
255
FL2
D
2048
Events
0
0
255
FL2
E
2048
Events
0
0
255
FL2

Figure 8

APPENDIX

Pergamon

Bioorganic & Medicinal Chemistry, Vol. 5, No. 1, pp 165–177, 1997

PII: S0968-0896(96)00199-X
0968-0896/97 $17.00+0.00

Combinatorial Synthesis and Biological Evaluation of Library of Small-Molecule Ser/Thr-Protein Phosphatase Inhibitors

Peter Wipf,[a,*] April Cunningham,[a] Robert L. Rice[b] and John S. Lazo[b,*]
Departments of [a]Chemistry and [b]Pharmacology, University of Pittsburgh, Pittsburgh, PA 15260, U.S.A.

Abstract—In eukaryotes, phosphorylation of serine, threonine, and tyrosine residues on proteins is a fundamental posttranslational regulatory process for such functions as signal transduction, gene transcription, RNA splicing, cellular adhesion, apoptosis, and cell cycle control. Based on functional groups present in natural product serine/threonine protein phosphatase (PSTPase) inhibitors, we have designed pharmacophore model **1** and demonstrated the feasibility of a combinatorial chemistry approach for the preparation of functional analogues of **1**. Preliminary biological testing of 18 structural variants of **1** has identified two compounds with growth inhibitory activity against cultured human breast cancer cells. In vitro inhibition of the PSTPase PP2A was demonstrated with compound **1d**. Using flow cytometry we observed that compound **1f** caused prominent inhibition in the G1 phase of the cell cycle. Thus, the combinatorial modifications of the minimal pharmacophore **1** can generate biologically interesting antiproliferative agents. Copyright © 1997 Elsevier Science Ltd

Introduction

Many eukaryotic cell functions, such as signal transduction, cell adhesion, gene transcription, RNA splicing, apoptosis, and cell proliferation, are controlled by protein phosphorylation, which is regulated by the dynamic relationship between both kinases and phosphatases.[1] Indeed, the principal role of many second messengers is to modulate kinase selectivity. In an effort to intervene early in the initiation stage of cellular events and in recognition of the tumor promoting effects of phorbol ester based protein kinase C activators, the lion's share of synthetic chemistry research in this area has focused on protein kinases.[2] However, there is substantial recent biological evidence for the multiple regulatory functions of protein phosphatases and a clear link between phosphatase inhibition and apoptosis.[3–9]

Besides some minor phosphorylation of histidine, lysine, arginine, and, in bacteria, aspartate, most eukaryotic amino acid phosphate derivatives are found on serine, threonine, and tyrosine protein residues. Generally, the primary characterization of phosphatases follows these structural guidelines: Ser/Thr protein phosphatases (PSTPases), Tyr protein phosphatases (PTPases), and dual-specificity phosphatases (DSPases).[3]

PSTPases have been classified according to their substrate specificity, metal ion dependence and sensitivity to inhibition (Table 1).[10,11] cDNA cloning has revealed at least 40 different enzymes of this type. In addition to proteins (Inhibitor-1, Inhibitor-2, DARPP-32, NIPP-1),[4] several (mostly marine) toxins have been identified as potent inhibitors (Fig. 1).[12]

Okadaic acid is produced by several species of marine dinoflagellates and reversibly inhibits the catalytic subunits of the PSTPase subtypes PP1, PP2A, and PP3.[4] SAR studies showed that the carboxyl group as well as the four hydroxyl groups were important for activity.[13,14] Calyculin A was identified as a cytotoxic component of the marine sponge *Discodermia calyx*. It has an extremely high affinity to PP1, PP2A, and PP3 with an IC_{50} in the 0.3 nM range.[4] Microcystins are potent cyclic hepta- and pentapeptide toxins of the general structure cyclo[D-Ala-X-D-*erythro*-β-methyl-*iso*-Asp-Y-Adda-D-*iso*-Glu-*N*-methyldehydro-Ala] where X and Y are variable L-amino acids.[4] They are known to promote tumors in vivo, but, with the exception of hepatocytes, are impermeable to most cells in vitro.[4]

The large number of naturally occurring microcystins makes it possible to carry out a limited SAR study.[15] Apparent IC_{50}s for microcystins range between 0.05 and 5 nM, with similar preference for PP1, PP2A, and PP3 as found for okadaic acid and calyculin A.[4] The

Table 1. Ser/Thr protein phosphatase classification[3,4]

Family	Subfamily	Characteristic
PSTPases	PP1	IC_{50} for okadaic acid 10–50 nM
	PP2A	IC_{50} for okadaic acid 0.5 nM
	PP2B (calcineurin)	Ca(II)-dependent; IC_{50} for okadaic acid >2000 nM
	PP2C	Mg(II)-dependent; not inhibited by okadaic acid
	PP3	IC_{50} for okadaic acid 4 nM

substitution of alanine for arginine has little effect on phosphatase inhibitory potency; there is, however, a difference in relative cytotoxicity.[15] The dehydroamino acid residue and the *N*-methyl substituents are also not critical. Crucial are the glutamic acid unit, since esterification leads to inactive compounds, and the overall shape of the Adda residue, since the (6*Z*)-isomer is inactive. Some variations in the Adda unit, specifically the *O*-demethyl and the *O*-demethyl-*O*-acetyl analogues, exert little effect on bioactivity, however. Considerably less information is available in the nodularin series, since fewer compounds are available;

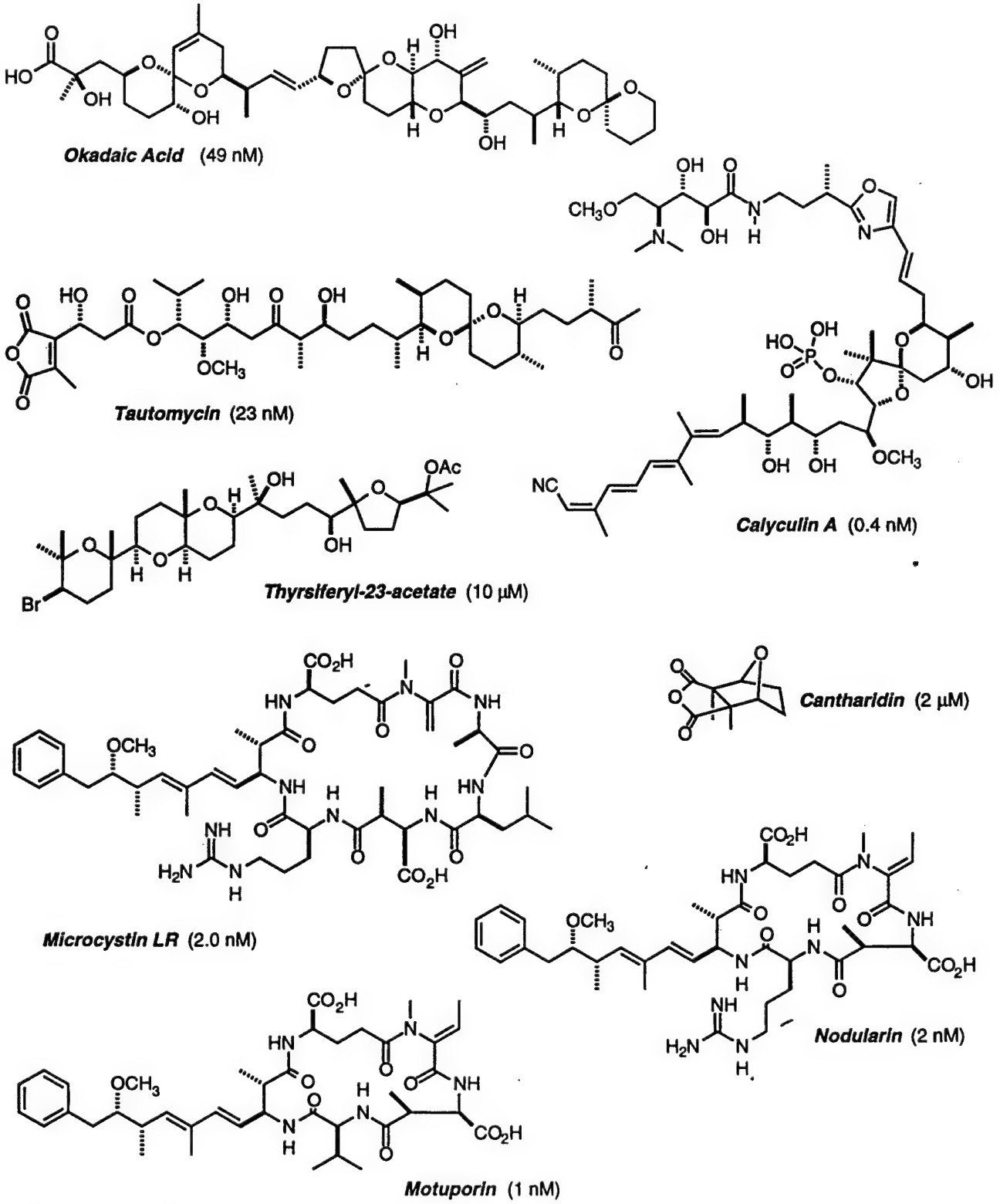

Figure 1. Natural product inhibitors of PSTPases (IC_{50} vs PP1).

however, the general SAR appears similar to the microcystins.[15] There are only slight differences in the inhibition profile; IC_{50}s for PP1 and PP3 are 2 and 1 nM, respectively, which is about 50 times higher than the IC_{50} for PP2A. The recently isolated motuporin (=[L-Val^2]nodularin) is even more potent with an IC_{50} <1 nM for PP1.[16,17] This secondary metabolite was isolated from a Papua New Guinea sponge and is the only member of the greater microcystin family that has thus far yielded to total synthesis.[18]

Tautomycin is produced by a terrestrial *Streptomyces* strain. This relatively unstable molecule inhibits PP1, PP2A and PP3 indiscriminately with an IC_{50} in the 15 nM range.[4] The remaining natural product inhibitors, thyrsiferyl-23-acetate and cantharidine, were shown to be somewhat selective, though weak (IC_{50} 0.16–10 μM) inhibitor of PP2A.[19–22]

Despite some recent total synthesis efforts,[23] no SAR for calyculin A, tautomycin[24] or thyrsiferyl acetate were reported. High toxicity, especially hepatotoxicity, is commonly found with all natural PSTPase inhibitors, often limiting the range of feasible pharmacological studies, and appears to be intrinsically associated with a non-specific phosphatase inhibition.[25] Importantly, based on kinetic and competition binding studies, okadaic acid, calyculin A, tautomycin, and the microcystins appear to bind competitively at the same site of PSTPases.[26–29] Since phosphatases are ubiquitous, precise tools in membrane and post-membrane signal transduction pathways, the development of selective inhibitors or activators of PSTPases that are cell-permeable, non-hepatotoxic, or broadly cytotoxic is of major significance for future progress in this field.

Design and Synthesis of Calyculin A Analogues

The design of our PSTPase inhibitor library was based on the SAR available for the natural product inhibitors and assumed that the presence of a carboxylate, a nonpolar aromatic function, and hydrogen-bond acceptors and donors (e.g. a peptidomimetic group) in suitable spatial arrangements are sufficient for strong and selective binding. A pharmacophore model that addresses these criteria is shown in Figure 2. Traditional computational studies by Quinn *et al.* have identified a related structural model based on molecular modeling of okadaic acid, calyculin A, and microcystin LR.[30] Whereas computational studies of the minimal structural requirements for PSTPase inhibition aim for an accurate prediction of the important conformational and electronic features of the lead structures, our combinatorial[31,32] analysis achieves this goal via a random optimization of the steric and electronic properties of the pharmacophore. Most marine natural products have evolved along an optimization of broad-range activity rather than specificity.[33] The structural variation present in a library of PSTPase inhibitors will allow the simultaneous exploration of high-affinity and high-specificity features providing selectivity beyond the natural product model.

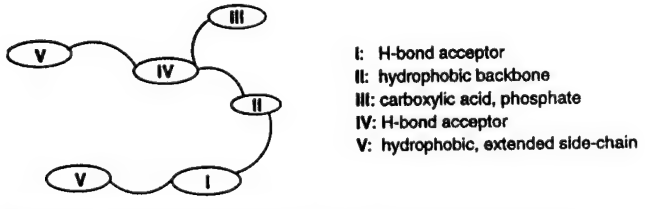

Figure 2. Pharmacophore model for PSTPase inhibitor library.

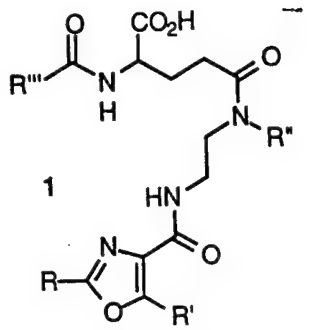

Figure 3. Parent structure for PSTPase inhibitor library synthesis.

Specifically, we have designed compounds of structure **1** to provide a platform for functional group variation according to our pharmacophore model (Fig. 3). The carboxylic acid moiety, crucial for bioactivity, is derived from glutamic acid. The substituent R attached to the oxazole moiety of **1** can be varied within a broad range and should probably be mostly hydrophobic in nature. To a lesser extent, direct substitutions at the oxazole R′ are possible that will explore the tolerance for bulky residues at this site. A variable and relatively flexible diamine segment serves as the spacer between oxazole moiety and carboxylic acid side chain in place of the synthetically less readily accessible spiroketal of calyculin A. A related *N*-methyl dehydroalanine residue is found in microcystin LR. The hydrophobicity of this subunit is modulated by *N*-alkylation with residues R″. An acyl portion R‴CO is responsible for providing the molecule with a relatively rigid hydrophobic tail similar to the Adda amino acid side chain in microcystins and the tetraene cyanide in calyculin A.

Initially, the development of an efficient approach for the combinatorial synthesis of target structures **1** focused on the optimization of the solution-phase synthesis of model compound **2** (Scheme 1). L-Glutamic acid (**3**) was protected in 62% yield as the γ-allyl ester using allyl alcohol and chlorotrimethylsilane.[34] Treatment with Fmoc-Cl followed by coupling to benzyl alcohol using 1-ethyl-3-[3-(dimethylamino-)propyl]-carbodiimide hydrochloride (EDCI) provided the tri-protected amino acid **6** in 82% yield. The Fmoc protective group was subsequently removed by exposure to DMAP and the free amine was acylated in situ with decanoyl chloride to give amide **7** in 63% yield. Pd(0)-catalyzed deprotection[35] of the allyl ester and coupling of the resulting acid **8** to ethylene diamine **9** in the presence of (1H-1,2,3-benzotriazol-1-yloxy)tris(dimethylamino)phosphonium hexafluoro-

phosphate (BOP)[36] led to amide **10** in 75% yield. A versatile general route to monoprotected ethylene diamines was easily achieved by carbamoylation of 2-chloroethylamine monohydrochloride (**12**), Finkelstein reaction, and aminolysis (Scheme 2).

Deprotection of the Alloc-group gave a primary amine which was coupled, in situ, to oxazole acid (**11**) using BOP as a coupling agent. The desired amide **2** was obtained in 57% yield for the two steps. The heterocyclic moiety **11** was efficiently prepared from *N*-benzoyl threonine (**14**) by side-chain oxidation and cyclodehydration with Dess–Martin reagent and electrophilic phosphorus, respectively,[37] followed by saponification of oxazole **15** (Scheme 3).

The solution-phase preparation of calyculin analogue **2** established the necessary general protocols for the preparation of a library of structural variants of the pharmacophore model **1** on solid-support. We have successfully applied this basic strategy for the parallel synthesis of 18 structural analogues (Scheme 4, Table 2). Coupling of diprotected glutamate **5** to the polystyrene-based Wang resin[38] with EDCI was performed on large scale and provided a supply of solid phase beads. The base-labile Fmoc protective group was removed by treatment with piperidine and THF, and the resin was distributed to three specially designed Schlenk filters equipped with suction adapters and inert gas inlets for maintaining steady bubbling. After the addition of solvent, hydrophobic residues R'''COCl were added to each flask, which provided three different amide derivatives **17**. After filtration and rinsing of the resin, allyl esters **17** were deprotected via Pd(0) chemistry and each batch was distributed over three modified Schlenk filters, providing nine different reaction sites for acylation. Addition of three different *N*-allyloxycarbonyl protected diamines

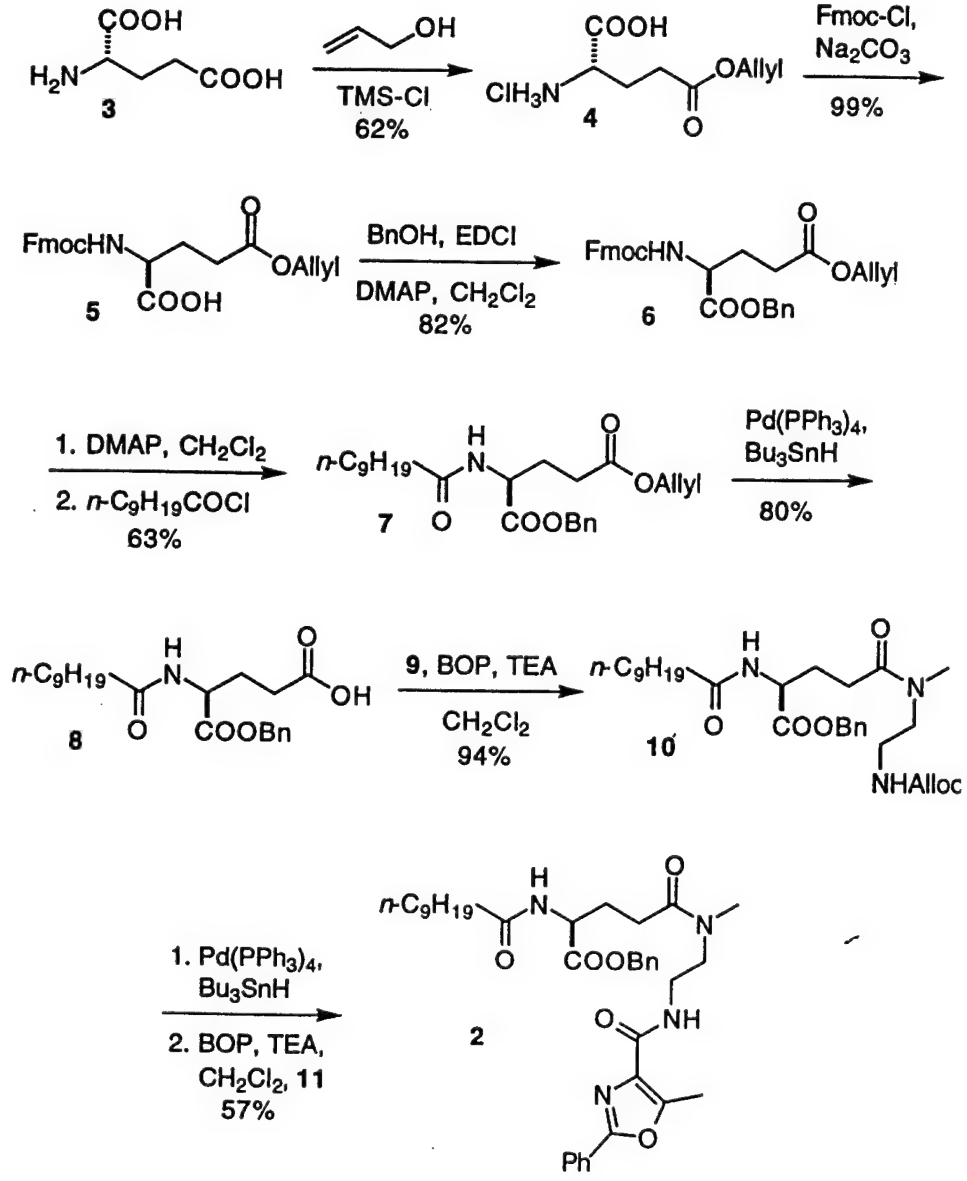

Scheme 1.

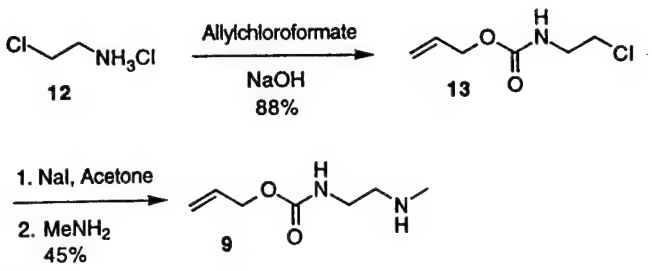

Scheme 2.

in the presence of PyBroP[39] or CloP[40] as coupling agents extended the side chain carboxyl terminus of glutamic acid toward the desired heterocyclic moiety in **1**. The resulting nine compounds (**18**) were each deprotected at the N-terminus and distributed over two additional Schlenk filters for the final segment condensation. Coupling with two different oxazole carboxylic acids in the presence of CloP and final purification by rinsing with solvent provided the phosphatase library **1** still attached to the solid support. Complete or partial cleavage with 50% trifluoroacidic acid was necessary to release the carboxylate which is required for biological activity. After filtration of the solid support and evaporation of the resulting mother liquor, the desired compounds **1** were obtained in a chemically pure and structurally well defined fashion ready for rapid throughput biological screening. In each case, the purity of the final compound was >60% according to spectroscopic analysis (^{1}H NMR, MS). The contamination was derived from incomplete couplings to the sterically hindered secondary amine moiety of Alloc-NHCH$_2$CH$_2$NH(R″). A small sample of resin had been routinely cleaved for reaction monitoring, but this coupling was difficult to drive to completion. Mass recovery was essentially quantitative. We are still in the process of further optimizing the reaction sequence and are confident that purities of >80% for the final material **1** can routinely be achieved after improvement of the coupling step.

Preliminary Biochemical and Biological Analysis of Library 1

We have begun to evaluate the ability of compounds **1a–r** to inhibit PP1 and PP2A. Initial studies were conducted in collaboration with Drs A. Boynton and D. Messner,[41] with their previously described assay.[25,29] These preliminary studies demonstrated that several members of our library inhibit protein phosphatases PP1 or PP2A by >50% at concentrations of 100 μM. We have further examined the ability of one member of the library to inhibit the catalytic activity of PP2A. As demonstrated in Figure 4, calyculin A inhibited PP2A activity at 10 nM, and compound **1d** caused 50% inhibition at 100 μM. These results document that our minimal structure retained the ability to inhibit the catalytic activity of Ser/Thr phosphatase. More comprehensive analyses are currently being conducted.

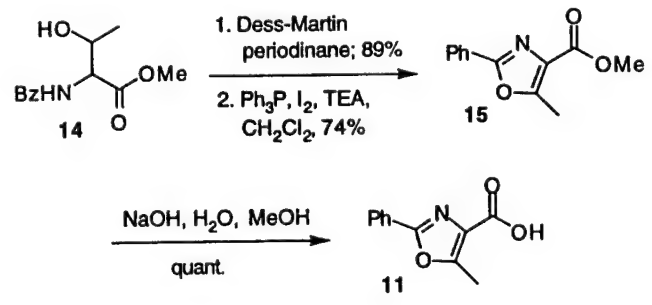

Scheme 3.

PSTPases are intracellular targets and, thus, we have examined the antiproliferative effects of members of the library to indirectly assess whether our compounds might enter cells. Exponentially growing human MDA-MB-231 breast carcinoma cells were exposed to all compounds at the highest available concentrations, which ranged from 30 to 100 μM. With the exception of two compounds, all lacked significant growth inhibitory activity. Compound **1i** caused 50% growth inhibition at 20 μM but had no further cytotoxicity at higher drug concentrations. Compound **1f** caused 50% growth inhibition at 100 μM and had a clear concentration-dependency (Fig. 5). Cell proliferation is coordinated by phosphorylation of cyclin-dependent kinases and tightly regulated by both kinases and phosphatases.[42] Thus, inhibition of Ser/Thr phosphatases such as PP2A or PP1 can result in disrupted cell cycle transition with restriction at discrete points in the cell cycle. Exponentially growing human MDA-MB-231 breast cancer cell populations (population doubling time of approximately 30–35 h) typically have approximately 50% of all cells in the S or DNA synthetic phase of the cell cycle (Fig. 6A,C). In contrast, when MDA-MB-231 cells were incubated for 48 h with 88 μM compound **1f**, there was prominent accumulation in the G1 phase with a concomitant decrease in both S and G2/M phases (Fig. 6B,C). Incubation of MDA-MB-231 cells for 72 h with 88 μM **1f** also caused a prominent accumulation in the G1 phase (Fig. 6D).

Discussion

Due to the limited character of previous SAR studies of the available natural product serine/threonine phosphatase inhibitors, the design of a small-molecule pharmacophore model has to allow for considerable structural variation. The combinatorial chemistry strategy is therefore ideally suited to address this problem. Among the characteristic structural features of calyculin A and the microcystins, the presence of a carboxylate, amide, oxazole, and lipophilic moieties are important features shared with our first generation lead structure **1**. The use of traditional amide coupling protocols combined with transition metal susceptible protective groups provided the basis for the parallel synthesis of 18 analogues of **1** via a solid-phase chemistry. We have begun to test this library both for biochemical and biological activity. Figure 4 demonstrates that the basic pharmacophore that we have

identified retains the ability to inhibit Ser/Thr phosphatases. We have not yet evaluated other members of our library with this assay, but inhibition of PP2A and PP1 has been established in preliminary studies for several members of our library. Compounds **1a–r** were further subjected to an assay for cytotoxicity and apoptosis in human breast carcinoma cells, and two members (**1h** and **f**) with an IC_{50} of <100 μM were found.[43] Interestingly, **1d**, which can block PP2A activity did not appear to be cytotoxic. This lack of biological activity may be due to poor cell penetration of cellular metabolism. Compound **1h** did not suppress cell-proliferation significantly more than 50% in our assay and thus was not examined further. Compound **1f**, however, exhibited a concentration-dependent inhibition in proliferation of MDA-MB-231 cells and flow cytometry data confirmed blockage in cell cycle progression at the G1 checkpoint. Although PSTPase inhibitors such as okadaic acid and calyculin A often are found to block cells in G2/M, a concentration-depended cell cycle arrest at the G1/S interface similar to that seen by us has been detected with some cells.[44] An additional attractive target

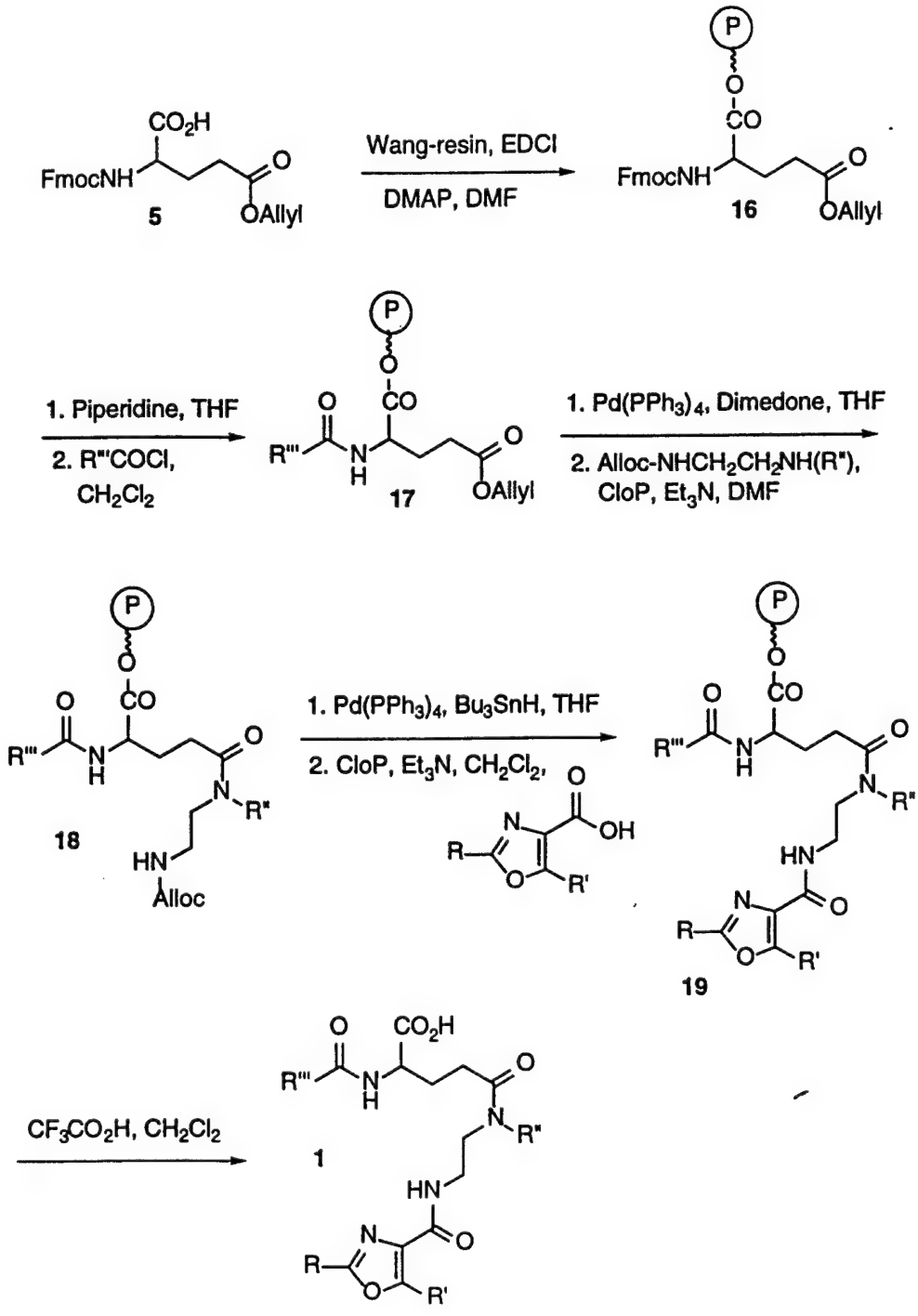

Scheme 4.

Table 2. Test library of 18 structural variants of pharmacophore model **1** prepared according to *Scheme 4*

Compound	R	R′	R″	R‴
1a	Ph	CH_3	CH_3	n-C_9H_{19}
1b	Ph	CH_3	n-C_6H_{13}	n-C_9H_{19}
1c	Ph	CH_3	Bn	n-C_9H_{19}
1d	Ph	Ph	CH_3	n-C_9H_{19}
1e	Ph	Ph	n-C_6H_{13}	n-C_9H_{19}
1f	Ph	Ph	Bn	n-C_9H_{19}
1g	Ph	CH_3	CH_3	$PhCH_2CH_2$
1h	Ph	CH_3	n-C_6H_{13}	$PhCH_2CH_2$
1i	Ph	CH_3	Bn	$PhCH_2CH_2$
1j	Ph	Ph	CH_3	$PhCH_2CH_2$
1k	Ph	Ph	n-C_6H_{13}	$PhCH_2CH_2$
1l	Ph	Ph	Bn	$PhCH_2CH_2$
1m	Ph	CH_3	CH_3	PhCH=CH
1n	Ph	CH_3	n-C_6H_{13}	PhCH=CH
1o	Ph	CH_3	Bn	PhCH=CH
1p	Ph	Ph	CH_3	PhCH=CH
1q	Ph	Ph	n-C_6H_{13}	PhCH=CH
1r	Ph	Ph	Bn	PhCH=CH

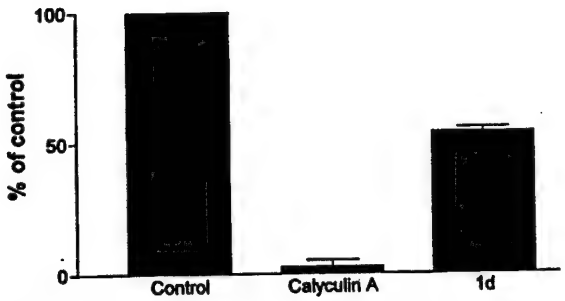

Figure 4. Inhibition of PP2A activity by compound **1d**. The catalytic subunit of PP2A was incubated with vehicle alone (control), calyculin A (10 nM), or **1d** (100 μM), and the dephosphorylation of the substrate fluorescein diphosphate determined spectrofluorometrically. Mean results to two independent experiments are shown; bars indicate the range.

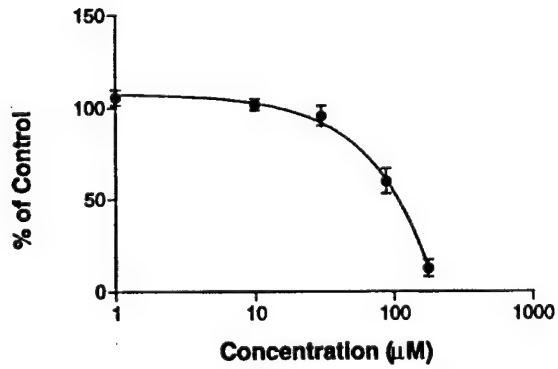

Figure 5. Antiproliferative effect of compound **1f** against human MDA-MB-231 breast cancer cells.

phosphatase that might control the G1/S transtion would be the dual specificity phophatase cdc25A.[45] Studies of the effect of **1a–r** on cdc25A and other phosphatases that may control cell cycle checkpoints are currently in progress.

These results clearly demonstrate the feasibility of using a combinatorial approach based on a natural product lead to identify novel antiproliferative and potential antineoplastic agents. Since cellular signal transduction is regulated by reversible enzymatic phosphorylation of serine, threonine and tyrosine residues on proteins, we expect that appropriately substituted, phosphatase-specific isomers of **1** will become important probes for transcription factor regulation, cell cycle control, and membrane and post-membrane signaling pathways. We are actively pursuing the synthesis and rapid-screening assays of much larger libraries based on **1** to identify more potent and more specific analogues.

Experimental Section

General methods

All glassware was dried in an oven at 150 °C prior to use. THF and dioxane were dried by distillation over Na/benzophenone under a nitrogen atmosphere. Dry CH_2Cl_2, DMF and CH_3CN were obtained by distillation from CaH_2.

2-Amino-pentanedioic acid 5-allyl ester (4). To a stirred suspension of 2.5 g (16.9 mmol) of L-glutamic acid (**3**) in 40 mL of dry allyl alcohol was added dropwise 5.4 mL (42.3 mmol) of chlorotrimethylsilane. The suspension was stirred at 22 °C for 18 h and poured into 300 mL of Et_2O. The resulting white solid was filtered off, washed with Et_2O, and dried in vacuo to provide 3.80 g (62%) of **4**: mp 133–134.5 °C (Et_2O); IR (KBr) 3152, 2972, 2557, 1738, 1607, 1489, 1450, 1289, 1366, 1264, 1223, 1177, 1146, 1121, 1084 cm^{-1}; ^1H NMR (D_2O): δ 5.8–5.7 (m, 1 H), 5.14 (dd, 1 H, J= 1.4, 17.3 Hz), 5.09 (dd, 1 H, J= 1.0, 10.4 Hz), 4.44 (d, 2 H, J= 5.6 Hz), 3.92 (t, 1 H, J= 6.8 Hz), 2.48 (t, 2 H, J= 7.0 Hz), 2.1–2.0 (m, 2 H); ^{13}C NMR (DMSO-d_6): δ 171.5, 170.6, 132.7, 117.9, 64.7, 51.2, 29.3, 25.2; MS (EI) *m/z* (relative intensity) 188 (63), 142 (72), 128 (27), 100 (21), 85 (100), 74 (32), 56 (73).

2-(9-H-Fluoren-9-ylmethoxycarbonlyamino)-pentanedioic acid 5-allyl ester (5). To 20 mL of dioxane was added 1.5 g (6.7 mmol) of ester **4**. The resulting suspension was treated with 16.8 mmol (17.7 mL of a 10% soln) of Na_2CO_3 at 0 °C, stirred for 5 min and treated with 1.74 g (6.7 mmol) of Fmoc-Cl dissolved in 10 mL of dioxane. The reaction mixture was warmed to 22 °C, stirred for 3 h, poured into 50 mL of H_2O and extracted with Et_2O (2 × 25 mL). The aq layer was cooled to 0 °C, acidified to pH 1 with conc HCl, and extracted with EtOAc (3 × 25 mL). The resulting organic layer was dried (Na_2SO_4) and concd in vacuo to give 2.72 g (99%) of **5** as a viscous oil: $[\alpha]_D$ +8.5° (*c*

2.8, $CHCl_3$, 21 °C); IR (neat) 3312, 3061, 2951, 2361, 2349, 2332, 1725, 1528,1447, 1414, 1325, 1254, 1117, 1078, 1049 cm^{-1}; ^1H NMR: δ 11.09 (br s, 1 H), 7.73 (d, 2H, J= 7.5 Hz), 7.57 (d, 2H, J=5.1 Hz), 7.4–7.25 (m, 4H), 6.0–5.85 (m, 1 H), 5.76 (d, 1H, J=8.1 Hz), 5.30 (d, 1H, J=19.5 Hz), 5.21 (d, 1H, J=10.5 Hz), 4.6–4.35 (m, 5H), 4.19 (t, 1H, J=6.6 Hz), 2.5–2.2 (m, 4H); ^{13}C NMR: δ175.6, 172.6, 156.2, 143.7, 143.5, 141.2, 131.7, 127.6, 127.0, 125.0, 119.9, 118.4, 67.1, 65.4, 53.1, 46.9, 30.2, 27.1; MS (EI) *m/e* (rel. int.) 409 (7), 351 (19), 338 (12), 280 (11), 239 (11), 196 (12), 178 (100), 165 (40); HRMS (EI) calcd for $C_{23}H_{23}NO_6$: 409.1525, found: 409.1501.

2-(9H-Fluoren-9-ylmethoxycarbonylamino)-pentanedioic acid 5-allyl ester 1-benzyl ester (6). To a soln of 1.5 g (36.6 mmol) of **5** in 5 mL of CH_2Cl_2 was added 0.42 mL (40.3 mmol) of benzyl alcohol, 0.912 g (47.6 mmol) of EDCI, and 45 mg (3.66 mmol) of dimethylaminopyridine (DMAP). The reaction mixture was stirred at 22 °C for 6 h, diluted with 20 mL of CH_2Cl_2, and extracted with H_2O (1 × 15 mL), 0.1 M HCl (2 × 15 mL), and brine (2 × 10 mL). The organic layer was dried (Na_2SO_4), concd in vacuo, and chromatographed on SiO_2 (hexanes:EtOAc, 5:1) to give 1.83 g (82%) of **6** as a white solid: mp 66.2–67.1 °C (EtOAc:hexanes); $[\alpha]_D$ +1.4° (*c* 1.64, $CHCl_3$, 21 °C); IR (neat) 3314, 1726, 1682, 1527, 1443, 1414, 1383, 1254, 1173, 1099, 1082, 980, 754, 735 cm^{-1}; ^1H NMR: δ 7.75 (d, 2 H, J=7.4 Hz), 7.59 (d, 2H, J=7.1 Hz), 7.41–7.27 (m, 9H), 5.95–5.85 (m, 1H), 5.44 (d, 1H, J=8.2 Hz), 5.34–5.19 (m, 4H), 4.56 (d, 2H, J=5.6 Hz), 4.5–4.4 (m, 3H), 4.21 (t, 1H, J=7.0 Hz), 2.5–2.0 (m, 4H); ^{13}C NMR: δ 172.2, 171.6, 155.8, 143.7, 143.5, 141.1, 135.0, 131.8, 128.5, 128.3, 128.1, 127.6, 126.9, 124.9, 119.8, 118.3, 67.2, 66.9, 66.2, 53.3, 47.0, 28.0, 27.3; MS (FAB, MNBA/MeOH) *m/z* (rel. int.) 500 ($[M+H]^+$, 40), 465 (8), 448 (14), 433 (12), 413 (8), 386 (38), 371 (24), 349 (9), 324 (16), 309 (26), 293 (11), 265 (10), 247 (24), 231 (56), 215 (39), 202 (26), 191 (24), 179 (67), 165 (48), 154 (67), 143 (31), 133 (71), 117 (100).

2-Decanoylamino-pentanedioic acid 5-allyl ester 1-benzyl ester (7). To a suspension of 1 g (2.0 mmol) of **6** in 10 mL of CH_2Cl_2 was added 1 g (8.2 mmol) of DMAP. The reaction mixture was stirred at 22 °C for

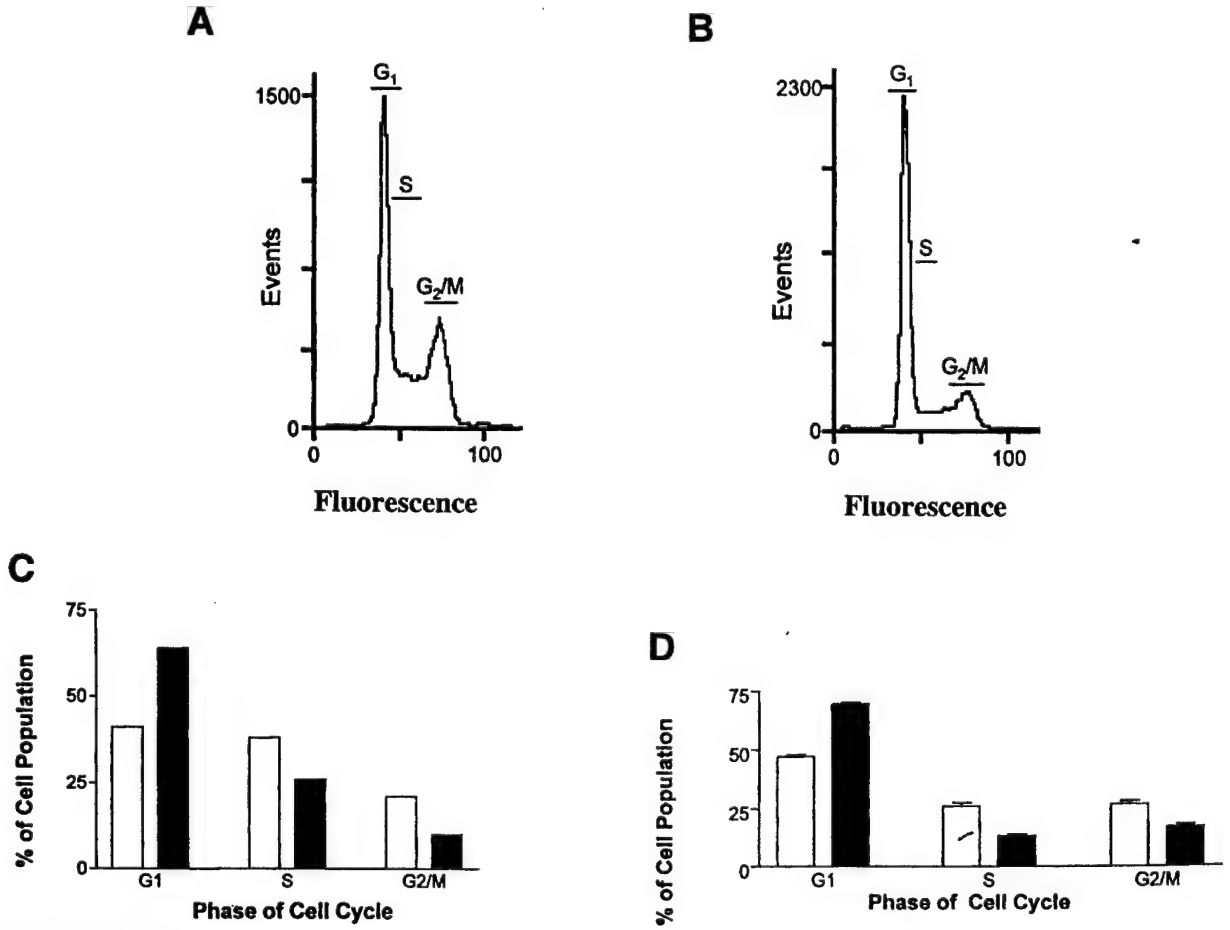

Figure 6. Cell cycle distribution of human breast cancer cells after treatment with compound **1f** determined by flow cytometry. Panel A. Flow cytometry analysis of MDA-MB-231 cells treated with vehicle alone. Panel B. Flow cytometry analysis 48 h after treatment with 88 μM compound **1f**. Fluorescence channel measures intracellular propidium iodide concentration, an index of DNA content. Horizontal bars are the gating positions that allow for cell cycle analysis. Panel C. MDA-MB-231 cell cycle distribution 48 h after continuous treatment with 88 μM compound **1f**. This is the result of one experiment. Open bars are control cells and black bars are cells treated with **1f**. Panel D. Cell cycle distribution 72 h after continuous treatment with 88 μM **1f**. The mean values were obtained from three independent determinations. Open bars are control cells and black bars are cells treated with 88 μM **1f**. The SE of the mean are displayed.

24 h, treated with 0.62 mL (3.0 mmol) of decanoyl chloride, stirred for 2 h at 22 °C, and extracted with satd Na_2CO_3 (2 × 10 mL). The organic layer was dried (Na_2SO_4), evapd to dryness, and the residue was chromatographed on SiO_2 (hexanes:EtOAc, 5:1) to give 548 mg (63%) of **7** as a viscous oil: IR (neat) 3293, 3063, 2924, 2855, 1740, 1649, 1534, 1453, 1379, 1175, 986, 930 cm^{-1}; ^1H NMR: δ 7.26 (s, 5H), 6.68 (d, 1H, J=7.8 Hz), 5.85–5.75 (m, 1H), 5.22 (d, 1H, J=17.3 Hz), 5.14 (d, 1H, J=10.4 Hz), 5.08 (s, 2H), 4.63–4.57 (m, 1H), 4.48 (d, 2H, J=5.6 Hz), 2.38–2.28 (m, 2H), 2.2–2.1 (m, 3H), 2.0–1.9 (m, 1H), 1.55 (t, 2H, J=6.9 Hz), 1.20 (bs, 12H), 0.82 (t, 3 H, J=5.9 Hz); ^{13}C NMR δ 173.0, 172.1, 171.6, 135.0, 131.7, 128.2, 128.1, 127.8, 117.9, 66.8, 64.9, 51.3, 36.0, 31.6, 29.9, 29.1, 29.0, 26.8, 25.3, 22.3, 13.8; MS (EI) *m/z* (rel. int.) 431 (12), 319 (21), 296 (51), 142 (100), 124 (31), 91 (91); HRMS (EI) *m/z* calcd for $C_{25}H_{37}NO_5$: 431.2672, found: 431.2673.

2-Decanoylamino-pentanedioic acid 1-benzyl ester (8). To a soln of 752 mg (1.74 mmol) of 2-decanoylamino-pentanedioic acid **7** in 10 mL of CH_2Cl_2 was added 100 mg (0.087 mmol) of tetrakistriphenylphosphine Pd(0) followed by 0.52 mL (1.9 mmol) of tributyltin hydride. After 15 min, the reaction mixture was quenched with 10 mL of a 10% HCl soln. The aq layer was reextracted with 15 mL of CH_2Cl_2 and the organic layer dried (Na_2SO_4), concd in vacuo, and chromatographed on SiO_2 (hexanes:EtOAc, 9:1) to provide 545 mg (79.9%) of **8** as a thick oil: $[\alpha]_D$ +2.8° (*c* 1.2, $CHCl_3$, 21 °C); IR (neat) 3351, 3064, 2995, 2852, 1738, 1712, 1657, 1536, 1454, 1380, 1364, 1265, 1209, 1183, 1121, 739 cm^{-1}; ^1H NMR: δ 10.9–10.7 (br s, 1 H), 7.22 (s, 5 H), 6.58 (d, 1H, J=7.8 Hz), 5.09 (s, 2H), 4.63 (dd, 1H, J=8.1, 12.9 Hz), 2.4–2.25 (m, 2H), 2.2–2.1 (m, 3H), 2.0–1.9 (m, 1H), (m, 6H), 1.53 (t, 2H, J=6.6 Hz), 1.19 (br s, 12H), 0.81 (t, 3H, J=6.0 Hz); ^{13}C NMR: δ 176.9, 174.0, 171.8, 134.9, 128.5, 128.4, 128.1, 67.3, 51.4, 36.2, 31.7, 29.9, 29.3, 29.2, 29.1, 27.0, 25.5, 22.5, 14.0; MS (EI) *m/z* (rel. int.) 391 (54), 373 (62), 279 (13), 256 (19), 178 (27), 178 (23), 155 (13), 146 (6), 130 (7), 102 (100); HRMS (EI) *m/z* calcd for $C_{22}H_{33}NO_5$: 391.2358, found: 391.2350.

4-[(2-Allyloxycarbonylamino-ethyl)-methyl-carbamoyl]-2-decanoylamino-butyric acid benzyl ester (10). To a soln of 526 mg (1.3 mmol) of **8** in 10 mL of CH_2Cl_2 was added 225 μL (1.61 mmol) of triethylamine and 320 mg (2.0 mmol) of secondary amine **9**. The solution was stirred at 22 °C for 5 min, treated with 710 mg (1.61 mmol) of benzotriazol-1-yloxy-tris(dimethylamino)-phosphonium hexafluorophosphate (BOP reagent), stirred at 22 °C for 10 min, concd in vacuo, dissolved in 15 mL of EtOAc, and extracted with 2 M HCl soln. The organic layer was chromatographed on SiO_2 (hexanes:EtOAC, 1:3) to give 715 mg (94%) of **10** as a clear oil: $[\alpha]_D$ +5.3 (*c* 0.58, $CHCl_3$, 21 °C); IR (neat) 3420, 3250, 2924, 1713, 1680, 1657, 1642, 1632, 1537, 1495, 1470, 1455, 1252, 845 cm^{-1}; ^1H NMR: δ 7.35–7.2 (br s, 5 H), 6.97 (d, 0.3H, J=7.5 Hz), 6.82 (d, 0.7 H, J=7.3 Hz), 5.9–5.6 (m, 2H), 5.3–5.1 (m, 4H), 4.65–4.5 (m, 1H), 4.50 (d, 2H, J=4.9 Hz); 3.55 (t, 1H, J=7.0 Hz), 3.35–3.1 (m, 3H), 2.85 (s, 3H), 2.4–1.8 (m, 6H), 1.65–1.5 (m, 2H), 1.22 (bs, 12H), 0.84 (t, 3H, J=6.1 Hz); ^{13}C NMR (MeOD): δ 176.4, 176.3, 174.4, 174.2, 173.2, 158.6, 137.1, 134.3, 134.2, 132.9, 129.5, 129.2, 129.1, 117.6, 117.4, 67.8, 66.3, 66.2, 53.5, 53.3, 39.6, 39.3, 36.7, 36.6, 34.2, 32.9, 30.5, 30.4, 30.3, 30.2, 29.7, 27.6, 26.8, 23.6, 14.5; MS (EI) *m/z* (rel. int.) 531 (16), 473 (37), 418 (16), 396 (26), 374 (38), 361 (17), 338 (87), 220 (54), 184 (52), 155 (36), 130 (29), 101 (37), 91 (100); HRMS (EI) *m/z* calcd for $C_{29}H_{45}N_3O_6$: 531.3308, found: 531.3316.

2-Decanoylamino-4-(methyl-{3-[5-methyl-2-phenyl-oxazole-4-carbonyl]-ethyl}-carbamoyl)-butyric acid benzyl ester (2). To a soln of 193 mg (0.363 mmol) of **10** in 15 mL of CH_2Cl_2 was added 20 mg (0.018 mmol) of tetrakistriphenylphosphine Pd(0), 127 μL (0.472 mmol) of tributyltin hydride, and 20 μL of H_2O. The reaction mixture was stirred at 22 °C for 5 min, filtered through a plug of basic Al_2O_3 and treated with 150 mg (0.726 mmol) of oxazole **11**, 60 mL (0.436 mmol) of triethylamine, and 192 mg (0.436 mmol) of BOP reagent. The reaction mixture was stirred for 30 min at 22 °C, diluted with 10 mL of CH_2Cl_2, and extracted with satd $NaHCO_3$ soln, 1 M HCl, and brine. The organic layer was concd in vacuo and chromatographed on SiO_2 (hexanes:EtOAc, 1:1) to give 131 mg (57%) of **2** as a viscous oil: $[\alpha]_D$ −0.8° (*c* 1.32, $CHCl_3$, 21 °C); IR (neat) 3476, 3415, 3311, 3065, 2925, 2854, 1741, 1649, 1526, 1491, 1379, 1338, 1264, 1240, 1200, 1174, 1070, 711 cm^{-1}; ^1H NMR: δ 8.0–7.95 (m, 2H), 7.5–7.4 (m, 2H), 7.33 (br s, 6 H), 6.93 (d, 0.3H, J=7.0 Hz), 6.85 (d, 0.7H, J=7.2 Hz), 5.18–5.07 (m, 2H), 4.65–4.55 (m, 1H), 3.7–3.3 (m, 4H), 2.98 (s, 1H), 2.96 (s, 2H), 2.71 (d, 3H, J=2.6 Hz), 2.6–2.0 (m, 6H), 1.58 (t, 2H, J=6.8 Hz), 1.3–1.1 (br s, 12H), 0.86 (t, 3H, J=6.9 Hz); ^{13}C NMR: δ 173.3, 172.8, 172.0, 171.9, 182.5, 158.6, 153.2, 152.8, 135.9, 130.7, 130.6, 129.7, 128.8, 128.5, 128.3, 128.2, 126.7, 126.5, 126.2, 66.9, 52.2, 52.1, 48.9, 47.6, 37.2, 37.1, 36.4, 36.3, 36.2, 34.1, 31.8, 29.6, 29.5, 29.4, 29.3, 29.2, 28.9, 26.8, 26.6, 25.5, 22.8, 14.1, 11.8; MS (EI) *m/z* (rel. int.) 632 (38), 497 (9), 405 (18), 374 (22), 260(21), 220 (42), 186 (56), 105 (18), 91 (100); HRMS calcd for $C_{36}H_{48}N_4O_6$: 632.3574, found: 632.3572.

(2-Chloro-ethyl)-carbamic acid allyl ester (13). A soln of 2.5 g (22 mmol) of chloroethylamine hydrochloride in 10 mL of 6 M NaOH was cooled to 0 °C and treated dropwise with 2.7 mL (25.9 mmol) of allyl chloroformate while keeping the pH at 9 by addition of 6 M NaOH soln. The reaction was then warmed to 22 °C, stirred for 2 h, and extracted with THF. The organic layer was dried (Na_2SO_4), concd in vacuo, and chromatographed on SiO_2 (hexanes:EtOAc, 9:1) to give 3.1 g (88%) of **13** as a yellow oil: IR (neat) 3333, 2949, 2348, 1705, 1647, 1529, 1433, 1368, 1248, 1190, 1144, 1061, 991, 929, 776 cm^{-1}; ^1H NMR: δ 6.05–5.85 (m, 1H), 5.55–5.35 (br s, 1H), 5.26 (dd, 1H, J=1.5, 17.1 Hz), 5.18 (dd, 1H, J=1.0, 10.4), 4.54 (d, 2H, J=5.5 Hz), 3.57 (t, 2H, J=5.5 Hz), 3.5–3.35 (m, 2H); ^{13}C NMR: δ 156.0, 132.5, 117.7, 65.6, 43.8, 42.7.

(2-Methylamino-ethyl)-carbamic acid allyl ester (9). A soln of 14 g (86 mmol) of **13** and 25 g (172 mmol) of NaI in 40 mL of acetone was refluxed for 18 h, concd in vacuo, dissolved in H_2O, and extracted with CH_2Cl_2. The organic layer was dried (Na_2SO_4) and cooled to 0 °C. Methyl amine was bubbled through the reaction mixture until the solution was satd. The reaction mixture was warmed to 22 °C, stirred for 36 h, concd in vacuo and chromatographed on SiO_2 (EtOAc) to produce 6.14 g (45%) of **9** as a yellow oil: IR (neat) 3306, 2938, 2313, 1844, 1703, 1651, 1525, 1460, 1383, 1256, 1144, 995, 927, 775 cm^{-1}; ^1H NMR: δ 5.95–5.8 (m, 1 H), 5.28 (dd, 1H, J=1.4, 17.3 Hz), 5.18 (d, 1H, J=10.4 Hz), 4.54 (d, 2H, J=5.3 Hz), 4.9–4.6 (br s, 1 H), 3.34 (q, 2H, J=5.6 Hz), 2.79 (t, 2H, J=5.6 Hz), 2.47 (s, 3H); ^{13}C NMR: δ 157.2, 132.8, 117.6, 65.5, 50.7, 39.7, 35.4; MS (EI) *m/e* (rel. int.) 158 (32), 138 (17), 129 (25), 101 (13), 84 (12), 73 (13), 57 (100).

5-Methyl-2-phenyl-oxazole-4-carboxylic acid methyl ester (15). A soln of 750 mg (3.2 mmol) of **14** in 10 mL of CH_2Cl_2 was treated with 1.61g (3.8 mmol) of Dess–Martin reagent. The reaction was stirred at 22 °C for 10 min, concd in vacuo, and chromatographed on SiO_2 (hexanes:EtOAc, 3:2) to give 658 mg (89%) of 2-benzoylamino-3-oxo-butyric acid methyl ester. Alternatively, a soln of 9.12 g (38 mmol) of **14** in 80 mL of CH_2Cl_2 was cooled to −23 °C and treated with 16.1 mL (115 mmol) of triethylamine and a soln of 18.3 g (115 mmol) of SO_3–pyridine complex in 60 mL of dry DMSO. The reaction mixture was warmed to 22 °C, stirred for 30 min, then cooled to −48 °C and quenched with 20 mL of satd $NaHCO_3$. The soln was extracted with 50 mL of hexanes:EtOAc (2:1). The aq layer was reextracted with hexanes:Et_2O (2:1) and the combined organic layers were washed with brine, dried (Na_2SO_4), and chromatographed (hexanes:EtOAc, 3:2) to give 7.1 g (79%) of 2-benzoylamino-3-oxo-butyric acid methyl ester as a white solid: mp 112.7–113.3 °C (hexanes:EtOAc); IR (neat) 3402, 1734, 1662, 1599, 1578, 1510, 1478, 1435, 1354, 1269, 1156, 1121, 912, 804, 714 cm^{-1}; ^1H NMR: δ 8.2–8.1 (br s, 1H), 8.0–7.4 (m, 5H), 5.49 (s, 1H), 3.86 (s, 3H), 2.33 (s, 3H); ^{13}C NMR: δ 168.2, 167.2, 132.6, 132.5, 132.1, 128.7, 127.3, 83.9, 54.2, 23.2; MS (EI) *m/e* (rel. int.) 235 (13), 208 (18), 192 (8), 121 (7), 105 (100), 77 (58).

A soln of 277 mg (1.06 mmol) of triphenylphosphine, 268 mg (1.06 mmol) of iodine, and 0.29 mL (2.11 mmol) of triethylamine in 5 mL of CH_2Cl_2 was cooled to −48 °C and treated with a soln of 124 mg (0.528 mmol) of 2-benzoylamino-3-oxo-butyric acid methyl ester in 5 mL of CH_2Cl_2. The reaction mixture was warmed to 22 °C, stirred for 20 min, transferred to a separatory funnel and extracted with aq $Na_2S_2O_7$ followed by satd Na_2CO_3. The organic layer was concd in vacuo and chromatographed on SiO_2 (hexanes: EtOAc, 9:1) to give 84.4 mg (74%) of **15** as a white solid: mp 89.3–89.9 °C (hexanes:EtOAc); IR (neat) 3025, 1717, 1610, 1561, 1485, 1436, 1348, 1323, 1302, 1285, 1235, 1188, 1103, 1072, 1057, 1022 cm^{-1}; ^1H NMR 8.1–7.95 (m, 2H), 7.5–7.3 (m, 3H), 3.92 (s, 3H), 2.68 (s, 3H); ^{13}C NMR: δ 162.7, 159.5, 156.3, 130.8, 128.8, 128.6, 128.3, 126.4, 51.9, 11.98; MS (EI) *m/z* (relative intensity) 231 (6), 217 (51), 185 (55), 105 (100), 77 (41), 44 (64); HRMS (EI) *m/z* calcd for $C_{12}H_{11}NO_3$: 217.0739, found: 217.0729.

5-Methyl-2-phenyl-oxazole-4-carboxylic acid (11). A solution of 2.07 g (9.5 mmol) of **15** in 20 mL of 3 M NaOH and 12 mL of MeOH was stirred at 22 °C for 2 h and extracted with Et_2O. The aq layer was acidified to pH 1 with concd HCl and extracted with EtOAc. The organic layer was dried (Na_2SO_4), and concd in vacuo to give 1.84 g (95%) of **11** as an off-white solid: mp 182.3–182.6 °C (EtOAc:hexanes); IR (neat) 3200, 2950, 2932, 2890, 2363, 2336, 1694, 1682, 1611, 1563, 1483, 1450, 1337, 1255, 1192, 1117, 1053, 1020 cm^{-1}; ^1H NMR: δ 10.2–9.9 (br s, 1H), 8.2–7.9 (m, 2H), 7.6–7.4 (m, 3H), 2.75 (s, 3H); ^{13}C NMR: (CD_3OD) δ 164.6, 160.7, 157.4, 131.9, 129.8, 129.6, 127.3, 127.2, 12.1; MS (EI) *m/z* (rel. int.) 203 (53), 185 (24), 157 (13), 116 (17), 105 (100), 89 (21), 77 (33), 63 (16); HRMS calcd for $C_{11}H_9NO_3$: 203.0582, found: 203.0583.

Solid-phase chemistry

Step 1, 5→16. In a medium porosity Schlenk filter aparatus was placed 750 mg Wang resin (0.96 mmol/g, 0.72 mmol of active sites). The resin was suspended in 12 mL of dry DMF and a stream of nitrogen was forced up through the filter at a rate which allowed the solvent to gently bubble. To this reaction mixture was added 1.47 g (3.6 mmol) of **5**. The suspension was agitated for 5 min and treated with 26 mg (0.216 mmol) of DMAP and 550 mg (2.88 mmol) of EDCI, agitated at 22 °C for 18 h and filtered, and the resin was washed with DMF (2 × 10 mL), H_2O (3 × 10 mL), THF (3 × 10 mL), and CH_2Cl_2 (3 × 10 mL). The resin was dried under vacuum and the remaining active sites were capped by addition of 10 mL of CH_2Cl_2 and 10 mL of acetic anhydride along with 26 mg (2.88 mmol) of DMAP to the resin. Bubbling was continued at 22 °C for 3 h and the resin was then washed with CH_2Cl_2 (6 × 15 mL) and dried in vacuo. To test the loading on the resin, 30 mg of resin was removed and suspended in 2 mL of trifluoroacetic acid for 5 min at 22 °C, filtered and washed (3 × 3 mL) with CH_2Cl_2. The filtrate was concentrated in vacuo to give 7.3 mg (85%) of **5**.

Step 2, 16→17. A suspension of 690 mg (0.576 mmol) of 2-(9H-fluoren-9-ylmethoxycarbonylamino)-pentanedioic acid 5-allyl ester linked to Wang resin (**16**) in 15 mL of THF was treated with 6 mL (57.6 mmol) of piperidine, agitated by bubbling for 30 min, filtered and washed with CH_2Cl_2 (6 × 10 mL). The resin was dried in vacuo. A suspension of this resin in 10 mL of CH_2Cl_2 was treated with 0.48 mL (2.31 mmol) of decanoyl chloride and 14 mg (0.115 mmol) of DMAP. The reaction mixture was agitated at 22 °C for 6 h, filtered and the resin was washed with CH_2Cl_2 (6 × 10 mL) and dried in vacuo.

Step 3, 17→18. A suspension of 690 mg (0.576 mmol) of 2-decanoylamino-pentanedioic acid 5-allyl ester linked to Wang resin (**17**) in 10 mL of THF was treated with 67 mg (0.0576 mmol) of tetrakis(triphenylphosphine)palladium(0) and 806 mg (5.75 mmol) of dimedone, and agitated by bubbling at 22 °C for 18 h. The resin was then filtered, washed with THF (2 × 10 mL), CH_2Cl_2 (2 × 10 mL), MeOH (2 × 10 mL), H_2O (2 × 10 mL), 1% HOAc soln (2 × x10 mL), H_2O (2 × 10 mL), MeOH (2 × 10 mL), CH_2Cl_2 (2 × 10 mL), and dried in vacuo. Cleavage and examination of 40 mg of resin by ^1H NMR showed full deprotection of the allyl ester.

A suspension of this resin in 12 mL of DMF was treated with 0.22 mL (1.572 mmol) of triethylamine and 414.1 mg (2.62 mmol) of Alloc-$NHCH_2CH_2NHMe$. After agitating the reaction mixture for 5 min to ensure proper mixing, 540 mg (1.572 mmol) of CloP was added. The reaction mixture was agitated with bubbling for 18 h at 30 °C, cooled to 22 °C, and the resin was filtered and washed with DMF (2 × 10 mL), CH_2Cl_2 (2 × 10 mL), MeOH (2 × 10 mL), H_2O (2 × 10 mL), THF (2 × 10 mL), and CH_2Cl_2 (2 × 10 mL). The resin was dried in vacuo and 40 mg of resin was cleaved with CF_3CO_2H. The ^1H NMR of the residue showed that coupling had occurred to nearly 100%.

Step 5, 18→19. A suspension of 200 mg (0.192 mmol) of 4-[(2-allyloxycarbonylamino-ethyl)-methyl-carbamoyl]-2-decanoylamino-butyric acid linked to Wang resin (**18**) in 6 mL of CH_2Cl_2 was treated with 12 mg (0.0096 mmol) of tetrakistriphenylphosphine Pd(0), 62 ml (0.230 mmol) of tributyltin hydride, and 10 µl of H_2O. The reaction mixture was agitated with bubbling N_2 for 15 min, filtered, and the resin was washed with 10 mL portions of CH_2Cl_2, THF, acetone, MeOH, H_2O, acetone, EtOAc, hexanes, THF, and CH_2Cl_2. The resin was then dried in vacuo and 15 mg was removed for testing. The ^1H NMR of the TFA-cleaved residue showed full deprotection as well as full removal of all tin side products.

A suspension of 185 mg (0.190 mmol) of this resin in 8 mL of CH_2Cl_2 was treated with 117 mg (0.576 mmol) of oxazole carboxylic acid, 198 mg (0.576 mg) of CloP, and 80 µl (0.576 mmol) of triethylamine. The reaction mixture was agitated by bubbling with N_2 for 3 h, filtered, and washed with 20 mL of CH_2Cl_2, acetone, water, acetone, and CH_2Cl_2. The resin was dried in vacuo and 15 mg was removed for testing. The ^1H NMR of the residue showed that the reaction had gone to 60% completion. The resin was subsequently submitted to a second coupling cycle.

Step 6, 19→1. A suspension of 115 mg (0.12 mmol) of 2-decanoylamino-4-(methyl-{3-[5-methyl-2-phenyl-oxazole-4-carbonyl]-ethyl}-carbamoyl)-butyric acid linked to Wang resin (**19**) in 3 mL of TFA was stirred for 5 min, filtered, and washed with 5 mL of CH_2Cl_2. The extract was concd in vacuo to provide 33.1 mg (100% for step 2 to step 6) of **1**. A ^1H NMR showed the product to be 66% pure with 2-acylamino-pentanedioic acid as the major impurity. Acid **1a** was dissolved in 3 mL of CH_2Cl_2 and treated with 0.016 mL (0.138 mmol) of benzyl bromide and 0.02 mL (0.138 mmol) of DBU to provide material identical with the benzyl ester **2** prepared by solution phase chemistry.

Cell culture

Human MDA-MB-231 breast carcinoma cells were obtained from the American Type Culture Collection at passage 28 and were maintained for no longer than 20 passages. The cells were grown in RPMI-1640 supplemented with 1% penicillin (100 µg/mL) and streptomycin (100 µg/mL), 1% L-glutamate, and 10% fetal bovine serum in a humidified incubator at 37 °C under 5% CO_2 in air. Cells were routinely found free of mycoplasma. To remove cells from the monolayer for passage or flow cytometry, we washed them two times with phosphate buffer and briefly (< 3 min) treated the cells with 0.05% trypsin/2 mM EDTA at room temperature. After the addition of at least two volumes of growth medium containing 10% fetal bovine serum, the cells were centrifuged at 1000 *g* for 5 min. Compounds were made into stock solns using DMSO, and stored at −20 °C. All compounds and controls were added to obtain a final concn of 0.1–0.2% (v/v) of the final soln for experiments.

PP2A assay

The activity of the catalytic subunit of bovine cardiac muscle PP2A (Gibco-BRL, Gaithersburg, MD) was measured with fluorescein diphosphate (Molecular Probes, Inc., Eugene, OR) as a substrate in 96-well microtiter plates. The final incubation mixture (150 µL) comprised 25 mM Tris (pH 7.5), 5 mM EDTA, 33 µg/mL BSA, and 20 µM fluorescein diphosphate. Inhibitors were resuspended in DMSO, which was also used as the vehicle control. Reactions were initiated by adding 0.2 units of PP2A and incubated at room temperature overnight. Fluorescence emission from the product was measure with Perseptive Biosystems Cytoflour II (exciton filter, 485 nm; emission filter, 530 nm) (Framingham, MA).

Cell proliferation assay

The antiproliferative activity of newly synthesized compounds was determined by our previously described method.[46] Briefly, cells (6.5×10^3 cells/cm^2) were plated in 96 well flat bottom plates for the cytotoxicity studies and incubated at 37 °C for 48 h. The plating medium was aspirated off 96 well plates and 200 µL of growth medium containing drug was added per well. Plates were incubated for 72 h, and then washed 4× with serum free medium. After washing, 50 µL of 3-[4,5-dimethylthiazol-2-yl]-2,5-diphenyl tetrazolium bromide soln (2 mg/mL) was added to each well, followed by 150 µL of complete growth medium. Plates were then incubated an additional 4 h at 37 °C. The soln was aspirated off, 200 µL of DMSO added, and the plates were shaken for 30 min at room

temperature. Absorbance at 540 nm was determined with a Titertek Multiskan Plus plate reader. Biologically active compounds were tested at least three independent times.

Measurement of cell cycle kinetics

Cells (6.5×10^5/cm^2) were plated and incubated at 37 °C for 48 h. The plating medium was then aspirated off, and medium containing a concentration of compound **1f** that caused approximately 50% growth inhibition (88–100 μM) was added for 48–72 h. Untreated cells at a similar cell density were used as control populations. Single cell preparations were fixed in ice-cold 1% paraformaldehyde, centrifugation at 1000 *g* for 5 min, resuspended in Puck's saline, centrifuged, and resuspended in ice-cold 70% ethanol overnight. The cells were removed from fixatives by centrifugation (1000 *g* for 5 min) and stained with a 5 μg/mL propidium iodide and 50 μg/mL RNase A solution. Flow cytometry analyses were conducted with a Becton Dickinson FACS Star. Single parameter DNA histograms were collected for 10,000 cells, and cell cycle kinetic parameters calculated using DNA cell cycle analysis software version C (Becton Dickinson). Experiments at 72 h were performed at least three independent times.

Acknowledgment

Funding was provided by the American Cancer Society (Junior Faculty Research Award to P.W.), Upjohn Co., the Alfred P. Sloan Foundation. and a United States Army Breast Cancer Predoctoral Fellowship. We thank Drs Boynton and Messner for their preliminary biochemical evaluation of **1a-r**.

References and Notes

1. Johnson, L. N.; Barford, D. *Annu. Rev. Biophys. Biomol. Struct.* **1993**, *22*, 199.

2. (a) Murray, K. J.; Warrington, B. H. In *Comprehensive Medicinal Chemistry;* (Sammes, P. G.; Taylor, J. B., Eds.; Pergamon Press: Oxford, 1990; Vol. 2; Chapter 8.7; p 531. (b) Murray, K. J.; Coates, W. J. *Annu. Rep. Med. Chem.* **1994**, *29*, 255.

3. Zolnierowicz, S.; Hemmings, B. A. *Trends in Cell Biol.* **1994**, *4*, 61.

4. Honkanen, R. E.; Boynton, A. L. In *Protein kinase C*; J. F. Kuo, Ed.; Oxford University Press: Oxford, 1994; Chapter, 12; p 305, and references cited therein.

5. Song, Q.; Baxter, G. D.; Kovacs, E. M.; Findik, D.; Lavin, M. F. *J. Cell. Phys.* **1992**, *153*, 550.

6. Haldari, S.; Jena, N.; Croce, C. M. *Proc. Natl Acad. Sci. U.S.A.* **1995**, *92*, 4507.

7. Boe, R.; Gjertsen, B. T.; Vintermyr, O. K.; Houge, G.; Lanotte, M.; Doskeland, S. O. *Exp. Cell. Res.* **1991**, *195*, 237.

8. Kiguchi, K.; Glesne, D.; Chubb, C. H.; Fujiki, H.; Huberman, E. *Cell Growth Differentiation* **1994**, *5*, 995.

9. Xia, Z.; Dickens, M.; Raingeaud, J.; Davis, R. J.; Greenberg, M. E. *Science* **1995**, *270*, 1326.

10. Mumby, M. C.; Walter, G. *Physiol. Rev.* **1993**, *73*, 673.

11. Wera, S.; Hemmings, B. A. *Biochem. J.* **1995**, *311*, 17.

12. Fujiki, H.; Suganuma, M.; Yatsunami, J.; Komori, A.; Okabe, S.; Nishiwakimatsushima, R.; Ohta, T. *Gazz. Chim. Ital.* **1993**, *123*, 309.

13. Nishiwaki, S.; Fujiki, H.; Suganuma, M.; Furuya-Suguri, H. *Carcinogenesis* **1990**, *11*, 1837.

14. (a) Takai, A.; Murata, M.; Torigoe, K.; Isobe, M.; Mieskes, G.; Yasumoto, T. *Biochem. J.* **1992**, *284*, 539. (b) Sasaki, K.; Murata, M.; Yasumoto, T.; Mieskes, G.; Takai, A. *Biochem. J.* **1994**, *288*, 259.

15. Rinehart, K. L.; Namikoshi, M.; Choi, B. W. *J. Appl. Phycol.* **1994**, *6*, 159.

16. De Silva, E. D.; Williams, D. E.; Andersen, R. J.; Klix, H.; Holmes, C. F. B.; Allen, T. M. *Tetrahedron Lett.* **1992**, *33*, 1561.

17. Bagu, J. R.; Sonnichsen, F. D.; Williams, D.; Andersen, R. J.; Sykes, B. D.; Holmes, C. F. *Nature Struct. Biol.* **1995**, *1*, 114.

18. Valentekovich, R. J.; Schreiber, S. L. *J. Am. Chem. Soc.* **1995**, *117*, 9069.

19. Matsuzawa, S.; Suzuki, T.; Suzuki, M.; Matsuda, A.; Kawamura, T.; Mizuno, Y.; Kikuchi, K. *FEBS Lett.* **1994**, *356*, 272.

20. Li, Y.-M.; Casida, J. E. *Proc. Natl Acad. Sci. U.S.A.* **1992**, *89*, 11867.

21. Eldridge, R.; Casida, J. E. *Tox. Appl. Pharm.* **1995**, *130*, 95.

22. Li, V. M.; Mackintosh, C.; Casida, J. E. *Biochem. Pharm.* **1993**, *46*, 1435.

23. (a) Evans, D. A.; Gage, J. R.; Leighton, J. L. *J. Am. Chem. Soc.* **1992**, *114*, 9434. (b) Ichikawa, Y.; Tsuboi, K.; Jiang, Y.; Naganawa, A.; Isobe, M. *Tetrahedron Lett.* **1995**, *36*, 7101.

24. Very recently, it was reported that tautomycin acts in its hydrolysed, bis-carboxylic acid form: Sugiyama, Y.; Ohtani, I. I.; Isobe, M.; Takai, A.; Ubukata, M.; Isono, K. *Bioorg. Med. Chem. Lett.* **1996**, *6*, 3.

25. Honkanen, R. E.; Codispoti, B.; Tse, K.; Boynton, A. L. *Toxicon* **1994**, *32*, 339.

26. Takai, A.; Sasaki, K.; Nagai, H.; Mieskes, G.; Isobe, M.; Isono, K.; Yasumoto, T. *Biochem. J.* **1995**, *306*, 657.

27. Yoshizawa, S.; Matsushima, R.; Watanabe, M. F.; Harada, K.; Ichihara, A.; Carmichael, W. W. *Cancer Res. Clin. Oncol.* **1990**, *116*, 609.

28. MacKintosh, C.; Klumpp, S. *FEBS Lett.* **1990**, *277*, 137.

29. Honkanen, R. E.; Zwiller, J.; Moore, R. E.; Daily, S. L.; Khatra, B. S.; Dukelow, M.; Boynton, A. L. *J. Biol. Chem.* **1990**, *265*, 19401.

30. (a) Quinn, R. J.; Taylor, C.; Suganuma, M.; Fujiki, H. *Bioorg. Med. Chem. Lett.* **1993**, *3*, 1029. (b) Taylor, C.; Quinn, R. J.; McCulloch, R.; Nishiwaki-Matsushima, R.; Fujiki, H. *Bioorg. Med. Chem. Lett.* **1992**, *2*, 299.

31. (a) Gallop, M. A.; Barrett, R. W.; Dower, W. J.; Fodor, S. P. A.; Gordon, E. M. *J. Med. Chem.* **1994**, *37*, 1233. (b) Gordon, E. M.; Barrett, R. W.; Dower, W. J.; Fodor, S. P. A.; Gallop, M. A. *J. Med. Chem.* **1994**, *37*, 1385.

32. Wipf, P.; Cunningham, A. *Tetrahedron Lett.* **1995**, *36*, 7819.

33. Wipf, P. *Chem. Rev.* **1995**, *95*, 2115, and references cited therein.

34. Belshaw, P.J.; Mzengeza, S.; Lajoie, G. *Syn. Commun.* **1990**, *20*, 3157.

35. Dangles, O.; Guibe, F.; Balavoine, G.; Lavielle, S.; Marquet, A. *J. Org. Chem.* **1987**, *52*, 4984.

36. Castro, B.; Dormoy, J.-R.; Evin, G.; Selve, C.; *Tetrahedron Lett.* **1975**, *14*, 1219.

37. Wipf, P.; Miller, C. P. *J. Org. Chem.* **1993**, *58*, 3604.

38. Wang, S.-S. *J. Am. Chem. Soc.* **1973**, *95*, 1328.

39. Coste, J.; Frerot, E.; Jouin, P. *J. Org. Chem.* **1994**, *59*, 2437.

40. Dormoy, J.; Castro, B. *Tetrahedron Lett.* **1979**, *35*, 3321.

41. Department of Molecular Medicine, Northwest Hospital, Seattle, WA.

42. Hunter, T.; Pines, J. *Cell* **1994**, *79*, 573.

43. Rice, R. L.; Wipf, P.; Cunningham, A.; Lazo, J. S. *Proc. Am. Assoc. Cancer Res.* **1996**, *37*, 2896.

44. Ishida, Y.; Furukawa, Y.; Decaprio, J. A.; Saito, M.; Griffin, J. D. *J. Cell. Physiol.* **1992**, *150*, 484.

45. Jinno, S.; Suto, K.; Nagata, A.; Igarashi, M.; Kanaoka, Y.; Nojima, H.; Okayama, H. *EMBO J.* **1994**, *13*, 1549.

46. Lazo, J. S.; Kondo, Y.; Dellapiazza, D.; Michalska, A. E.; Choo, K. H.; Pitt, B.R. *J. Biol. Chem.* **1995**, *270*, 5506.

(*Received in U.S.A.* 2 *February* 1996; *accepted* 31 *May* 1996)

A Targeted Library of Small-Molecule, Tyrosine, and Dual-Specificity Phosphatase Inhibitors Derived from a Rational Core Design and Random Side Chain Variation

Robert L. Rice, James M. Rusnak, Fumiaki Yokokawa, Shiho Yokokawa, Donald J. Messner, Alton L. Boynton, Peter Wipf, and John S. Lazo

Departments of Pharmacology and Chemistry, University of Pittsburgh, Pittsburgh, Pennsylvania 15261, and Department of Molecular Medicine, Northwest Hospital, Seattle, Washington 98125

Biochemistry®

Reprinted from
Volume 36, Number 50, Pages 15965–15974

A Targeted Library of Small-Molecule, Tyrosine, and Dual-Specificity Phosphatase Inhibitors Derived from a Rational Core Design and Random Side Chain Variation†

Robert L. Rice,‡ James M. Rusnak,‡ Fumiaki Yokokawa,§ Shiho Yokokawa,§ Donald J. Messner,∥ Alton L. Boynton,∥ Peter Wipf,§ and John S. Lazo*,‡

Departments of Pharmacology and Chemistry, University of Pittsburgh, Pittsburgh, Pennsylvania 15261, and Department of Molecular Medicine, Northwest Hospital, Seattle, Washington 98125

Received June 5, 1997; Revised Manuscript Received August 25, 1997®

ABSTRACT: Tyrosine phosphatases (PTPases) dephosphorylate phosphotyrosines while dual-specificity phosphatases (DSPases) dephosphorylate contiguous and semicontiguous phosphothreonine and phosphotyrosine on cyclin dependent kinases and mitogen-activated protein kinases. Consequently, PTPases and DSPases have a central role controlling signal transduction and cell cycle progression. Currently, there are few readily available potent inhibitors of PTPases or DSPases other than vanadate. Using a pharmacophore modeled on natural product inhibitors of phosphothreonine phosphatases, we generated a refined library of novel, phosphate-free, small-molecule compounds synthesized by a parallel, solid-phase combinatorial-based approach. Among the initial 18 members of this targeted diversity library, we identified several inhibitors of DSPases: Cdc25A, -B, and -C and the PTPase PTP1B. These compounds at 100 μM did not significantly inhibit the protein serine/threonine phosphatases PP1 and PP2A. Kinetic studies with two members of this library indicated competitive inhibition for Cdc25 DSPases and noncompetitive inhibition for PTP1B. Compound AC-$\alpha\alpha$69 had a K_i of approximately 10 μM for recombinant human Cdc25A, -B, and -C, and a K_i of 0.85 μM for the PTP1B. The marked differences in Cdc25 inhibition as compared to PTP1B inhibition seen with relatively modest chemical modifications in the modular side chains demonstrate the structurally demanding nature of the DSPase catalytic site distinct from the PTPase catalytic site. These results represent the first fundamental advance toward a readily modifiable pharmacophore for synthetic PTPase and DSPase inhibitors and illustrate the significant potential of a combinatorial-based strategy that supplements the rational design of a core structure by a randomized variation of peripheral substituents.

Reversible covalent modification of proteins by the addition and removal of phosphate residues dominates as the method used by mammalian cells in intracellular signaling. A complex cascade of interrelated protein kinases and protein phosphatases dynamically regulate intracellular protein phosphorylation. Two broad families of eukaryotic protein phosphatases have been defined: protein serine/threonine phosphatases (PSTPase)[1] and protein tyrosine phosphatases (PTPase). More recently a subfamily of PTPases, the dual-specificity phosphatases (DSPase), has been identified, which dephosphorylate tyrosine and threonine residues on the same substrate (*1*). Two major members of the DSPase family are the Cdc25 phosphatases, which dephosphorylate a contiguous TY motif, and the mitogen-activated protein kinase (MAPK) phosphatases, which dephosphorylate a semicontiguous TXY, where X is G, P, or E.

Investigation of the biological role of PSTPases has been greatly facilitated by the discovery of natural low-molecular weight enzyme inhibitors. Okadaic acid, a polyether fatty acid produced by a marine dinoflagellate, was the first broadly characterized PSTPase inhibitor, and more recently other natural products, such as microcystins and calyculin A, also have been found to be excellent active site inhibitors (*2*−*5*). These potent PSTPase inhibitors are widely used to decipher intracellular signal transduction pathways, but all have limitations such as poor cell permeability, chemical instability, and finite supply. Moreover, the known PSTPase inhibitors also have restricted PSTPase isotype specificity and have little, if any, activity toward PTPases. Studies of the intracellular function of PTPases and particularly DSPases have been severely hampered by the lack of potent inhibitors. Vanadate, which has been widely used as an inhibitor of both PTPases and DSPases, is one of the few

† This work was supported in part by Army Breast Cancer Predoctoral Research Fellowship DAMD17-94-J4193, the Fiske Drug Discovery Fund, and USPHS NIH Grants CA 61299, CA 39745, CA 53861, and AI 34914.

* Address correspondence to this author at Department of Pharmacology, Biomedical Science Tower E-1340, University of Pittsburgh, Pittsburgh, PA 15261. Telephone: (412) 648-9319. Fax: (412) 648-2229. E-mail: lazo@pop.pitt.edu.

‡ Department of Pharmacology, University of Pittsburgh.

§ Department of Chemistry, University of Pittsburgh.

∥ Northwest Hospital.

® Abstract published in *Advance ACS Abstracts,* December 1, 1997.

[1] Abbreviations: AEBSF, 4-(2-aminoethyl)benzenesulfonyl fluoride; BopCl, bis(2-oxo-3-oxazolidinyl)phosphinic chloride; DPPA, diphenylphosphoryl azide; DSPases, dual-specificity phosphatases; DTT, DL-dithiothreitol; FDP, 3,6-fluorescein diphosphate; GST, glutathione-S-transferase; IC_{50}, half-maximal inhibitory concentration; IPTG, isopropyl β-D-thiogalactopyranoside; MAPK, mitogen-activated protein kinase; MAPKP, mitogen-activated protein kinase phosphatase; pNPP, *para*-nitrophenyl phosphate; SC, solution chemistry; PSTPases, protein serine/threonine phosphatases; PTPases, protein tyrosine phosphatases.

S0006-2960(97)01338-X CCC: $14.00

inhibitors readily available (*6*−*9*). For several DSPases, namely Cdc25A and -B, the endogenous substrates are not known. The natural products dnacin, dysidiolide, and a RK-682 analogue appear to inhibit Cdc25 DSPases (*9*−*11*), but there is little information on the nature of their inhibition, their selectivity, or their cell permeability, and, as they are natural products, limited supplies restrict their widespread use. The best reported inhibitor of PTPase is a competitive cyclic peptide inhibitor with a K_i of 0.73 μM that has the disadvantages associated with a peptide inhibitor (*12*). Thus, good artificial inhibitors would facilitate analyses of the biological role of PTPases and DSPases.

Although some investigators have reported structural similarities between the PSTPases and DSPases (*13*), recent thoughtful analyses of the active site structures of protein phosphatases (*1, 14, 15*) suggest that sufficient differences exist among the protein phosphatase classes to permit the identification of selective inhibitors. Thus, we have begun to devise strategies to generate selective, small-molecule, active site inhibitors of protein phosphatases. We purposefully focused on small molecules and excluded phosphates in our design to enhance the likelihood that the resulting compounds would enter cells. In our initial attempt to generate PSTPase isotype selective inhibitors, a core moiety for phosphatase inhibition was chosen based on the readily available structure−activity relationship profile for natural product PSTPase inhibitors (*16, 17*). To complement this design, we adapted a combinatorial synthetic approach for the random variation of substituents to ensure chemical diversity and maximum flexibility. We synthesized an initial library on solid support to establish the overall synthetic approach and documented that at least one member of the library retained some ability to inhibit the PSTPase PP2A (*17*). In the current study we have markedly extended our analysis to include the entire library and a significant number of protein phosphatases, namely, the PSTPases PP1 and PP2A, the DSPases Cdc25A, Cdc25B, Cdc25C, and CL100, and the PTPase PTP1B. Surprisingly, among the initial 18 members of the targeted diversity library, we identified several competitive inhibitors of Cdc25 phosphatase and noncompetitive inhibitors of PTP1B that have little activity against the PSTPase PP1 and PP2A. These results represent the first fundamental advance toward identifying a readily modifiable pharmacophore for the design of nonelectrophilic, small-molecule PTPase and DSPase inhibitors. Moreover, the marked differences in Cdc25 inhibition as compared to PTP1B inhibition seen with relatively modest chemical modifications in modular side chains demonstrate the structurally demanding nature of the DSPase active site that was distinct from the PTP1B catalytic site.

MATERIALS AND METHODS

Chemical Compounds. The generation of the compounds in the combinatorial library has been previously described (*17*), although we have now adopted a new, more descriptive nomenclature for ease of discussion. The new nomenclature and the compound structures are listed in Figure 1 and Table 1. The basic combinatorial pharmacophore is now termed AC (Figure 1); addition of a phenyl moiety is termed α, a phenethyl is β, benzyl is δ, a styryl is γ, and alkyl chains are designated on the basis of the carbon length. Compounds were synthesized using solid bead combinatorial methods, and their predicted structural identity and purity (>60%) were

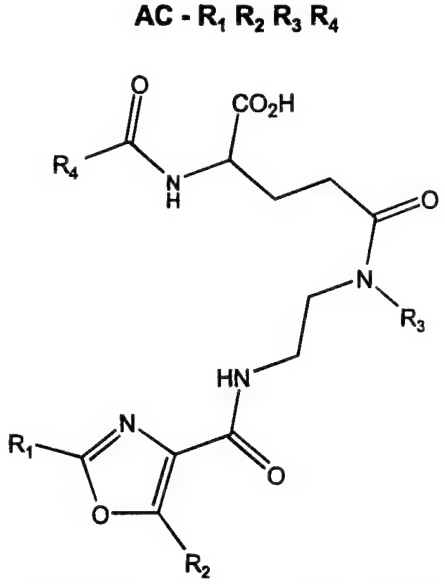

FIGURE 1: General chemical structure of pharmacophore.

Table 1

Compound	R_1	R_2	R_3	R_4
AC-α119	⬡	CH_3	CH_3	n-C_9H_{19}
AC-α169	⬡	CH_3	n-C_6H_{13}	n-C_9H_{19}
AC-α1δ9	⬡	CH_3	⬡	n-C_9H_{19}
AC-αα19	⬡	⬡	CH_3	n-C_9H_{19}
AC-αα69	⬡	⬡	n-C_6H_{13}	n-C_9H_{19}
AC-ααδ9	⬡	⬡	⬡	n-C_9H_{19}
AC-α11β	⬡	CH_3	CH_3	⬡
AC-α16β	⬡	CH_3	n-C_6H_{13}	⬡
AC-α1δβ	⬡	CH_3	⬡	⬡
AC-αα1β	⬡	⬡	CH_3	⬡
AC-αα6β	⬡	⬡	n-C_6H_{13}	⬡
AC-ααδβ	⬡	⬡	⬡	⬡
AC-α11γ	⬡	CH_3	CH_3	⬡
AC-α16γ	⬡	CH_3	n-C_6H_{13}	⬡
AC-α1δγ	⬡	CH_3	⬡	⬡
AC-αα1γ	⬡	⬡	CH_3	⬡
AC-αα6γ	⬡	⬡	n-C_6H_{13}	⬡
AC-ααδγ	⬡	⬡	⬡	⬡

confirmed by ^{1}H NMR and mass spectroscopy (*17*). Several discrete compounds, namely, AC-ααδ9 and AC-αα69, were synthesized using solution chemistry (SC) according to (*17*) and are referred to as SC compounds throughout this manuscript to differentiate them from compounds synthesized by solid bead-based combinatorial methods. For the resynthesis of these compounds, 2,2,2-trichlorethoxycarbonyl and allyloxycarbonyl protective groups were used, and amide coupling was effected with BopCl (*18*) and DPPA (*19*) coupling agents. We also synthesized for the first time SC-α109 and SC-αα09 for structural hypothesis testing and used the same procedure as mentioned above for SC-ααδ9 and SC-αα69. The SC compounds were >90% pure on the basis

of previously described ^{1}H NMR and mass spectroscopy methods (*17*). All compounds were resuspended for biological testing in DMSO as a stock solution of 10 mM and stored in the dark at −70 °C in aliquots for use in individual experiments. In contrast to the solid-phase library, which was enriched in the L-stereoisomers, the SC compounds were racemic.

Plasmids and Reagents. Plasmid pGEX2T for glutathione-*S*-transferase (GST) fusion of full-length human Cdc25A was a gift from Dr. Robert T. Abraham (Mayo Clinic, Rochester, MN), and the plasmids pGEX2T-KG and pGEX2T containing the GST fusion of full-length human Cdc25B and -C, respectively, were a gift from Dr. David Beach (Cold Spring Harbor Laboratory, Cold Spring Harbor, NY). The plasmid pET15b containing the histidine-tagged CL100 was a gift from Dr. Stephen M. Keyse (University of Dundee, Dundee, U.K.). The substrate 3,6-fluorescein diphosphate (FDP) was purchased from Molecular Probes Inc. (Eugene, OR), *para*-nitrophenyl phosphate (pNPP) was obtained from Sigma (St. Louis, MO), and Ni-NTA was purchased from Qiagen Inc (Chatsworth, CA). The inhibitory activity of SC-ααδ9 and SC-αα69 against PP1 and PP2A was measured with the phosphatase assay kit from Gibco-BRL (Grand Island, NY) using PP1 and PP2A catalytic units purified from rabbit skeletal muscle obtained from Upstate Biotechnology (Lake Placid, NY). Phosphorylase *b* was radiolabeled with Redivue [^{32}P]γATP, which was from Amersham (Arlington Heights, IL). Alkaline phosphatase from calf intestine was purchased from Promega (Madison, WI). Recombinant PTP1B was obtained from Upstate Biotechnology (Lake Placid, NY).

Bacterial Growth and Fusion Protein Production. Escherichia coli strain BL21 (DE3) was used for transfection with plasmids containing the fusion constructs encoding GST and Cdc25A, -B, or -C under the transcriptional control of isopropyl β-D-thiogalactopyranoside (IPTG). *E. coli* were first grown overnight at 37 °C in the presence of LB media with 100 μg/mL ampicillin. A 4 mL aliquot of this preculture was used to inoculate 1 L of LB containing 100 μg/mL of ampicillin. The cultures were incubated at 37 °C for 4−5 h. IPTG (1 mM final concentration) was then added, and the cultures were incubated at 37 °C for an additional 3 h. Cells were harvested by centrifugation at 3500*g* for 10 min at 4 °C. The resultant bacterial pellets were kept frozen at −80 °C until extraction. His_6-tagged CL100 was produced similarly except the *E. coli* strain DH5a was used in place of BL21 (DE3).

Purification of GST Fusion Proteins. The bacterial pellet was disrupted by sonication at 4 °C in lysis buffer containing 10 μg/mL of aprotinin, 10 μg/mL of leupeptin, 100 μg/mL of AEBSF, and 10 mM DTT. The homogenate was then centrifuged for 10 min at 4 °C at 10000*g*. The resulting supernatant fraction was immediately mixed and rotated with glutathione beads (equilibrated with lysis buffer) for 1 h at 4 °C (5 vol of supernatant/1 vol of 50% bead slurry). The glutathione beads were washed two times with 10 vol of lysis buffer and then twice with 10 vol of 2× reaction buffer (60 mM Tris, pH 8.5, 150 mM NaCl, 1.34 mM EDTA, 0.066% BSA) containing 10 μg/mL of aprotinin, 10 μg/mL of leupeptin, 100 μg/mL of AEBSF, and 10 mM DTT. The fusion protein was eluted with three successive washes using 10 mM glutathione in 2× reaction buffer. The efficiency of the elution was monitored by the phosphatase assay described below. Active fractions were pooled and supplemented with 20% glycerol prior to storage at −80 °C. His_6-tagged CL100 was purified using the same procedure except 20 mM β-mercaptoethanol was used in place of DTT for all steps of the purification and 100 mM imidazole was used instead of 10 mM glutathione for the elution.

Serine/Threonine Phosphatase Assay. The catalytic subunits of PP1 and PP2A were purified from oysters and phosphatase activity was determined with a radiolabeled phosphohistone substrate (histone HI) was determine by the liberation of ^{32}P using previously described procedures (*20, 21*). Briefly, assays were conducted in a final volume of 80 μL containing 50 mM Tris buffer (pH 7.4), 0.5 mM DTT, 1 mM EDTA (assay buffer), phosphohistone (1−2 μM PO_4), and the catalytic subunits of either PP1 or PP2A. Okadaic acid (1 nM) was included in some PP1 preparations to suppress endogenous PP2A activity and had no apparent affect on the inhibitory activity of the compounds tested. Dephosphorylation of ^{32}P-labeled histone was determined after a 10−20 min incubation with or without 100 μM combinatorial compounds by extraction as a phosphomolybdate complex as described previously (*20, 21*). The reaction was directly dependent on enzyme concentration and time under these conditions. The inhibitory activity of SC-ααδ9 and SC-αα69 against PP1 and PP2A was also measured with rabbit skeletal muscle PP1 and PP2A and ^{32}P-labeled phosphorylase A as a substrate by the commercially available method of Gibco-BRL.

PTPase and Dual-Specificity Phosphatase Assay. The activity of the GST fusion or His_6-tagged DSPase and PTPase was measured with FDP (Molecular Probes, Inc., Eugene, OR), which is readily metabolized to the fluorescent fluorescein monophosphate (*7*), as a substrate in a 96-well microtiter plates. The final incubation mixture (150 μL) comprised 30 mM Tris (pH 8.5), 75 mM NaCl, 0.67 mM EDTA, 0.033% bovine serum albumin, 1 mM DTT, and 20 μM FDP for Cdc25 phosphatases. The same final incubation mixture was used for CL100 and PTP1B, with the appropriate pH optimum, namely, pH 7.0 and 7.5, respectively. Inhibitors were resuspended in DMSO, and all reactions including controls were performed at a final concentration of 7% DMSO. Reactions were initiated by adding ∼0.25 μg of fusion protein and incubated at ambient temperature for 1 h for Cdc25 and CL100 phosphatase and 30 min for PTP1B. Fluorescence emission from the product was measured with a multiwell plate reader (Perseptive Biosystems Cytofluor II, Framingham, MA; excitation filter, 485/20; emission filter, 530/30). For all enzymes the reaction was linear over 2 h of incubation, well within the time used in the experiments, and was directly proportional to both the enzyme and substrate concentration.

Alkaline Phosphatase Assay. The activity of alkaline phosphatase was measured in a 96-well microtiter plate with FDP (Molecular Probes, Inc., Eugene, OR) as a substrate, which was readily metabolized to the fluorescent fluorescein monophosphate (*7*). The final incubation mixture (150 μL) contained 30 mM Tris (pH 7.3), 75 mM NaCl, 0.67 mM EDTA, 0.033% bovine serum albumin, 1 mM DTT, and 1 μM FDP (∼K_m). Inhibitors were resuspended in DMSO, and all reactions including controls were performed at a final concentration of 7% DMSO. Reactions were initiated by adding ∼0.1 unit of alkaline phosphatase and incubated at ambient temperature for 5 min. Fluorescence emission from the product was measured with a multiwell plate reader (Perseptive Biosystems Cytofluor II, Framingham, MA;

excitation filter, 485/20; emission filter, 530/30). For all enzymes the reaction was linear over the time of incubation and directly proportional to both the enzyme and substrate concentration.

Thin-Layer Chromatography. To ensure that only a single product was produced with the FDP substrate, we incubated FDP and phosphatases under our standard reaction conditions for 0.5 to 1 h and spotted 2.5 μL of the reaction from each microtiter plate well on a Whatman reversed phase TLC LKC_{18} plate. The resolving conditions were room temperature and a methanol/water (3:2 vol) solvent. Compounds and products were viewed under long UV wavelength (366 nm) to illuminate the potential fluorescein monophosphate and fluorescein product. FDP has no fluorescent intensity at this wavelength. The R_f values for fluorescein monophosphate and fluorescein were 0.9 and 0.8, respectively. We found that only the fluorescein monophosphate was produced under our reaction conditions with the PTPase and DSPases used. Thus, despite the ability of Cdc25 to dephosphorylate fluorescein monophosphate (*22*), under the reaction conditions used the diphosphate fluorescein was the preferred substrate as previously suggested (*13*).

Steady-State Kinetics. Reactions with GST-Cdc25A, -B, and -C were conducted in 30 mM Tris (pH 8.5), 75 mM NaCl, 0.67 mM EDTA, 0.033% bovine serum albumin, and 1 mM DTT. Reactions with CL100 were conducted in 30 mM Tris (pH 7.0), 75 mM NaCl, 0.67 mM EDTA, 0.033% BSA, 1 mM DTT, and 20 mM imidazole. Reactions with GST-PTP1B were conducted in 30 mM Tris (pH 7.5), 75 mM NaCl, 0.67 mM EDTA, 0.033% bovine serum albumin, and 1 mM DTT. DMSO was kept at 7% in reaction mixtures to ensure compound solubility. All reactions were carried out at room temperature, and product formation was determined in an multiwell plate reader (Perseptive Biosystems Cytofluor II, Framingham, MA; excitation filter, 485/20; emission filter, 530/30). Data were collected at 10 min intervals for 1 h for Cdc25 and CL100 phosphatases and 30 min for PTP1B. The V_0 was determined for each substrate concentration and then fit to the Michaelis−Menten equation (eq 1):

$$V_o = V_{max}[S]/(K_m + [S]) \quad (1)$$

using Prism 2.01 (GraphPad Software Inc.). The correlation coefficient for each experiment and substrate concentration was always >0.9. The substrate concentrations used to determine the steady-state kinetics for Cdc25A, -B, and -C were 10, 20, 30, 40, 50, 75, 100, and 200 mM FDP; for CL100 the concentrations were 75, 100, 200, 300, 400, 500, and 750 μM FDP; and for PTP1B the concentrations were 1, 5, 10, 25, 50, 75, 100, 150 μM FDP.

Determination of Inhibition Constant. The inhibition constants for SC-ααδ9 and SC-αα69 were determined for the Cdc25A, -B, and -C, CL100, and PTP1B hydrolysis of FDP. At various fixed concentrations of inhibitor, the initial rates with different concentrations of FDP were measured. The data were then fit to eq 2 to obtain the inhibition constant (K_i) for the competitive model or eq 3 for the noncompetitive model.

$$V_o = V_{max}[S]/(K_m(1 + [I]/K_i) + [S]) \quad (2)$$

$$V_o = V_{max}[S]/((K_m + [S])(1 + [I]/K_i)) \quad (3)$$

Table 2: Percent Inhibition of PSTPase Activity with 100 μM Combinatorial Compound[a]

	PP1		PP2A	
compound	mean	SEM	mean	SEM
AC-α119	0	0	0	0
AC-α169	4	10	14	15
AC-α1δ9	11	3	33	13
AC-αα19	0	0	0	0
AC-αα69	0	0	0	0
AC-ααδ9	9	7	5	11
AC-α11β	12	6	15	11
AC-α16β	11	5	31	10
AC-α1$\delta\beta$	13	1	48	8
AC-αα1β	22	2	20	4
AC-αα6β	1	19	32	21
AC-αα$\delta\beta$	32	5	47	6
AC-α11γ	11	4	13	4
AC-α16γ	27	9	23	2
AC-α1$\delta\gamma$	25	3	35	4
AC-αα1γ	27	5	8	11
AC-αα6γ	17	9	40	9
AC-αα$\delta\gamma$	24	9	46	8

[a] Each value is the percent inhibition from untreated control and the mean from three independent determinations.

At least four concentrations of SC-ααδ9 and SC-αα69 ranging from 0 to 30 μM were used with Cdc25A or -B. The K_i of Cdc25C was calculated using at least 4 concentrations of drugs that ranged from 0 to 100 μM of SC-αα69 and SC-ααδ9. At least four concentrations of SC-ααδ9 and SC-αα69 ranging from 0 to 3 μM were used with PTP1B. The K_i of CL100 was determined using three different concentrations of SC-ααδ9: 30, 100, and 300 μM.

RESULTS AND DISCUSSION

Phosphatase Inhibition by Solid Phase-Derived Compounds. All members of the current library contained a phenyl substituent on the oxazole C_2 (i.e., R_1) (Table 1). Because the fundamental pharmacophore was based on the PSTPase inhibitors calyculin A, microcystins, and okadaic acid, we initially examined the library for its ability to disrupt two established PSTPases. One-third of the library members completely failed to inhibit PP1 at 100 μM (Table 2) while more than two-thirds of the library members inhibited PTP1B with >50% inhibition at 100 μM (Table 4). Several compounds demonstrated >40% inhibition of PTP1B at 3 μM. Only modest inhibition of PP1 was observed with most library compounds and the maximum reduction in PP1 activity of 32% was seen with AC-αα$\delta\beta$, which interestingly was the one compound that failed to inhibit PTP1B at 100 μM (Table 4). We found at 100 μM approximately one-third of the library members caused >30% inhibition of PP2A with AC-α1$\delta\beta$, AC-αα$\delta\beta$, and AC-αα$\delta\gamma$, causing ~50% inhibition. Although in our preliminary analyses we observed AC-αα19 caused an approximate 50% inhibition of enzyme activity with the PP2A catalytic subunit from bovine cardiac muscle (*17*), we found no significant inhibition of oyster PP1 or PP2A (Table 2). Okadaic acid (100 μM) and calyculin A (10 nM) were highly effective in our assay and caused >99% inhibition of PP1 or PP2A activity (data not shown). Although no compound at 100 μM produced >60% inhibition of PP1 or PP2A (Table 2), a preference for compounds with aromatic substituents on R_3 and R_4 emerged for these PSTPases.

Table 3: Percent Inhibition of DSPase Activity with 100 μM Combinatorial Compound[a]

	Cdc25												MAPKP			
	Cdc25 A				Cdc25 B				Cdc25 C				CL100			
	exp. 1		exp. 2		exp. 1		exp. 2		exp. 1		exp. 2		exp. 1		exp. 2	
compound	mean	SEM	mean	SEM	mean	SEM	mean	SEM	mean	SEM	mean	SEM	mean	SEM	mean	SEM
AC-α119	35	3	30	1	0	0	0	0	6	3	0	0	10	3	5	6
AC-α169	86	2	86	2	53	1	60	1	11	1	28	1	16	4	21	5
AC-α1δ9	90	1	88	3	55	1	60	2	44	2	35	5	19	3	0	0
AC-αα19	0	0	3	2	9	2	8	1	33	2	21	2	0	0	18	6
AC-αα69	95	4	92	3	82	1	84	2	64	3	56	1	26	4	27	6
AC-ααδ9	97	2	97	1	84	1	87	5	56	3	60	2	0	0	12	10
AC-α11β	48	3	52	5	42	10	0	0	18	1	2	1	0	0	0	0
AC-α16β	70	2	58	4	44	4	18	3	17	2	14	2	0	0	0	0
AC-α1δβ	77	2	62	2	35	1	38	1	21	8	28	2	0	0	0	0
AC-αα1β	0	0	0	0	9	1	11	6	46	2	31	1	0	0	0	0
AC-αα6β	20	4	15	2	24	1	24	2	27	4	40	4	0	0	4	6
AC-ααδβ	48	1	29	1	30	2	32	3	57	5	51	2	0	0	0	0
AC-α11γ	85	4	77	1	53	1	57	1	54	1	52	2	0	0	0	0
AC-α16γ	78	5	64	1	34	1	34	3	30	2	33	1	0	0	0	0
AC-α1δγ	76	3	55	1	34	1	34	3	37	4	36	1	0	0	0	0
AC-αα1γ	31	3	27	4	7	5	20	3	48	2	51	2	0	0	4	6
AC-αα6γ	48	2	43	2	46	3	29	2	52	6	51	1	25	5	21	1
AC-ααδγ	73	2	43	3	57	3	31	6	66	3	56	3	0	0	0	0

[a] Each value is the percent inhibition from untreated control and the mean from an experiment done in triplicate.

Table 4: Percent Inhibition of PTPase Activity with Combinatorial Compound[a]

	3 μM		100 μM	
compound	mean	SEM	mean	SEM
AC-α119	0	0	32	7
AC-α169	15	6	77	7
AC-α1δ9	48	3	85	9
AC-αα19	3	7	38	10
AC-αα69	37	9	91	13
AC-ααδ9	40	2	92	3
AC-α11β	43	12	91	5
AC-α16β	50	7	61	14
AC-α1δβ	5	7	59	7
AC-αα1β	41	26	50	8
AC-αα6β	35	24	63	13
AC-ααδβ	3	10	1	16
AC-α11γ	0	0	45	3
AC-α16γ	38	3	74	8
AC-α1δγ	5	7	80	9
AC-αα1γ	41	26	52	7
AC-αα6γ	42	7	48	13
AC-ααδγ	42	7	79	12

[a] Each value is the percent inhibition from untreated control and the mean from at least three independent determinations.

Several library members also appeared to inhibit DSPases significantly at 100 μM (Table 3). Thus, AC-ααδ9 and AC-αα69 caused >90% inhibition of Cdc25A, AC-α169, AC-α1δ9, and AC-α11γ caused >80% inhibition of Cdc25A, while other compounds, such as AC-αα1β and AC-αα19, had no effect (Table 3). Minor structural modifications of the platform produced marked changes in inhibitory ability consistent with the concept of a restrictive catalytic site in Cdc25 as compared to the PTPase PTP1B. It was noteworthy, however, that the modification pattern for Cdc25 (Table 3) was distinct from that for PTP1B (Table 4).

In general, modification of the R_2 position produced minor changes with no obvious overall preference for phenyl versus methyl among the congeners for Cdc25 phosphatases. The best inhibitors of this series for Cdc25 phosphatases were found when both R_3 and R_4 contained hydrophobic moieties, such as aromatic or extended alkyl species. AC-αα69 and AC-αα6γ produced a modest (<30%) inhibition of CL100 activity at 100 μM, but all of the other members of the refined combinatorial library had little or no effect on this MAPK DSPase. Thus several compounds, such as AC-ααδ9, appeared to have some selectivity for the PTP1B PTPase and Cdc25 DSPases compared to either the MPKP DSPase CL100 or PSTPases.

Concentration Dependent Inhibition with Solid-Phase-Derived and SC Compounds. Analyses of combinatorial library elements required resynthesis of the predicted discrete compound with promising biochemical effects to ensure the inhibitory activity was not associated with a side reactant or contaminants (*23*). To investigate more extensively the inhibitory potential of the most active compounds against Cdc25, we next synthesized AC-ααδ9 and AC-αα69 by solution chemistry methods. As illustrated in Figure 2A–D, both solid-phase-derived AC-ααδ9 and solution phase derived SC-ααδ9 demonstrated a marked concentration-dependent inhibition of recombinant human Cdc25A and B activity. We observed a half-maximal inhibitory concentration (IC_{50}) of 75 μM for Cdc25A and -B when treated with AC-ααδ9, while SC-ααδ9 showed an IC_{50} of approximately 15 μM for Cdc25A and -B (Figure 2A and C). Thus, the SC compounds displayed a 5-fold greater inhibitory activity compared to the solid phase derived compounds, which could reflect the increased purity, the inclusion of *R* stereoisomers in the racemic SC compounds, or both. Similarly, both AC-αα69 and SC-αα69 samples caused a concentration-dependent inhibition of Cdc25A and -B with the racemic SC compound being approximately 5–6-fold more potent (Figure 2B and D). The widely used PTPase inhibitor vanadate had an IC_{50} of 1 μM for Cdc25A and -B in this assay. To ensure that SC-ααδ9 and SC-αα69 did not also gain significant activity against PSTPases, we tested these compounds against oyster (data not shown) and rabbit skeletal muscle (Figure 3) PP1 and PP2A catalytic subunit and observed no inhibition at 100 μM. We have seen no inhibition of calf intestine alkaline phosphatase activity with 100 μM of any of the combinatorial library members or with

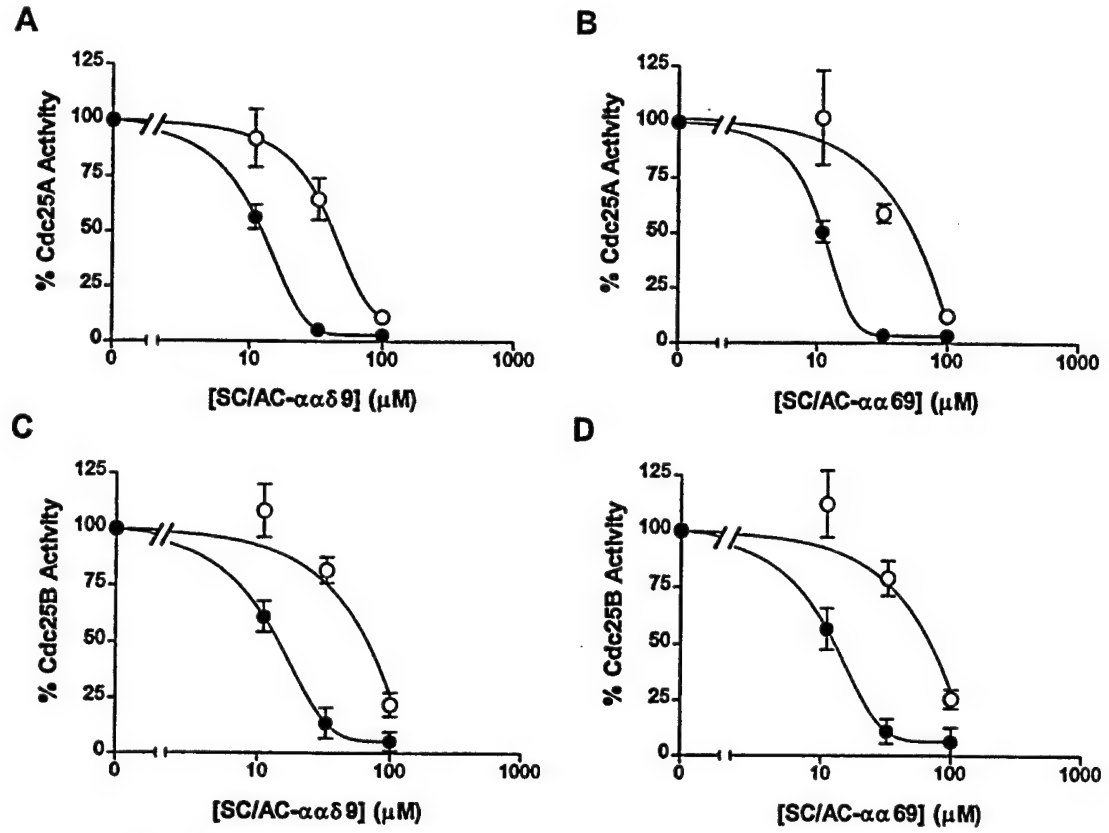

FIGURE 2: Concentration-dependent inhibition of Cdc25A and -B phosphatase by AC-αaδ9, SC-αaδ9, AC-αa69, and SC-αa69. Compounds AC-αaδ9 and AC-αa69 are indicated by open symbols and compounds SC-αaδ9 and SC-αa69 by closed symbols. (A) Inhibition of recombinant human Cdc25A phosphatase activity by SC-αaδ9 and AC-αaδ9. (B) Inhibition of recombinant human Cdc25A phosphatase activity by SC-αa69 and AC-αa69. (C) Inhibition of recombinant human Cdc25B phosphatase activity by SC-αaδ9 and AC-αaδ9. (D) Inhibition of recombinant human Cdc25B phosphatase activity by SC-αa69 and AC-αa69; $N = 3$; bar = SEM. Enzymatic activities were determined as outlined in Material and Methods and fit by the curve fitting program in Prism 2.01.

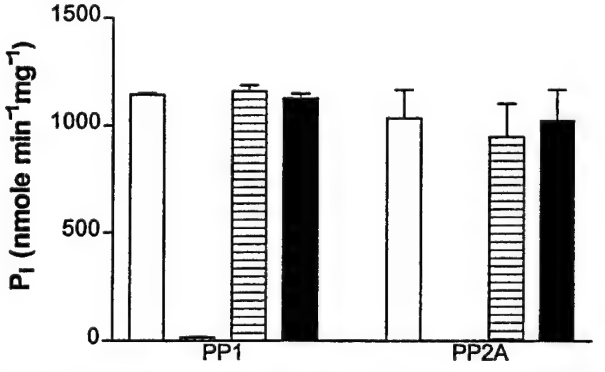

FIGURE 3: Inhibition of PP1 and PP2A by 100 μM SC-αaδ9 and SC-αa69. Controls are shown with open bars, cross-hatched bars represent 10 nM calyculin A treatment, and compounds SC-αa69 and SC-αaδ9 are indicated by horizontal and filled striped bars, respectively; $N = 3$; bar = SEM. Enzymatic activities were determined as outlined in the Material and Methods with rabbit skeletal muscle catalytic subunits.

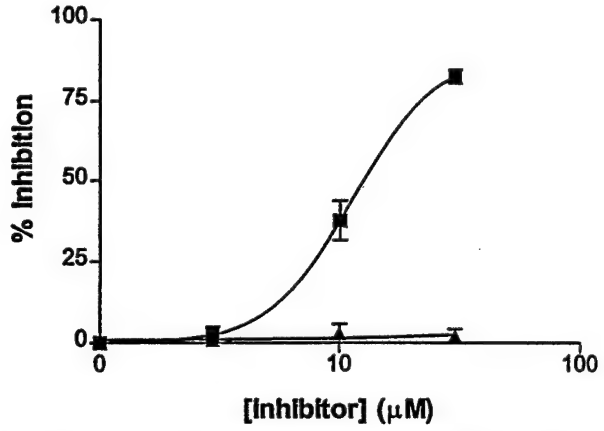

FIGURE 4: Effect of okadaic acid and SC-αaδ9 on Cdc25B phosphatase activity. Various concentrations of okadaic acid (▲) and SC-αaδ9 (■) were incubated with recombinant human Cdc25B as described in Material and Methods. The resulting data were fitted to the curve by Prism 2.01; $N = 3$; bar = SEM.

SC-αaδ9 or SC-αa69 (data not shown). Additionally, LeClerc and Meijer (personal communication) also found no inhibition of Cdc2 kinase activity as measure by their previously assay (*24*) with up to 100 μM SC-αaδ9. Furthermore, okadaic acid, a parent compound on which the pharmacophore platform was based, did not inhibit Cdc25B (Figure 4), demonstrating that the activity was not inherent in the parent compounds. To ensure that the inhibition was not dependent on the FDP substrate, we have also used pNPP as a substrate for Cdc25A and found marked inhibition with SC-αaδ9, although pNPP was a much poorer substrate than FDP (data not shown). These results confirm and extend studies of Gottlin et al. (*22*) indicating the aromatic substrate 3-*O*-methylfluorescein binds with higher affinity and reacts faster with Cdc25B than pNPP. In separate studies, LeClerc and Meijer (personal communication) have observed an IC_{50} of 4 μM with SC-αaδ9 and human recombinant Cdc25A using pNPP and their previously described method (*24*). Thus, the results with the solution phase compounds validated the initial observations with the combinatorial library.

Inhibition Kinetics of Compounds. We next determined the kinetic characteristics of DSPase and PTPase inhibition

Table 5: K_m and K_i of SC-ααδ9 and SC-αα69 for DSPases and PTPases

	K_m (μM)		K_i for SC-ααδ9 (μM)		K_i for SC-αα69 (μM)	
compound[a]	average	SEM	average	SEM	average	SEM
Cdc25A	45	3	9	2	8	3
Cdc25B	12	3	6	2	7	3
Cdc25C	22	1	11	3	11	2
CL100	192	72	229	115	ND[b]	ND
PTP1B	21	9	1.2	0.2	0.85	0.06

[a] $n = 3-10$ independent experiments. [b] ND, not determined.

with SC-ααδ9 and SC-αα69. We found the K_m with FDP for Cdc25A, Cdc25B, Cdc25C, CL100, and PTP1B were 45 ± 3 (SEM, $N =$ at least 4), 12 ± 3, 22 ± 1, 192 ± 72 and 21 ± 9 μM, respectively (Table 5). Therefore, FDP was a much better substrate for Cdc25 and PTP1B phosphatases than for the MAPK phosphatase CL100. Kinetic studies using SC-ααδ9 and SC-αα69 with Cdc25B were most consistent with a competitive inhibition model (Figure 5) while for PTP1B noncompetitive inhibition was the best model (Figure 6). We also concluded SC-ααδ9 competitively inhibits Cdc25A, Cdc25C and CL100 (data not shown) and SC-αα69 competitively inhibits Cdc25A and Cdc25C (data not shown). SC-αα69 had a K_i of 7 ± 3 μM for Cdc25B phosphatase and a K_i of 0.85 ± 0.06 μM for PTP1B (Table 5). The K_i for Cdc25A and Cdc25C were 8 ± 3 μM and 11 ± 2 μM, respectively (Table 5). The K_i for SC-ααδ9 for the MAPK phosphatase CL100 was 229 ± 115 μM. We have not yet determined the K_i for SC-αα69 and CL100.

On the basis of our initial studies with the library, we predicted that substitution of sterically enriched, hydrophobic moieties on this platform was critical for an efficient inhibitor of Cdc25 and PTP1B. To assess the relative importance of the bulky hydrophobic substitutents on the R_3 position, we synthesized two close congeners of SC-ααδ9 and SC-α1δ9, namely, SC-αα09 and SC-α109 (Figure 7A). SC-αα09 had markedly less inhibitory activity at 100 μM compared to SC-ααδ9, and SC-α109 also was less active than SC-α1δ9 (Figure 7B) indicating the importance of the bulky moiety in the R_3 position for Cdc25 phosphatase. SC-αα09 had the same strong inhibitory activity upon PTP1B as SC-ααδ9 demonstrating a bulky moiety at R_3 position was not critical for PTP1B inhibition (Figure 7C). Furthermore, both SC-αα09 and SC-ααδ9 produced similar inhibition of PTP1B of approximately 50% at 3 μM (data not shown).

Combinatorial chemistry provides a powerful new approach to diversify the structure of biologically active natural products (*23*). In this study we have developed a refined chemical scaffold for targeted combinatorial chemistry based on a predicted pharmacophore obtained from the structure activity relationship of several natural product inhibitors of PSTPases. Although the side chain composition and the size of the initial library are rather limited at this time, the

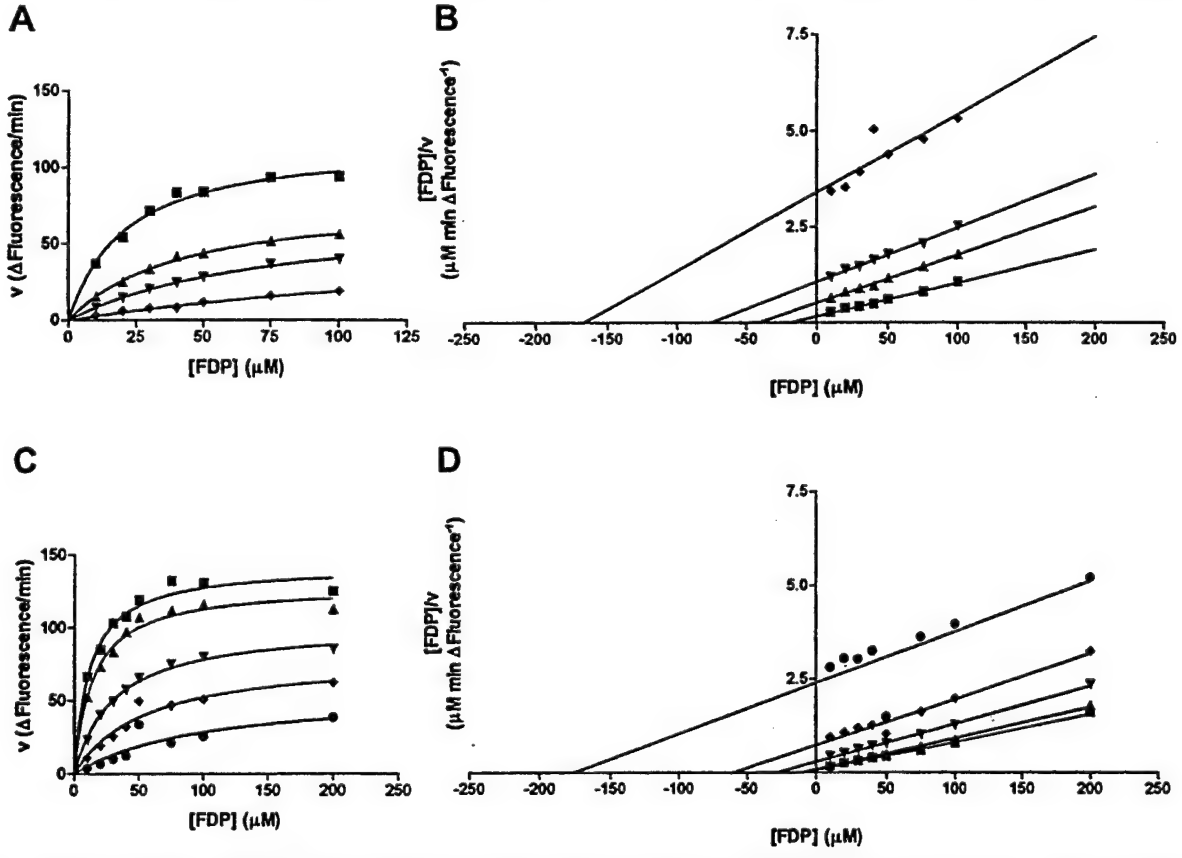

FIGURE 5: Kinetic analyses of Cdc25B inhibition by SC-ααδ9 and SC-αα69. (A, B) (■) 0 μM, (▲) 10 μM, (▼) 15 μM, and (◆) 30 μM inhibitor concentration. (C, D) (■) 0 μM, (▲) 3 μM, (▼) 10 μM, (◆) 15 μM, and (●) 30 μM inhibitor concentration. (A) Michaelis–Menten plot of Cdc25B inhibition by SC-ααδ9. (B) Hanes–Woolf plot of Cdc25B inhibition by SC-ααδ9. (C) Michaelis–Menten plot of Cdc25B inhibition by SC-αα69. (D) Hanes–Woolf plot of Cdc25B inhibition by SC-αα69; $N = 5$. Enzyme activities were determined as outlined in Materials and Methods, and the data were fit to the nonlinear Michaelis–Menten equation while all the data points were also fit simultaneously to the Hanes–Woolf equation for competitive inhibition for the Hanes–Woolf plot by the curve fitting program Prism 2.01. The values reported under Results for K_m and K_i were calculated from a nonlinear fit of the data to the Michaelis–Menten equation for competitive inhibition using the same program.

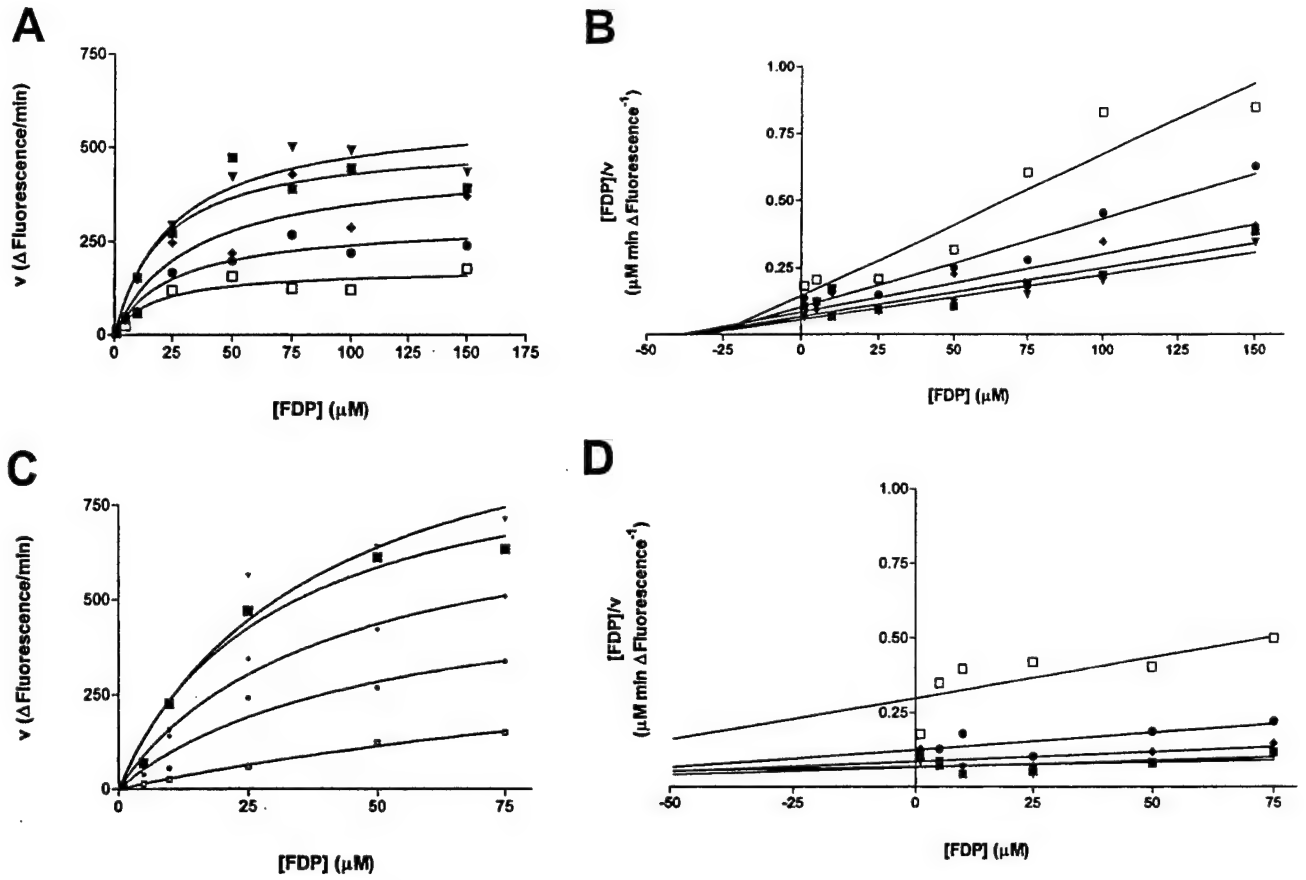

FIGURE 6: Kinetic analyses of PTP1B inhibition by SC-ααδ9 and SC-αα69. (A, B) (■) 0 μM, (▼) 0.1 mM, (◆) 0.3 μM, (●) 1 μM, and (□) 3 μM inhibitor concentration. (A) Michaelis–Menten plot of PTP1B inhibition by SC-ααδ9. (B) Hanes–Woolf plot of PTP1B inhibition by SC-ααδ9. (C) Michaelis–Menten plot of PTP1B inhibition by SC-αα69. (D) Hanes–Woolf plot of PTP1B inhibition by SC-αα69, $N = 4$. Enzyme activities were determined as outlined in Materials and Methods, and the data were fit to the nonlinear Michaelis–Menten equation while all the data points were also fit simultaneously to the Hanes–Woolf equation for competitive inhibition for the Hanes–Woolf plot by the curve fitting program Prism 2.01. The values reported under Results for K_m and K_i were calculated from a nonlinear fit of the data to the Michaelis–Menten equation for noncompetitive inhibition using the same program.

pharmacophore was readily functionalized and proved to be a most promising platform for future compound syntheses. It is noteworthy that none of the compounds in the library had highly efficacious inhibitory activity against PSTPases despite the use of a pharmacophore that owed its original design to natural product PSTPase inhibitors.

A detailed analysis of the structure–activity profile is limited by the relatively small library size; however, certain observations can be made concerning the inhibition of PSTPase, Cdc25 phosphatase and the PTPase PTP1B. Clearly the ability of some of the library compounds, such as AC-αα$\delta\beta$, to modestly inhibit both PP2A and Cdc25 phosphatases while having little effect on PTP1B indicates some overlapping inhibitor specificity between the PSTPases and Cdc25 enzyme. Nonetheless, distinct specificity emerged between PP2A phosphatase and the Cdc25 and PTP1B phosphatases, which might be expected considering the differences in the catalytic mechanisms in the broad PSTPase and PTPase families (*1*). The nonyl moiety has greater steric bulk and is more hydrophobic ($\log P > 4$) compared to either the phenethyl ($\log P = 3.15$) or styryl ($\log P = 2.95$) moieties. Substitution of the nonyl moiety at the R_4 site of a compound containing a phenyl at R_2 and a benzyl at R_3 (Figure 1) caused a significant increase in Cdc25 phosphatase inhibition and a complete loss of PSTPase inhibition as compared to the substitution of the phenethyl or styryl moiety at R_4. This may reflect a hydrophobic region on Cdc25 near the active site. Interestingly, Sodeoka et al. (*11*) found the hydrophobic side chain of RK-682 was important for the inhibitory activity against Cdc25 but not VHR. In contrast to Cdc25 phosphatases, the PSTPases were much less tolerant of bulky, hydrophobic substitutions at R_4 and none of the R_4 nonyl compounds were effective inhibitor of PP1 or PP2A while AC-α169 and AC-α1δ9 were respectable inhibitors of Cdc25A and -B and PTP1B phosphatase (Tables 3 and 4). In contrast to the inhibitory profile with Cdc25 phosphatases, AC-ααδ9 and AC-ααδγ reproducibly inhibited PTP1B equally well.

The identification of inhibitors that clearly prefer PTPases over PSTPases most likely reflects the lack of sequence similarity between these enzyme classes and the distinct fundamental catalytic mechanisms that exist between PSTPases and the enzyme superfamily of PTPases, which includes the DSPases (*1, 22, 25*). The crystal structure of the catalytic sites of prototype PSTPase, PTPases, and DSPases also suggests that they would accommodate different substrates and inhibitors consistent with previous biochemical studies (*1, 25, 26*). Consequently, the identification of inhibitors for the Cdc25 class of DSPase and the PTPase PTP1B is consistent with our current understanding of these phosphatases. Interestingly, these inhibitors were not very effective against the MAPK phosphatase class, which probably reflects the lack of common intervening amino acids in the critical HCXXXXXR active. Because

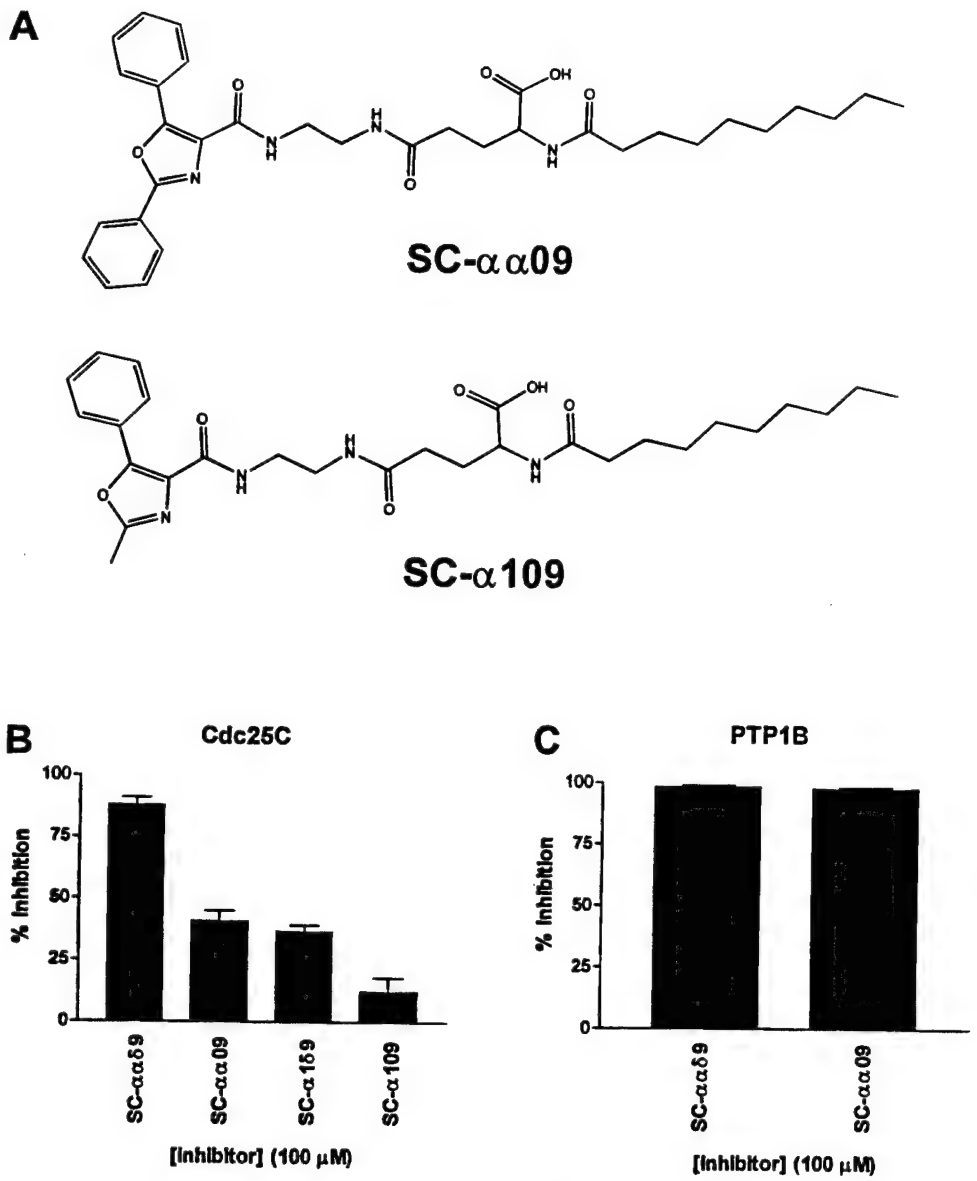

FIGURE 7: Chemical structure and inhibition of SC-αα09 and SC-α109. (A) Chemical structures of SC-αα09 and SC-α109. (B) Inhibition of Cdc25C phosphatase activity as described by the procedures in Materials and Methods. All values are expressed as a percent of vehicle control and the compound concentration was 100 μM; $N = 3$; bars = SEM. (C) Inhibition of PTP1B phosphatase activity as described by the procedures in the Materials and Methods. All values are expressed as a percent of vehicle control, and the compound concentration was 100 μM; $N = 3$; bars = SEM.

the catalytic regions of the Cdc25 enzymes, namely HCEF-SSER, are identical, the similar K_i values for Cdc25A, -B, or -C with SC-ααδ9 or SC-αα69 are not surprising.

In summary, we have identified a new class of small-molecule, competitive, inhibitors of human Cdc25 DSPases and noncompetitive inhibitors of PTP1B PTPase that are readily synthesized. Moreover, there is some evidence that PP2A and Cdc25 phosphatases have overlapping yet distinct inhibitor specificity. These compounds are small and have chemical structures unlike known PTP1B or Cdc25 inhibitors (*10, 11, 12, 27*). We previously demonstrated (*17*) that AC-ααδ9 caused a concentration-dependent inhibition of human breast cancer MDA-MB-21 cell proliferation and a G_1 cell cycle block consistent with intracellular entry. We are currently attempting to determine if these cellular effects are mediated by phosphatase inhibition. The pharmacophore used in our present studies should provide an excellent platform for future analog development. Our results illustrate the potential usefulness of this combinatorial-based approach in generating lead structures for selective inhibitors for phosphatases.

ACKNOWLEDGMENT

We are grateful for the constructive comments of Drs. Guillermo Romero and Andreas Vogt (University of Pittsburgh). We also thank Drs. LeClerc and Meijer (CNRS, Roscoff, France) for assaying our compounds, Dr. Stephen M. Keyse (University of Dundee, U.K.), Dr. Jehangir Mistry (Diagnostic Systems Labs, Webster, TX) for TLC advice, Dr. David Beach (Cold Spring Harbor Laboratories, NY), and Robert T. Abraham (Mayo Clinic) for reagents used in these studies, and Mark Stroud (Northwest Hospital) for his technical assistance with the PP1 and PP2A assay.

REFERENCES

1. Denu, J. M., Stuckey, J. A., Saper, M. A., and Dixon, J. E. (1996) *Cell 87*, 361−364.

2. Honkanen, R. E., Zwiller, J., Moore, R. E., Daily, S. L., Khatra, B. S., Dukelow, M., and Boynton, A. L. (1990) *J. Biol. Chem. 265*, 19401−19404.
3. Takai, A., Sasaki, K., Nagai, H., Mieskes, G., Isobe, M., Isono, K., and Yasumoto, T. (1995) *Biochem. J. 306*, 657−665.
4. Yoshizawa, S., Matsushima, R., Watanabe, M. F., Harada, K., Ichihara, A., Carmichael, W. W., and Fujiki, H. (1990) *J. Cancer Res. Clin. Oncol. 116*, 609−614.
5. MacKintosh, C., and Klumpp, S. (1990) *FEBS Lett. 277*, 137−140.
6. Keyse, S. M., and Emslie, E. A. (1992) *Nature 359*, 644−647.
7. Schmidt, A., Rutledge, S. J., Endo, N., Opas, E. E., Tanaka, H., Wesolowski, G., Leu, C. T., Huang, Z., Ramachandaran, C., Rodan, S. B., and Rodan, G. A. (1996) *Proc. Nat. Acad. Sci. U.S.A. 93*, 3068−3073.
8. Groom, L. A., Sneddon, A. A., Alessi, D. R., Dowd, S., and Keyse, S. M. (1996) *EMBO J. 15*, 3621−3632.
9. Horiguchi, T., Nishi, K., Hakoda, S., Tanida, S., Nagata, A., and Okayama, H. (1994) *Biochem. Pharmacol. 48*, 2139−2141.
10. Gunasekera, S. P., McCarthy, P. J., and Kelly-Borges, M. (1996) *J. Am. Chem. Soc. 118*, 8759−8760.
11. Sodeoka, M., Sampe, R., Kagamizono, T., and Osada, H. (1996) *Tetrahedron Lett. 37*, 8775−8778.
12. Akamatsu, M., Roller, P. P., Chen, L., Zhang, Z. Y., Ye, B. and Burke, T. R., Jr. (1997) *Bioorg. Med. Chem. 5*, 157−163.
13. Chen, L., Montserat, J., Lawrence, D. S., and Zhang, Z. Y. (1996) *Biochemistry 35*, 9349−9354.
14. Eckstein, J. W., Beer-Romero, P., and Berdo, I. (1996) *Protein Sci. 5*, 5−12.
15. Quinn, R. J., Taylor, C., Suganuma, M., and Fujiki, H. (1993) *Bioorg. Med. Chem. Lett. 3*, 1029−1034.
16. Bell, J. R., Ollivier, Emmanuelle, O., and Guerucci, M.-A. (1992) *Biol. Cell 75*, 139−142.
17. Wipf, P., Cunningham, A., Rice, R. L., and Lazo, J. S. (1997) *Bioorg. Med. Chem. 5*, 165−178.
18. Coste, J., Frerot, E., and Jouin, P. (1994) *J. Org. Chem. 59*, 2437−2446.
19. Shioiri, T., Ninomiya, K., and Yamada, S. (1972) *J. Am. Chem. Soc. 94*, 6203−6205.
20. Honkanen, R. E., Codispoti, B., Tse, K., and Boynton, A. L. (1994) *Toxicon 32*, 339−350.
21. Honkanen, R. E., Dukelow, M., Zwiller, J., Moore, R. E., Khatra, B. S., and Boynton, A. L. (1991) *Mol. Pharmacol. 40*, 577−583.
22. Gottlin, E. B., Xu, X., Epstein, D. M., Burke, S. P., Eckstein, J. W., Ballou, D. P., and Dixon, J. E. (1996) *J. Biol. Chem. 271*, 27445−27449.
23. Ellman, J., Stoddard, B., and Wells, J. (1997) *Proc. Natl. Acad. Sci. U.S.A. 94*, 2779−2782.
24. Baratte, B., Meijer, L., Galaktionov, K., and Beach, D. (1992) *Anticancer Res. 12*, 873−880.
25. Yuvaniyama, J., Denu, J. M., Dixon, J. E., and Saper, M. A. (1996) *Science 272*, 1328−133.
26. Draetta, G., and Eckstein, J. (1997) *Biochem. Biophys. Acta 1332*, M53−M63.
27. Watanabe, T., Takeuchi, T., Otsuka, M., Tanaka, S. I., and Umezawa, K. (1995) *J. Antibiotics 48*, 1460−1466.

BI971338H

J. Pharmacol. Exper. Therap.
In Press

Disruption of IGF-1 signaling and downregulation of Cdc2 by SC-ααδ9, a novel small molecule antisignaling agent identified in a targeted array library

Andreas Vogt, Robert L. Rice, Catherine E. Settineri, Fumiaki Yokokawa, Shiho Yokokawa, Peter Wipf, and John S. Lazo

Department of Pharmacology, School of Medicine (A.V., R.L.R., C.E.S., J.S.L.), and Department of Chemistry, College of Arts and Science (F.Y., S.Y., P.W.), University of Pittsburgh, Pittsburgh, Pennsylvania

Running title : Novel antisignaling agent from targeted array

Correspondence: John S. Lazo, University of Pittsburgh, School of Medicine, Department of Pharmacology, Pittsburgh, PA 15261, (412) 648 9319. E-mail: lazo@pop.pitt.edu

Pages : 34

Tables : 2

Figures : 7

References : 36

Abstract : 230 words

Introduction : 680 words

Discussion : 863 words

Abbreviations : SC-ααδ9, 4-(benzyl-(2-[(2,5-diphenyl-oxazole-4-carbonyl)-amino]-ethyl)-carbamoyl)-2-decanoylamino butyric acid; DSPase, dual specificity phosphatase; IGF-1, Insulin-like growth factor-1; MEF, mouse embryonic fibroblasts; MAPK, mitogen-activated protein kinase; MTT, 3-[4,5-dimethylthiazol-2-yl]-2,5-diphenyltetrazolium bromide; PSTPase, protein serine/threonine phosphatase; PTPase, protein tyrosine phosphatase; SDS-PAGE, sodium dodecyl sulfate-polyacrylamide gel electrophoresis; SV40, simian virus 40 large T antigen.

Abstract

We previously reported the generation of a library of hydrophobic oxazole-based small molecules designed as inhibitors of phosphatases involved in cellular signaling and cell cycle control. One member of the targeted array library, SC-ααδ9, inhibited cell growth in the G0/G1 phase of the cell cycle. To investigate potential mechanisms for SC-ααδ9 antiproliferative activity, we have used mouse embryonic fibroblasts transformed with SV40 large T antigen (SV40 MEF) as a model system for a malignant phenotype that depends on overexpression of cell cycle regulators and autocrine stimulation by insulin-like growth factor-1 (IGF-1). Structure activity relationship studies with SC-ααδ9 and four library congeners demonstrated that antiproliferative activity was not a result of overall hydrophobicity. Rather, SC-ααδ9 decreased IGF-1 receptor tyrosine phosphorylation, receptor expression, mitogen-activated protein kinase (MAPK) activation, and levels of the cyclin dependent kinase Cdc2. Less toxic congeners only partially affected receptor expression, receptor tyrosine phosphorylation and Cdc2 levels. Thus SC-ααδ9, which is structurally distinct from other known small molecules that decrease intracellular Cdc2 levels, has profound effects on intracellular signaling. Furthermore, SC-ααδ9, but not vanadate or okadaic acid, selectively inhibited the growth of SV40 MEF compared to the parental cells. These results suggest that overexpression of Cdc2 and increased dependence on IGF-1 autocrine stimulation are responsible for the increased sensitivity of SV40 MEF to SC-ααδ9. The SC-ααδ9 pharmacophore could be a useful platform for the development of novel antisignaling agents.

An improved understanding of oncogenesis and the roles that oncogenes and tumor suppressors play in the regulation of cell proliferation has led to more rational approaches for the design and development of neoplastic-specific, target-directed, anticancer drugs. Signal transduction pathways in general, and growth factor-mediated signaling in particular, have become prime targets for novel antiproliferative agents. It is generally assumed that agents aimed to correct aberrant signaling will have a distinct advantage over traditional anticancer therapies by selectively affecting growth of tumor cells over normal tissues.

Growth factors and cytokines play a pivotal role in regulating cell proliferation, cell cycle progression, and cell survival. Many tumors overproduce growth factors, and autocrine stimulation appears to be a major factor in the establishment and maintenance of the malignant phenotype. In addition, growth factors are key regulators of the cell cycle, and the mechanisms that link extracellular signals to transcriptional activation and cell cycle regulation are now being uncovered (Hill and Treisman, 1995).

The most prevalent mechanism used by cells to regulate growth factor signal transduction is reversible protein phosphorylation and dephosphorylation by kinases and phosphatases (Sun and Tonks, 1994). Both classes of enzymes are currently being explored as potential anticancer targets (Wipf et al., 1997; Mohammadi et al., 1997; Dudley et al., 1995; Baratte et al., 1992; Chen et al., 1996). Special emphasis has been placed on the development of nonelectrophilic, cell active, small molecules that inhibit signal transduction, as these agents should have several desirable attributes such as stability, potential oral availability, diffusibility, non-immunogenicity lacking in large molecules such as antibodies or peptides.

Using parallel chemistry, we have recently synthesized on solid support a library of small molecule, nonelectrophilic oxazoles that were modeled after antiphosphatase natural products, such as okadaic acid and calyculin A. Several members of the natural product-based library inhibited the growth of MDA-MB-231 breast cancer cells in culture, and one member, 4-(benzyl-(2-[(2,5-diphenyl-oxazole-4-carbonyl)-amino]-ethyl)-carbamoyl)-2-decanoylamino butyric acid (SC-ααδ9, Table 1), accumulated cells in the G0/G1 phase of the cell cycle (Wipf et al., 1997). *In vitro,* SC-ααδ9 effectively inhibited both the protein tyrosine phosphatase PTP1B and Cdc25 dual specificity phosphatases, but did not affect serine/threonine phosphatases, the DSPase CL100, or alkaline phosphatase (Rice et al., 1997). We have, however, no information concerning intracellular actions of this novel compound or the biochemical basis of its antiproliferative activity.

Any potential anticancer agent should display selectivity for the malignant phenotype. Thus, we have used cellular transformation by SV40 large T antigen (SV40) as a relevant model to investigate potential intracellular mechanisms of SC-ααδ9 growth inhibition and its selectivity toward a malignant phenotype. SV40 is a complete transforming agent (Ray et al., 1990; Ray and Kraemer, 1993), unlike other oncogenes (e.g. *ras*) that, in primary fibroblasts, induce a senescence-like phenotype and require other genetic alterations to achieve their full transforming potential (Weinberg, 1997; Serrano et al., 1997). SV40 transformation has been reported to elevate levels or activities of key mitotic regulators, such as cyclin A, cyclin B, and Cdc2 (Chang et al., 1997), and to increase expression of Cdc25B (Nagata et al., 1991) in human diploid

fibroblasts. SV40 directly transactivates Cdc2 promoter/reporter constructs and increases levels of Cdc2 mRNA in monkey kidney cells (Chen et al., 1996). In addition to its effects on cell cycle regulators, SV40 enhances promoter activity of the insulin-like growth factor-1 (IGF-1) gene (Porcu et al., 1994). Cells transfected with SV40 have high levels of IGF-1 mRNA, and secrete IGF-1 into the growth medium (Baserga, 1993). This reduces growth factor requirements and is likely to be important for SV40 transforming ability (Baserga, 1993). IGF-1 is also required for Cdc2 expression (Surmacz et al., 1992). Thus, SV40 transformation results in a model system that owes its transformed phenotype to both autocrine stimulation and overexpression of cell cycle regulators. Using this model system, we found that SC-ααδ9 is selectively toxic to the virally transformed cells and relate the growth inhibition to disrupted IGF-1 signaling pathways and decreased Cdc2 levels. The SC-ααδ9 pharmacophore may thus be useful in the development of agents in the treatment of tumors whose growth or survival depends on autocrine stimulation.

Methods

Chemical compounds. The general synthesis of compounds SC-ααδ9, SC-αα09, SC-α109 has been previously described (Wipf et al., 1997; Rice et al., 1997). A slightly modified strategy was used for the synthesis of the new compounds SC-ααδ6III and SC-ααδ4II. Briefly, *rac*-glutamate was selectively side-chain esterified with trimethylsilylchloride in allyl alcohol, *N*-protected with *β,β,β*-trichloroethoxycarbonyl chloride, and methylated to give fully protected N-Troc-allyl-methylglutamate. The diester was de-allylated, coupled with protected ethylene diamine and reacted with 2,5-diphenyl-oxazole-4-carboxylic acid in the presence of PyBroP as described (Frerot et al., 1991). After attachment of the oxazole moiety, the Troc group was removed with zinc in acetic acid, and a carbodiimide-mediated coupling provided substrates SC-ααδ6III and SC-ααδ4II. All intermediates and products were purified by chromatography on SiO_2 and characterized by nuclear magnetic resonance and high resolution mass spectrometry as described previously (Wipf et al., 1997; Rice et al., 1997).

Determination of cLog P values. Computation of cLog P, the calculated logarithm of the octanol-water partition coefficient, was performed on an Indigo2 R4400 workstation according to the protocol by Villar (Alkorta and Villar, 1992). Extended conformations of compounds were fully optimized using the semiempirical method PM3. Charges and other parameters for the regression analysis were also obtained with the PM3 module on Spartan 5.0 (Wavefunction, Inc., Irvine, CA).

Cell Culture. MEF were isolated from fetuses of 14.5-day pregnant mice (129 Ola x C57Bl/6) using previously described methods (Kondo et al., 1995). Cells were maintained in Dulbecco's Minimum Essential Medium containing 20% fetal bovine serum (FBS, HyClone, Logan, UT), and 1% penicillin-streptomycin (GIBCO BRL) in a humidified atmosphere of 5% CO at 37°C. Primary cultures of MEF were never extended beyond passage 15 to avoid entering of crisis. MEF cells were transformed using the plasmid pCC5 (a kind gift from Dr. Stephen Strom, University of Pittsburgh) expressing SV40 large T antigen under the control of its own promoter by means of a cationic lipid (Lipofectamine, GIBCO BRL) according to manufacturer's instructions. SV40 transformed MEF were grown in DMEM supplemented with 5% FBS and 1% penicillin-streptomycin (GIBCO BRL) to attempt to control for similar growth and plating efficiencies compared with MEF. As indicated, in some experiments both cell lines were grown and treated in DMEM containing 10% FBS and 1% penicillin-streptomycin.

Assay for antiproliferative activity. We used our previously described MTT microtiter assay (Kondo et al., 1995) to determine the antiproliferative activity of the newly synthesized compounds. Cells were plated at 2,000 cells/well in 96 well plates. After a 24 h incubation at 37° C, cells were exposed continuously for 48 h to each compound, incubated with MTT for 3 hours and total cell number determined by colorimetric quantitation of the blue formazane dye at 540 nm in DMSO as previously described (Kondo et al., 1995).

Colony formation. Long-term survival of MEF and SV40 MEF was determined in a clonogenic assay essentially as described (Freshney, 1994). Briefly, cells were plated (200 cells/well) in 6 well plates and treated the next day with vehicle (DMSO) or inhibitors without media change in

order to not disturb the cell attachment process. After 10 to 12 days in culture with continuous exposure to drug, colonies were exposed to staining solution containing 0.25% crystal violet and 10% formalin (35% v/v) in 80% methanol for 30 min, washed with water, and counted. Plating efficiency was determined as the fraction of cells that attached to the support and grew into colonies larger than 1 mm in diameter.

Western blotting. Cells were grown to subconfluency in 100 mm dishes, harvested, and lysed in lysis buffer (30 mM HEPES, pH 7.5, 1% Triton-X 100, 10% glycerol, 5 mM $MgCl_2$, 25 mM NaF, 1 mM EGTA, 10 mM NaCl, 2 mM Na_3VO_4, 10 µg/ml trypsin inhibitor, 10 µg/ml aprotinin, 25 µg/ml leupeptin, 2 mM PMSF, 6.4 mg/ml Sigma104 phosphatase substrate). Lysates were electrophoresed on 4-20% gradient gels (NOVEX, San Diego, CA), transferred to nitrocellulose and immunoblotted with antibodies against SV40 large T antigen (Ab-2, Oncogene Science, Manhasset, NY), Cdc25A (144), Cdc25B (C-20), Cdc25C (C-20), Cdc2 (17), or IGF-1 receptor beta subunit (C-20, all from Santa Cruz Biotechnology, Santa Cruz, CA), or anti-phosphotyrosine (PY20, Transduction Laboratories, Lexington, KY). Hyperphosphorylated and hypophosphorylated Cdc2 were separated on a large 10% polyacrylamide gel. For determination of Erk activation, lysates were separated on 15% SDS-PAGE and immunoblotted with an anti-Erk1 (K23, Santa Cruz Biotechnology, recognizes Erk 1 and Erk2) or Erk 2 (Upstate Biotechnology, Lake Placid, NY) antibodies. Positive antibody reactions were visualized using peroxidase-conjugated secondary antibodies (Jackson ImmunoResearch, West Grove, PA) and an enhanced chemiluminescence detection system (Renaissance, NEN, Boston, MA) according to manufacturer's instructions. Equal loading was ensured by reblotting with an anti-actin (H-196, Santa Cruz Biotechnology, Santa Cruz, CA). For quantitation of protein expression levels, X-ray

films were scanned on a Molecular Dynamics personal SI densitometer and analyzed using the ImageQuant software package (Ver. 4.1, Molecular Dynamics, Sunnyvale, CA).

In vitro phosphatase assays. Phosphatase-active GST-Cdc25B_2 was expressed and isolated from a plasmid (pGEX2T-KG) encoding GST-Cdc25B_2 fusion protein in *E. coli* strain BL21 (DE3) as described (Rice et al., 1997). The activity of GST-Cdc25B_2 was measured in our recently described fluorescence-based microtiter plate assay (Rice et al., 1997) except that 3-O-methylfluorescein monophosphate (OMFP, Sigma, St Louis, MO) was used as a substrate. Briefly, 100-250 ng of enzyme were incubated with the substrate for 5 min at room temperature in 150 µl assay buffer containing 30 mM Tris (pH 8.5), 50 mM NaCl, 1.5 mM EDTA, 0.033% bovine serum albumin, and 1 mM DTT. Inhibition studies were carried out at concentrations of OMFP that represented apparent K_m values (i.e. 40 µM). Inhibitors were dissolved in DMSO and added to the reaction mixture before the addition of enzyme. All reactions including controls were performed at a final concentration of 7% DMSO.

Results

Antiproliferative and antiphosphatase activity of a selected member of a targeted array library. We previously described the generation of a library of compounds modeled after calyculin A, microcystin LR, and okadaic acid, natural product inhibitors of PSTPases (Wipf et al., 1997). Surprisingly, *in vitro* inhibition studies for antiphosphatase activity revealed a number of compounds that were potent inhibitors of PTP1B (i.e. >50% inhibition at 3 μM), but had little effect on the PSTPases PP1 and PP2A or the closely related DSPase CL100 at concentrations as high as 100μM (Rice et al., 1997). SC-ααδ9, one of the most potent inhibitors of PTP1B, also inhibited Cdc25 A, B, and C (K_i ~10 μM) (Rice et al., 1997) and was cytotoxic to MDA-MB-231 breast cancer cells in culture (Wipf et al., 1997). We have now expanded the targeted array library by other structural analogs and chosen five closely related congeners to assess structural requirements for growth inhibitory activity. Table 1 shows the structures of the library members, which contain substituents of varying hydrophobicity and steric bulk in the R_2, R_3, and R_4 positions. Compounds SC-ααδ9, SC-αα09, and SC-α109 were synthesized as discrete compounds by traditional solution-phase chemistry as described (Wipf et al., 1997; Rice et al., 1997). The novel oligoether compounds SC-ααδ6III and SC-ααδ4II were synthesized by a slightly modified procedure as described in the Methods Section.

SV40 transformation resulted in elevated levels of Cdc25B and Cdc2 and increased tyrosine phosphorylation of the IGF-1 receptor. To generate a relevant model system for the analysis of the activity and selectivity of SC-ααδ9 against the malignant phenotype, we

transfected primary MEF with SV40. As expected, these cells grew in soft agar, exhibited reduced serum-dependence, and achieved higher saturation densities on plastic surfaces than the parental cells (data not shown). The presence of SV40 was confirmed by Western blotting (Figure 1A). In accordance with previously published data (Chang et al., 1997; Nagata et al., 1991), SV40 MEF showed a dramatic increase in Cdc25B and Cdc2 protein levels after SV40 transformation (Figure 1B and 1D), whereas levels of Cdc25A were unchanged (Figure 1C). The appearance of three higher molecular bands in the Cdc25 A immunoblot has been observed previously (Galaktionov et al., 1995), but their identity is unclear. We were unable to detect Cdc25C by Western blotting with a commercially available antibody (data not shown). Increased signaling through the IGF-1 receptor was assessed by sequential immunoblotting with antibodies to phosphotyrosine and the IGF-1 receptor. Figure 1E shows that the anti-phosphotyrosine antibody detected a major band of approximately 100 kDa. Reblotting with an anti-IGF-1 receptor antibody confirmed the identity of the 100 kDa band and also demonstrated equivalency in protein loading (Figure 1F). Thus, the transformed cells exhibited higher levels of IGF-1 receptor tyrosine phosphorylation presumably reflecting autocrine stimulation by IGF-1 (Baserga, 1993), whereas levels of the IGF-1 receptor itself were similar in both cell lines.

Structural requirements for cytotoxicity and *in vitro* inhibition of Cdc25B. The five library congeners from Table 1 containing structural variations in the R_2, R_3, and R_4 positions were assayed for their antiproliferative activity against SV40 MEF using the MTT assay as described in the Methods Section. Within compounds bearing a C_9 alkyl chain in the R_4 position, growth inhibitory activity decreased with decreasing bulk in the R_3 position (SC-αα09), and was

abolished after replacement of the phenyl group in R_2 with a sterically less demanding methyl substituent (SC-α109) (Table 2). Replacement of the highly hydrophobic C_9 alkyl chain in SC-ααδ9 with a more polar but sterically similar oligoether group (SC-ααδ6III) also resulted in a loss of antiproliferative activity. Shortening of the oligoether residue in the R_4 position accentuated loss of activity (SC-ααδ4II). Taken together, these results indicated a requirement for hydrophobic substituents, especially in the R_2 and R_4 position, for antiproliferative activity. To address the question whether the observed biological acitivity of the five congeners was merely due to their overall hydrophobic character, we calculated log P values (cLogP) for all compounds based on energy-minimized extended conformations by the method of Villar (Alkorta and Villar, 1992). Because the compounds are present as carboxylates under cell culture and *in vitro* phosphatase assay conditions, cLogP values were calculated for the compounds in their free acid and carboxylate forms. As expected, cLogP values were much lower for the compounds in their ionized forms. Irrespective of the charge characteristics of the compounds, however, both sets of values indicated that there was no obvious correlation between overall hydrophobicity and inhibition of cell proliferation. For example, SC-αα09 was more toxic than SC-α109, even though their cLog P values were similar. Furthermore, the oligoether compound SC-ααδ6III was about 1,000 times more polar than SC-αα09, yet both compounds were comparable in their antiproliferative activities. Thus, even though SC-ααδ9, the most active compound, was also the most hydrophobic, overall hydrophobicity was not the sole determinant of biological activity. Furthermore, the decrement in antiproliferative activity did not readily correlate with loss of *in vitro* Cdc25B inhibition (Table 2).

SC-ααδ9 decreased Cdc2 levels in SV40 transformed MEF. One of the putative substrates for both Cdc25B and Cdc25C is the cyclin dependent kinase Cdc2 (Sebastian et al., 1993). Thus, we treated SV40 MEF continuously for 48 h with increasing concentrations of SC-ααδ9 and analyzed cellular lysates by immunoblot analysis with an anti-Cdc2 antibody as described in the Methods Section. Hyperphosphorylation of Cdc2 results in the appearance of a slower migrating band on SDS-PAGE (Draetta and Beach, 1988). We found that a 48 h exposure to 30 or 60 μM SC-ααδ9 markedly decreased levels of Cdc2 (Figure 2, lanes 3 and 4). Reprobing of the Cdc2 immunoblot with an anti-actin antibody demonstrated approximately equal protein loading (Figure 2B). Densitometric scanning of both the upper (phosphorylated) and lower (unphosphorylated) bands of Cdc2 indicated that, at 10 and 30 μM, SC-ααδ9 did not alter the phosphorylation status of Cdc2. We hypothesized that the decrease in Cdc2 protein levels was a result of an intracellular action of SC-ααδ9. Thus, we investigated other events associated with a loss of Cdc2 that would account for SC-ααδ9's ability to inhibit cell growth and the previously observed G0/G1 phase accumulation.

SC-ααδ9 decreased IGF-1 receptor tyrosine phosphorylation and receptor expression. One of the known regulators of Cdc2 is IGF-1 (Surmacz et al., 1992). Because it had previously been shown that SV40 transformation enhances levels of IGF-1 mRNA and increases IGF-1 secretion (Baserga, 1993), we investigated whether the decrease in Cdc2 levels caused by SC-ααδ9 correlated with a reduction in IGF-1 signaling in SV40 transformed cells. SV40 MEF were treated with various concentrations of SC-ααδ9 for 48 h, lysates separated on SDS-PAGE and immunoblotted with antibodies against phosphotyrosine and the IGF-1 receptor. Figure 3A

shows that SC-ααδ9 decreased phosphotyrosine levels on a 100kDa protein (lanes 2 - 4). Reprobing of the same blot with an anti-IGF-1 receptor antibody revealed that the decrease in phosphotyrosine levels at the highest concentration of SC-ααδ9 was, in part, due to a decrease in IGF-1 receptor expression (Figure 3B). Thus, SC-ααδ9 interfered with IGF-1 mediated receptor signaling by reducing both receptor tyrosine phosphorylation and, unexpectedly, IGF-1 receptor levels. Concomitant with reduced receptor autophosphorylation, we also observed inactivation of MAPK (Erk2), a downstream target in the IGF-1 receptor signaling cascade. Figure 3C shows an anti-Erk2 immunoblot after separation of the identical lysates into the lower, unphosphorylated and the slower migrating, phosphorylated species as described in the Methods Section. SC-ααδ9 decreased Erk2 phosphorylation in a concentration-dependent manner (lanes 2-4). To determine whether MAPK inhibition alone was sufficient for inhibition of cell proliferation, we treated cells with PD-98059, a specific inhibitor of MEK, the direct upstream activating kinase of Erk (Dudley et al., 1995). PD-98059 (50 μM) completely inhibited MAPK phosphorylation (Figures 3C, lane 5), but in contrast to SC-ααδ9 did not affect IGF-1 receptor expression (Figure 3B lane 5) or cell proliferation (data not shown) and had only a partial effect on receptor tyrosine phosphorylation (Figure 3A, lane 5). Densitometric analysis of the immunoblots in Figures 2 and 3 indicated that IGF-1 receptor autophosphorylation, inactivation of Erk2, and the decrease in Cdc2 were all concentration-related, with an IC_{50} of approximately 30 μM (Figure 3E and Figure 5A), whereas loss of receptor was only observed at the highest concentration tested.

Less toxic library congeners and vanadate did not inhibit IGF-1 receptor signaling. We next examined the effects of the less toxic library congeners SC-ααα09 and SC-α109 on IGF-1 signaling. We found that SC-ααα09 partially affected receptor tyrosine phosphorylation, and that SC-α109 was inactive (Figure 4A, lanes 2 and 3). Neither SC-ααα09 nor SC-α109 markedly reduced IGF-1 receptor or Cdc2 levels (Figure 4B and 4E, lanes 2 and 3). At concentrations that were cytotoxic, vanadate markedly increased receptor tyrosine phosphorylation (Figure 4A, lane 4), suggesting a distinct mechanism of action from SC-αααδ9. Furthermore, SC-ααα09 and SC-α109 did not affect MAPK activation (Figure 4C and 4D, lanes 2 and 3). The apparent slight increase in MAPK phosphorylation and IGF-1 receptor autophosphorylation by SC-α109 (Figure 4A, 4C, and 4D, lane 3) was not reproducible. PD-98059 (50μM) caused essentially complete inhibition of both Erk1 and Erk2, but only partially decreased receptor autophosphorylation and levels of Cdc2 (Figure 4A and 4E, lane 5). These data indicate that, although the decrease in Erk phosphorylation by SC-αααδ9 correlated with an inhibition of IGF-1 signaling, inactivation of MAPK alone was not sufficient to cause a complete loss of Cdc2 or inhibition of cell proliferation.

SC-αααδ9, but not okadaic acid or vanadate, was selectively toxic to SV40 transformed MEF. Having demonstrated a profound effect on intracellular signaling by SC-αααδ9, we next examined the sensitivity of MEF and SV40 MEF to SC-αααδ9 and two classic antiphosphatases, vanadate and okadaic acid. Using a clonogenic assay, we found that SV40 MEF were two to three times more sensitive to SC-αααδ9 based on the concentration required for a 50% decrease in plating efficiency compared to the wild-type MEF (Figure 5). This selectivity was reproduced in

an MTT assay (Figure 6A) where it was seen also when both cell lines were grown in 10% fetal bovine serum (data not shown). We then treated both normal and SV40 transformed MEF with okadaic acid and vanadate, known inhibitors of PSTPases and PTPases, respectively (Mumby and Walter, 1993), and found that only SC-ααδ9 preferentially affected growth of the transformed cells (Figure 6A) whereas both okadaic and vanadate were equally effective in normal or transformed MEF (Figure 6B and 6C), even though okadaic acid was about 1,000 times more potent than SC-ααδ9 or vanadate. These results indicated a transformation-specific intracellular action of SC-ααδ9 compared to okadaic acid or vanadate.

SC-ααδ9 decreased IGF-1 receptor tyrosine phosphorylation and levels of Cdc2 in both MEF and SV40 MEF. Finally, we examined whether SC-ααδ9 differentially affected IGF-1 signaling and levels of Cdc2 in MEF or SV40 MEF. To control for the known effects of serum on Cdc2 expression (Surmacz et al., 1992), both cell lines were plated and treated with SC-ααδ9 in the presence of 10% fetal bovine serum. After 48 h, lysates were separated on SDS-PAGE and immunoblotted with antibodies against phosphotyrosine, IGF-1 receptor, and Cdc2. Figure 7 shows that SV40 MEF had much higher levels of Cdc2 and displayed higher phosphotyrosine content on the IGF-1 receptor, consistent with the results from Figure 1. Equal loading was ensured by immunoblotting with an anti-actin antibody (Figure 7D). As judged by cell numbers and morphology, SC-ααδ9 under these conditions was about two to threefold less toxic to normal MEF (data not shown), confirming the selective toxicity of SC-ααδ9 seen in Figures 5 and 6. Interestingly, SC-ααδ9 caused downregulation of Cdc2 (Figure 7C) and inhibition of IGF-1 receptor signaling (Figure 7 A and 7B) in both cell lines, although the absolute decrement

in Cdc2 levels and receptor tyrosine phosphorylation was much larger in the transformed cells. These results indicate that decreased Cdc2 levels and inhibition of IGF-1 signaling are not secondary to inhibition of cell proliferation, but suggest that SC-ααδ9 specifically affects a cellular target associated with IGF-1 signaling.

Discussion

Independence from growth factor control and loss of cell cycle regulation is a common feature of human malignancies. Many tumors overexpress growth factor receptors and depend on autocrine or paracrine stimulation (Baselga and Mendelsohn, 1994). Most growth factors utilize mechanisms involving protein phosphorylation and dephosphorylation to transduce extracellular signals to the nucleus. The roles of growth factors like platelet-derived growth factor (PDGF), epidermal growth factor (EGF), and IGF-1 in cell cycle progression from G0 to S-phase have been studied extensively (for a recent review see Winkles, 1998).

Mechanistic studies using SV40 large T antigen transformation have established a role of the IGF-1 receptor in the malignant phenotype. SV40 transformation causes an increase in IGF-1 mRNA expression and protein secretion (Baserga, 1993). Cells with a targeted disruption of the IGF-1 receptor gene are no longer transformed by SV40 (Sell et al., 1993). Because a number of human tumors have been shown to overexpress the IGF-1 receptor, aberrant signaling through the insulin-like growth factor-1 (IGF-1) receptor has become a target for anticancer drug design (Baserga, 1996).

Growth factors also regulate cell cycle dependent kinases. Serum stimulation of quiescent cells results in the expression of Cdc2, a key component of the mitosis-promoting factor comprising p34Cdc2 and cyclin B. In cells expressing high numbers of IGF-1 receptors, Cdc2 can be induced by IGF-1 alone, and this induction can be suppressed by an antisense

oligodeoxynucleotide against the IGF-1 receptor gene (Surmacz et al., 1992). Cdc2 is activated by dephosphorylation on threonine and tyrosine residues by the cell cycle phosphatases Cdc25B and Cdc25C (Sebastian et al., 1993), and Cdc2 as well as Cdc25B are overexpressed in SV40 transformed cells.

We have recently described the design and synthesis of a unique, small molecule, targeted array library that has antiphosphatase elements (Wipf et al., 1997). Several members of this library inhibited PTP1B and Cdc25, but not PSTPases at low micromolar concentrations *in vitro*. One compound, SC-ααδ9, selectively inhibited growth of transformed cells in culture. This selective toxicity was not shared by the phosphatase inhibitors vanadate and okadaic acid. Thus, SC-ααδ9 had a different activity profile than two classical antiphosphatase compounds, suggesting the antiproliferative effects may be associated with other pharmacological activities resident in this basic pharmacophore. Furthermore, although SC-ααδ9 was a potent inhibitor of Cdc25 *in vitro*, we saw no increased phosphorylation of Cdc2, a known substrate for Cdc25B and Cdc25C, in cultured cells, and growth inhibition was not strictly correlated with *in vitro* inhibition of Cdc25B. Thus, while we cannot formally exclude phosphatase inhibition as the cause of growth inhibition for SC-ααδ9, it seems more likely that these compounds exert their antiproliferative effects through another mechanism.

Structure-activity relationship studies using congeners with only slight structural modifications demonstrated that sterically demanding residues in the R_2 and R_3 positions or a hydrophobic alkyl chain in the R_4 position enhanced cytotoxicity. Log P values, however, calculated for the

five compounds in an extended energy-minimized conformation showed that antiproliferative activity was not a result of overall hydrophobicity, even though the most biologically active compound (SC-ααδ9) was also the most hydrophobic. These results are consistent with SC-ααδ9 having a specific intracellular site of action.

SC-ααδ9 decreased Cdc2 levels. This was an interesting result, because only few pharmacological agents, for example IFN-γ (Saunders and Jetten, 1994), retinoic acid (Zhu et al., 1997), and mezerein (Jiang et al., 1995) have been reported to reduce Cdc2 levels. Butyrolactone-I, a Cdc2 kinase inhibitor, decreased Cdc2 protein levels after prolonged exposure (Nishio et al., 1996). We have, however, seen no *in vitro* inhibition of Cdc2 kinase by SC-ααδ9 (Rice et al., 1997). The Cdc2 depletion is unlikely to be a result of cell cycle inhibition because Cdc2 levels, like those of many other cyclin-dependent kinases, appear to remain stable throughout the cell cycle (Draetta and Beach, 1988; Morgan, 1995), and are downregulated only in serum-deprived or senescent cells (Surmacz et al., 1992; Richter et al., 1991). Thus, the growth arrest caused by SC-ααδ9 is reminiscent of quiescence, senescence, or differentiation.

Consistent with the previously reported ability of IGF-1 to induce Cdc2, the loss of Cdc2 correlated with an inhibition of IGF-1 receptor signaling and MAPK activation. Interestingly, however, selective disruption of IGF-1 signaling at the MAPK level by the MEK-specific inhibitor PD-98059 only led to a partial decline in Cdc2 levels and did not result in inhibition of cell proliferation. This most likely reflects direct transactivation of Cdc2 by SV40 large T antigen, which would be independent of MAPK activation. In contrast to PD-98059, SC-ααδ9,

at concentrations that caused complete dephosphorylation of Erk, abolished Cdc2 expression. The precise mechanisms for the Cdc2 downregulation are unknown, and could be due to decreased transcription, translation, or increased protein degradation. Finally, we investigated possible mechanisms for SC-ααδ9 selectivity towards the transformed cells and found that the absolute reduction in Cdc2 levels caused by SC-ααδ9 was greater in SV40 MEF than in the parental cells. We propose that the increased sensitivity of the transformed cells to SC-ααδ9 is a result of their increased dependence on elevated Cdc2 expression and IGF-1 signaling. We suggest the SC-ααδ9 pharmacophore could prove useful in the further development of antiproliferative agents for the treatment of growth factor dependent tumors.

Acknowledgments

We thank Dr. Stephen Strom, University of Pittsburgh, for the SV40 cDNA, Donald Schwartz for performing the SV40 large T antigen transformation, Dr. David Beach (Cold Spring Harbor Laboratory, Cold Spring Harbor) for the pGEX2T-KG plasmid encoding GST-Cdc25B_2, and Angela Wang for excellent technical assistance.

References

Alkorta I and Villar HO (1992) Quantum mechanical parametrization of a conformationally dependent hydrophobicity index. *Int. J. Quant. Chem.* **44**: 203-218.

Baratte B, Meijer L, Galaktionov K and Beach D (1992) Screening for antimitotic compounds using the cdc25 tyrosine phosphatase, an activator of the mitosis-inducing p34cdc2/cyclinB-cdc13 protein kinase. *Anticancer Res.* **12**: 873-880.

Baselga J and Mendelsohn J (1994) Receptor blockade with monoclonal antibodies as anti-cancer therapy. *Pharmacol. Ther.* **64**: 127-154.

Baserga R (1993) Gene regulation by IGF-I. *Molecular Reproduction & Development* **35**: 353-356.

Baserga R (1996) Controlling IGF-receptor function: a possible strategy for tumor therapy. *Trends in Biotech.* **14**: 150-152.

Chang TH, Ray FA, Thompson DA and Schlegel R (1997) Disregulation of mitotic checkpoints and regulatory proteins following acute expression of SV40 large T antigen in diploid human cells. *Oncogene* **14**: 2383-2393.

Chen H, Campisi J and Padmanabhan R (1996) SV40 large T antigen transactivates the human cdc2 promoter by inducing a CCAAT box binding factor. *J. Biol. Chem.* **271**: 13959-13967.

Chen L, Montserat J, Lawrence DS and Zhang ZY (1996) VHR and PTP1 protein phosphatases exhibit remarkably different active site specificities toward low molecular weight nonpeptidic substrates. *Biochemistry* **35**: 9349-9354.

Draetta G and Beach D (1988) Activation of cdc2 protein kinase during mitosis in human cells: cell cycle-dependent phosphorylation and subunit rearrangement. *Cell* **54**: 17-26.

Dudley DT, Pang L, Decker SJ, Bridges AJ and Saltiel AR (1995) A synthetic inhibitor of the mitogen-activated protein kinase cascade. *Proc. Natl. Acad. Sci. U. S. A.* **92**: 7686-7689.

Frerot E, Coste J, Pantaloni A, Dufour M-N and Jouin P (1991) PyBOP and PyBroP: Two reagents for the difficult coupling of the α,α-dialkyl amino acid, Aib. *Tetrahedron* **47**: 259.

Freshney RI (1994) *Culture of Animal Cells: A Manual of Basic Technique.* Wiley-Liss, New York

Galaktionov, K, Jessus, C, and Beach, D (1995) Raf1 interaction with Cdc25 phosphatase ties mitogenic signal transduction to cell cycle activation. *Genes Dev.* **9**:1046-1058.

Hill CS and Treisman R (1995) Transcriptional regulation by extracellular signals: mechanisms and specificity. *Cell* **80**: 199-211.

Jiang H, Lin J, Young SM, Goldstein NI, Waxman S, Davila V, Chellappan SP and Fisher PB (1995) Cell cycle gene expression and E2F transcription factor complexes in human melanoma cells induced to terminally differentiate. *Oncogene* **11**: 1179-1189.

Kondo Y, Woo ES, Michalska AE, Choo KH and Lazo JS (1995) Metallothionein null cells have increased sensitivity to anticancer drugs. *Cancer Res.* **55**: 2021-2023.

Mohammadi M, McMahon G, Sun L, Tang C, Hirth P, Yeh BK, Hubbard SR and Schlessinger J (1997) Structures of the tyrosine kinase domain of fibroblast growth factor receptor in complex with inhibitors. *Science* **276**: 955-960.

Morgan DO (1995) Principles of CDK regulation. *Nature* **374**: 131-134.

Mumby MC and Walter G (1993) Protein serine/threonine phosphatases: structure, regulation, and functions in cell growth. *Physiol. Rev.* **73**: 673-699.

Nagata A, Igarashi M, Jinno S, Suto K and Okayama H (1991) An additional homolog of the fission yeast CDC25+ gene occurs in humans and is highly expressed in some cancer cells. *New Biologist* **3**: 959-968.

Nishio K, Ishida T, Arioka H, Kurokawa H, Fukuoka K, Nomoto T, Fukumoto H, Yokote H and Saijo N (1996) Antitumor effects of butyrolactone I, a selective cdc2 kinase inhibitor, on human lung cancer cell lines. *Anticancer Res.* **16**: 3387-3395.

Porcu P, Grana X, Li S, Swantek J, De Luca A, Giordano A and Baserga R (1994) An E2F binding sequence negatively regulates the response of the insulin-like growth factor 1 (IGF-I) promoter to simian virus 40T antigen and to serum. *Oncogene* **9**: 2125-2134.

Ray FA and Kraemer PM (1993) Iterative chromosome mutation and selection as a mechanism of complete transformation of human diploid fibroblasts by SV40 T antigen. *Carcinogenesis* **14**: 1511-1516.

Ray FA, Peabody DS, Cooper JL, Cram LS and Kraemer PM (1990) SV40 T antigen alone drives karyotype instability that precedes neoplastic transformation of human diploid fibroblasts. *J. Cell. Biochem.* **42**: 13-31.

Rice RL, Rusnak JM, Yokokawa F, Yokokawa S, Messner DJ, Boynton AL, Wipf P and Lazo JS (1997) A Targeted Library Of Small-Molecule, Tyrosine, And Dual- Specificity Phosphatase

Inhibitors Derived From A Rational Core Design And Random Side Chain Variation. *Biochemistry* **36**: 15965-15974.

Richter KH, Afshari CA, Annab LA, Burkhart BA, Owen RD, Boyd J and Barrett JC (1991) Down-regulation of cdc2 in senescent human and hamster cells. *Cancer Res.* **51**: 6010-6013.

Saunders NA and Jetten AM (1994) Control of growth regulatory and differentiation-specific genes in human epidermal keratinocytes by interferon gamma. Antagonism by retinoic acid and transforming growth factor beta 1. *J. Biol. Chem.* **269**: 2016-2022.

Sebastian B, Kakizuka A and Hunter T (1993) Cdc25M2 activation of cyclin-dependent kinases by dephosphorylation of threonine-14 and tyrosine-15. *Proc. Natl. Acad. Sci. U. S. A.* **90**: 3521-3524.

Sell C, Rubini M, Rubin R, Liu JP, Efstratiadis A and Baserga R (1993) Simian virus 40 large tumor antigen is unable to transform mouse embryonic fibroblasts lacking type 1 insulin-like growth factor receptor. *Proc. Natl. Acad. Sci. U. S. A.* **90**: 11217-11221.

Serrano M, Lin AW, McCurrach ME, Beach D and Lowe SW (1997) Oncogenic ras provokes premature cell senescence associated with accumulation of p53 and p16INK4a. *Cell* **88**: 593-602.

Sun H and Tonks NK (1994) The coordinated action of protein tyrosine phosphatases and kinases in cell signaling. *Trends in Biochem. Sci.* **19**: 480-485.

Surmacz E, Nugent P, Pietrzkowski Z and Baserga R (1992) The role of the IGF-1 receptor in the regulation of cdc2 mRNA levels in fibroblasts. *Exp. Cell Res.* **199**: 275-278.

Weinberg RA (1997) The cat and mouse games that genes, viruses, and cells play. *Cell* **88**: 573-575.

Winkles JA (1998) Serum- and polypeptide growth factor-inducible gene expression in mouse fibroblasts. *Prog. Nucl. Acid Res. Mol. Biol.* **58**: 41-78.

Wipf P, Cunningham A, Rice RL and Lazo JS (1997) Combinatorial Synthesis and Biological Evaluation of Library of Small-Molecule Ser/Thr-Protein Phosphatase Inhibitors. *Bioorg. Med. Chem.* **5**: 165-177.

Zhu WY, Jones CS, Kiss A, Matsukuma K, Amin S and De Luca LM (1997) Retinoic acid inhibition of cell cycle progression in MCF-7 human breast cancer cells. *Exp. Cell Res.* **234**: 293-299.

Footnotes

This work was supported by Army Breast Cancer Grant DAMD 17-1-7229, Army Breast Cancer Predoctoral Fellowship DAMD 17-94-J4103, The Fiske Drug Discovery Fund , and USPHS NIH grants CA-61229 and CA-39745.

Send reprint requests to :

John S. Lazo

Professor and Chairman

University of Pittsburgh School of Medicine

Department of Pharmacology, E 1314 BST

Pittsburgh, PA 15261, USA

Table 1. Structures and nomenclature of selected compounds from a targeted array library

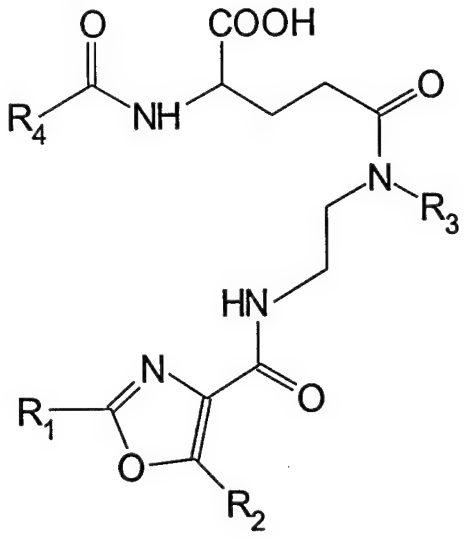

Compound	R_1	R_2	R_3	R_4
SC-ααδ9			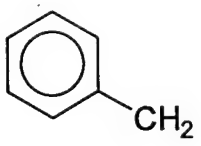	C_9H_{19}
SC-αα09			H	C_9H_{19}
SC-α109		CH_3	H	C_9H_{19}
SC-ααδ6III			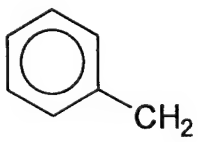	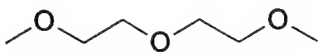
SC-ααδ4II			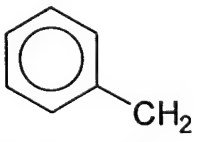	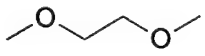

Table 2. Antiproliferative and antiphosphatase activity of library members

	cell survival *In culture*[a] (% of control)		$Cdc25B_2$ activity *In vitro*[b] (% of control)		cLog P values[d]	
compound	at 50μM	at 100μM	at 30μM	at 100μM	free acid	carboxylate
SC-ααδ9	2 ± 2 (4)	7 ± 3 (3)	32 ± 11 (3)	15 ± 2 (3)	4.9	1.2
SC-αα09	28 ± 8 (4)	20 (1)	82 ± 11 (3)	51 ± 27 (6)	3.5	-0.3
SC-α109	91 ± 10 (4)	79 ± 8 (2)	ND[c]	86 ± 11 (3)	3.9	-0.2
SC-ααδ6III	59 ± 16 (3)	10 ± 6 (3)	ND	87 ± 2 (3)	1.4	-2.0
SC-ααδ4II	73 ± 10 (3)	42 ± 6 (3)	ND	67 ± 2 (3)	1.9	-1.8

[a] determined by MTT assay in SV40 MEF. Data are the averages of (n) independent experiments ± SEM or range.
[b] measured by fluorescence-based assay as described in the Methods section. Data are the averages of (n) independent experiments ± SEM
[c] ND = not determined
[d] cLogP values represent logarithms of the octanol-water partition coefficient and were calculated based on energy-minimized extended conformations by the method of Alkorta and Villar (1992). Compounds with greater hydrophobicity had higher absolute values. As expected, cLogP values were lower for the compounds in their ionized (carboxylate) forms.

Figure Legends

Figure 1. SV40 large T antigen transformation results in increased levels of mitotic regulators and enhanced IGF-1 receptor autophosphorylation. Cell lysates were isolated from exponentially growing MEF and SV40 MEF, separated by SDS-PAGE on 4-20% gradient gels, and immunoblotted with antibodies against **(A)** SV40 large T antigen, **(B)** Cdc25B, **(C)** Cdc25A, **(D)** p34Cdc2, **(E)** phosphotyrosine (PY20) and **(F)** IGF-1 receptor as described in the Methods Section. Numbers indicate the positions of molecular weight markers in kDa. Data are representative of three independent experiments.

Figure 2. SC-ααδ9 decreases levels of Cdc2 in SV40 MEF. Cells were grown to 50% confluency in 100 mm dishes and treated for 48 h with vehicle or increasing concentrtions of SC-ααδ9. **(A)** Lysates were separated on 10% SDS-PAGE and immunoblotted with an anti-Cdc2 antibody. **(B)** Actin was immunolabeled as a loading control. *Lane 1*, vehicle control; *lanes 2-4*, 10, 30 and 60 μM SC-ααδ9. P and U denote the phosphorylated and non-phosphorylated forms of Cdc2.

Figure 3. SC-ααδ9 disrupts IGF-1 signaling. SV40 MEF were treated for 48 h with vehicle or inhibitors and lysed as described in the Methods Section. Lysates were separated on 4-20% SDS-PAGE and immunoblotted with **(A)** anti-phosphotyrosine (PY20), **(B)** anti-IGF-1 receptor, or **(C)** anti-Erk2 antibodies. **(D)** Blots were analyzed for β-actin to ensure equal protein loading. *Lane 1*, vehicle control; *lanes 2-4*, 10, 30, and 60 μM SC-ααδ9; *lane 5*, 50 μM PD-98059. P and U denote the unphosphorylated and phosphorylated forms of Erk2. **(E)** Graphical

representation of the results from panels A-D and Figure 2. Protein bands were quantitated by densitometric scanning and plotted as percent of vehicle control. MAPK phosphorylation is expressed as the percentage of the upper (phosphorylated) band on SDS-PAGE compared to total MAPK (upper and lower band), normalized to vehicle-treated control.

Figure 4. **Less toxic congeners of SC-ααδ9 do not affect IGF-1 signaling.** Lysates from vehicle or inhibitor-treated SV40 MEF were immunoblotted with **(A)** anti-phosphotyrosine (PY20), **(B)** anti-IGF-1 receptor , **(C)** anti-Erk2, **(D)** Erk1, or **(E)** p34Cdc2 antibodies. *Lane 1*, vehicle control; *lane 2*, 100 μM SC-αα09; *lane 3*, 100 μM SC-α109; *lane 4*, 30 μM sodium vanadate; *lane 5*, 50 μM PD-98059.

Figure 5. **SC-ααδ9 preferentially inhibits clonogenic growth of SV40 transformed cells.** MEF (□) and SV40 MEF (■) were plated in triplicate in 6 well plates and treated with vehicle or inhibitor as described in the Methods Section. After 10-12 days of continuous exposure to drug, cells were stained with crystal violet and colonies >1mm in diameter counted. Data are expressed as % of colonies compared to vehicle treated control and are representative of five independent experiments. Bars = SEM. Absolute plating efficiencies were 10 ± 3% for MEF and 14 ± 6% for SV40 MEF.

Figure 6. **Cytotoxicity of SC-ααδ9, okadaic acid and vanadate on normal and SV40 transformed MEF.** MEF (□) and SV40 MEF (■) were plated in 96 well plates and after 24 h treated with various concentrations of **(A)** SC-ααδ9, **(B)** okadaic acid, or **(C)** vanadate. Cell

survival was determined 48 h later using the MTT assay as described in the Methods Section. Each value is the mean of 3-5 independent experiments performed in quadruplicate. Bars=SEM.

Figure 7. Inhibition of IGF-1 signaling and Cdc2 expression in MEF and SV40 MEF. Cells were grown to 50% confluency in medium containing 10% FBS and treated with the indicated concentrations of SC-ααδ9 for 48 h. Western blotting was performed with antibodies against **(A)** anti-phosphotyrosine (PY20), **(B)** IGF-1 receptor, **(C)** p34Cdc2, and **(D)** β–actin (loading control) as described in the Methods Section. Data are representative of two independent experiments.

Index terms

signal transduction, anticancer drugs, Cdc2, Simian Virus 40 large T antigen, Insulin-like growth factor-1

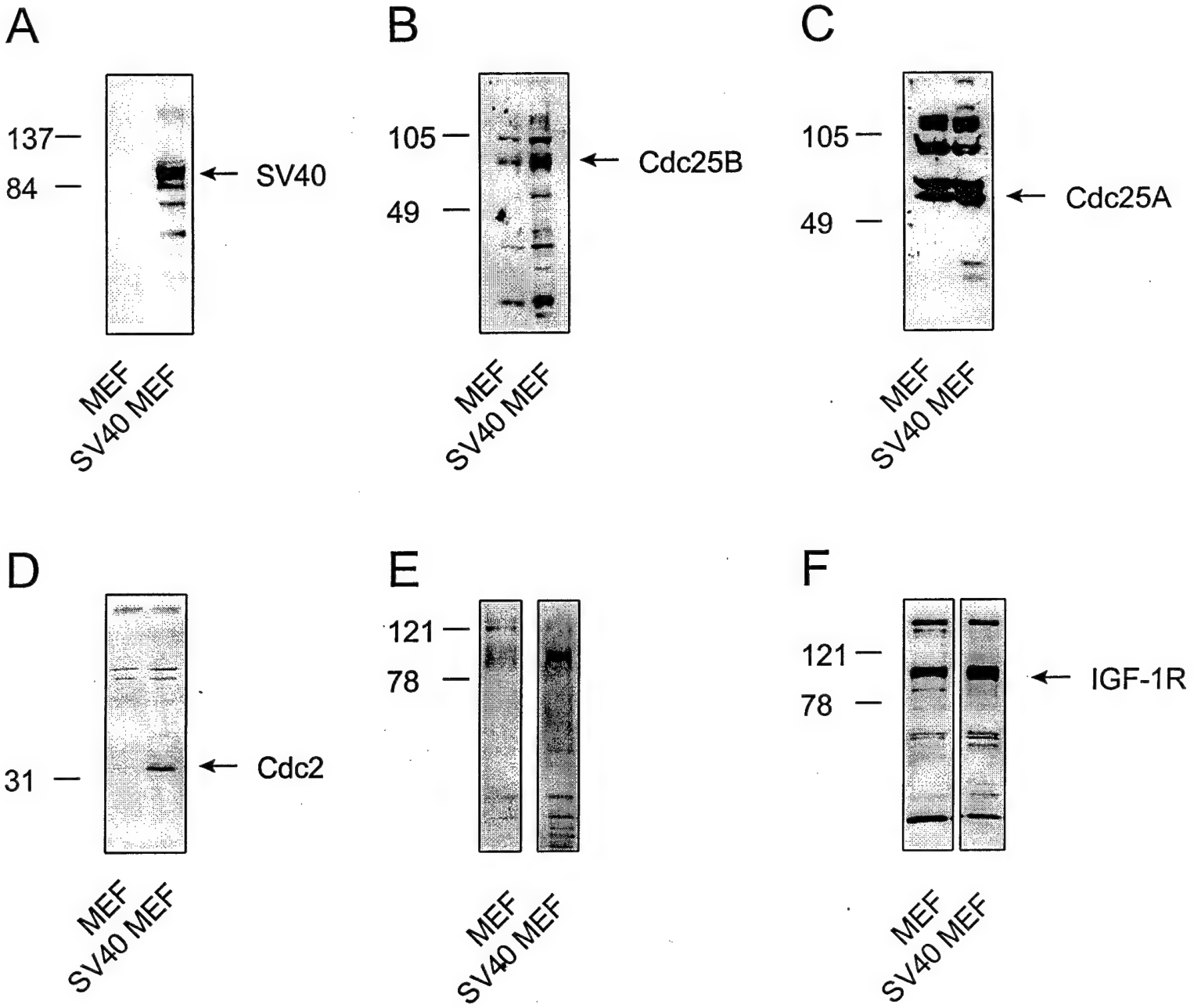
A
137
84
SV40
MEF
SV40 MEF
B
105
49
Cdc25B
MEF
SV40 MEF
C
105
49
Cdc25A
MEF
SV40 MEF
D
31
Cdc2
MEF
SV40 MEF
E
121
78
MEF
SV40 MEF
F
121
78
IGF-1R
MEF
SV40 MEF

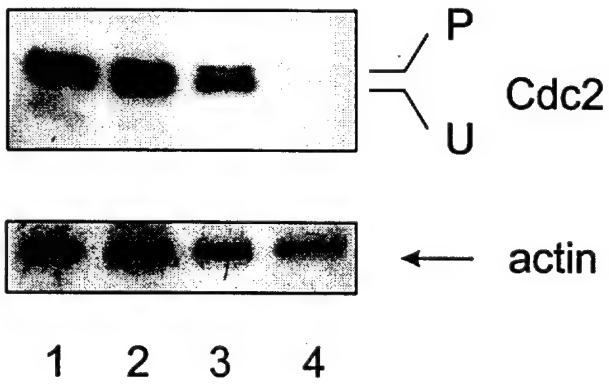
P
U
Cdc2
actin
1 2 3 4

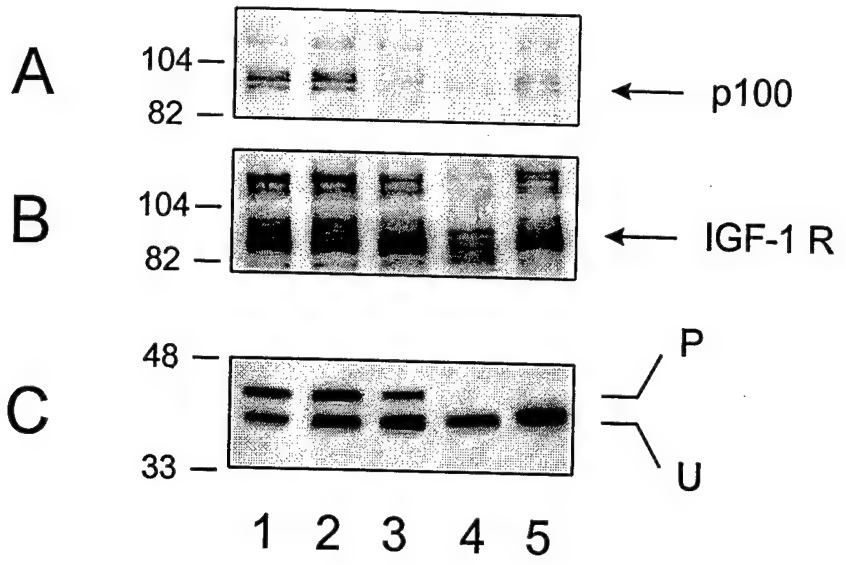
A
104
82
p100
B
104
82
IGF-1 R
C
48
33
P
U
1 2 3 4 5

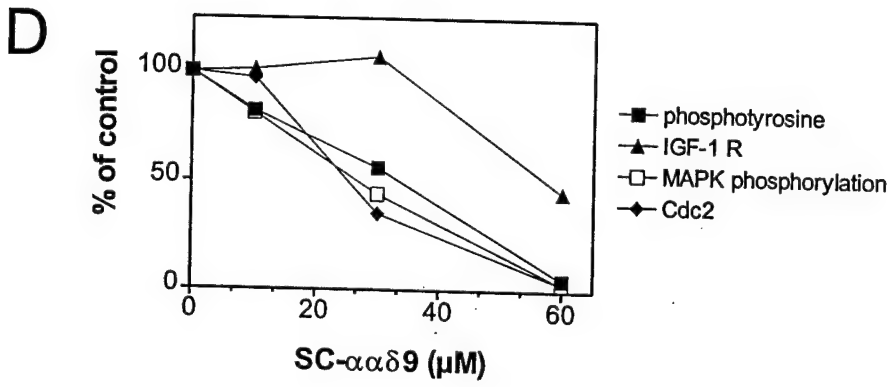
D
% of control
100
50
0
0
20
40
60
SC-ααδ9 (μM)
phosphotyrosine
IGF-1 R
MAPK phosphorylation
Cdc2

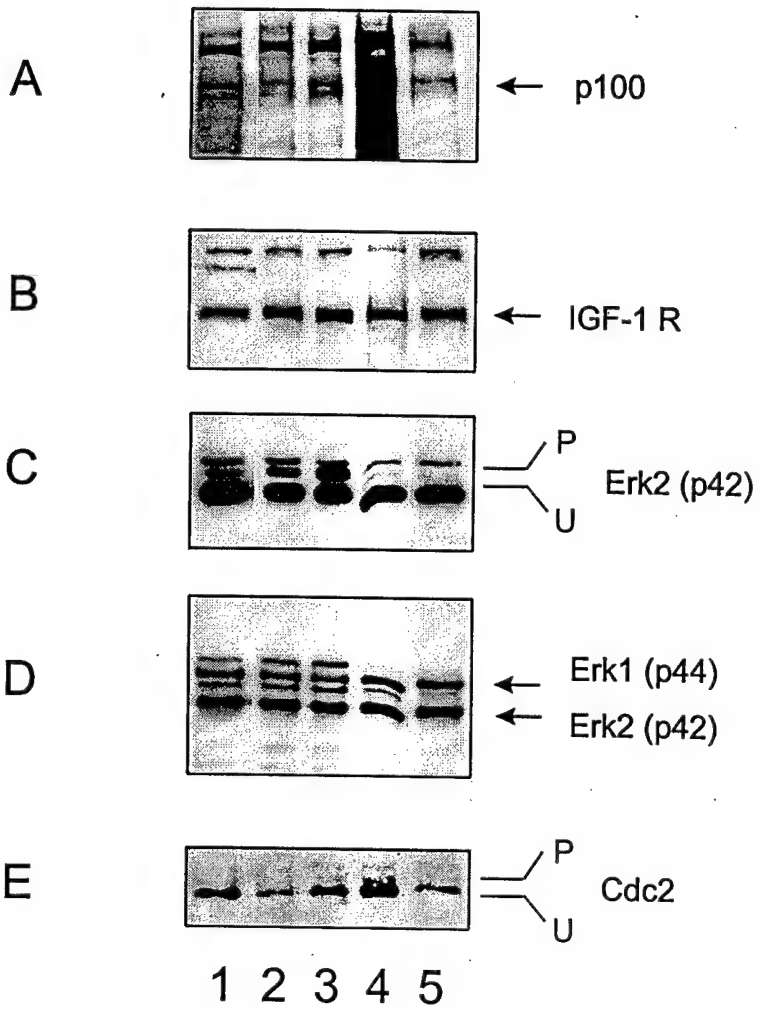
A
p100
B
IGF-1 R
C
P
U
Erk2 (p42)
D
Erk1 (p44)
Erk2 (p42)
E
P
U
Cdc2
1 2 3 4 5

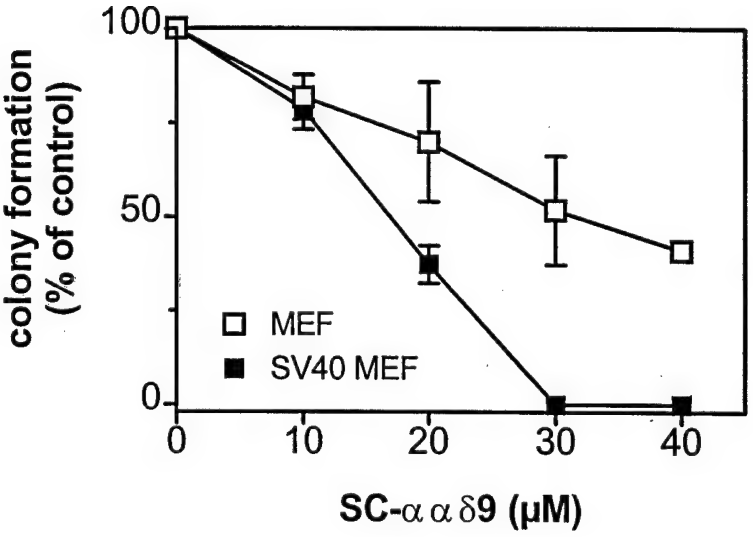
100
50
0
colony formation
(% of control)
MEF
SV40 MEF
0
10
20
30
40
SC-α α δ9 (μM)

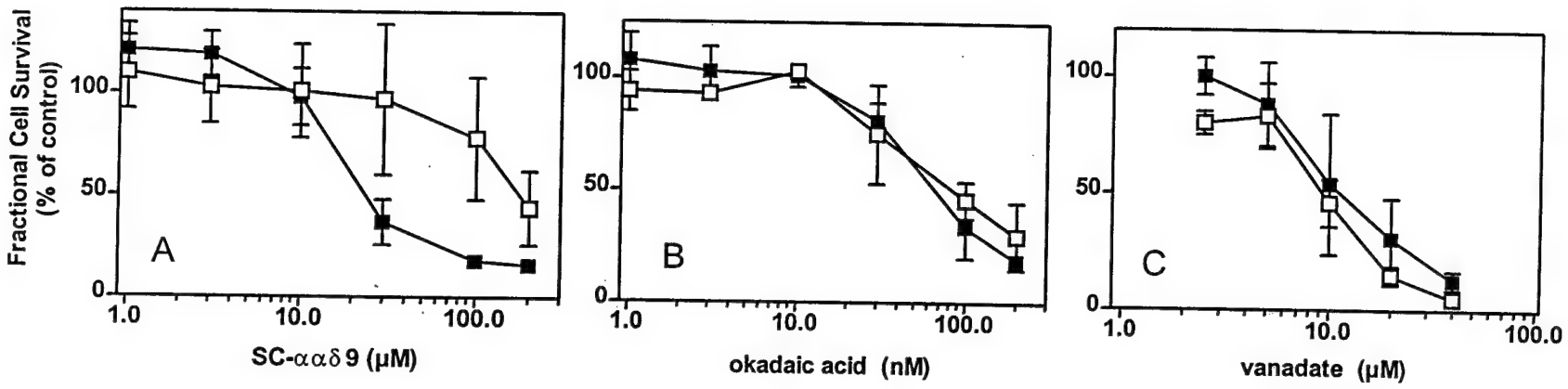
Fractional Cell Survival
(% of control)
100
50
0
A
1.0
10.0
100.0
SC-ααδ9 (μM)
100
50
0
B
1.0
10.0
100.0
okadaic acid (nM)
100
50
0
C
1.0
10.0
100.0
vanadate (μM)

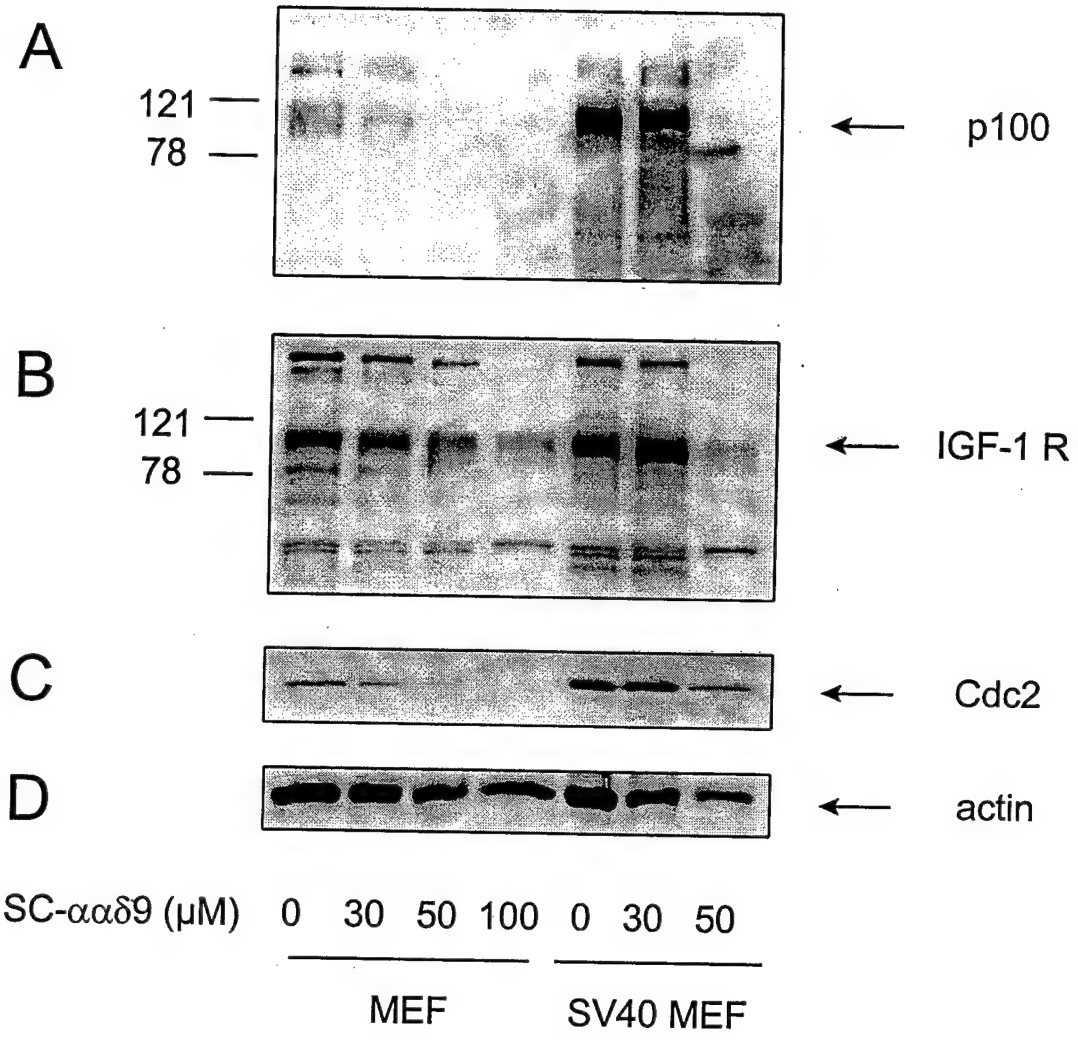
A
121
78
p100
B
121
78
IGF-1 R
C
Cdc2
D
actin
SC-ααδ9 (μM) 0 30 50 100 0 30 50
MEF
SV40 MEF

Identification of a selective inhibitor of VHR phosphatase in a novel, targeted small molecule library†.

Robert L. Rice[‡], Ronald J. Bernardi[‡], James M. Rusnak[‡¶], Fumiaki Yokokawa[§], Shiho Yokokawa[§], Peter Wipf[§] and John S. Lazo[‡*]

Departments of Pharmacology[‡] and Chemistry[§], the Combinatorial Chemistry Center and the Molecular Therapeutic/Drug Discovery Program of the University of Pittsburgh Cancer Institute, University of Pittsburgh, Pittsburgh, PA 15261.

Running title: Novel protein phosphatase inhibitors.

*Address for Correspondence: John S. Lazo, Department of Pharmacology, Biomedical Science Tower E-1340, University of Pittsburgh, Pittsburgh, PA 15261; Telephone: 412-648-9319; Fax: 412-648-2229; Email: lazo@pop.pitt.edu

[¶] Current address: Department of Medicine, Mayo Clinic, MN 55905.

†This work was supported in part by Army Breast Cancer Predoctoral Research Fellowship DAMD17-94-J4193 and Grant DAMD17-97-1-7229, the Fiske Drug Discovery Fund, and USPHS NIH Grants CA 78039 and GM 55433.

Abbreviations AEBSF, 4-(2-aminoethyl) benzenesulfonyl fluoride; DTT, DL-dithiothreitol; OMFP, 3,0-methyl -fluorescein monophosphate; GST, glutathione-S-transferase; IPTG, isopropyl β-D-thiogalactopyranoside; MAPK, mitogen-activated protein kinase; VHR, vaccinia human-related, phosphatase, MAPKP, mitogen-activated protein kinase phosphatase; PTPases, protein tyrosine phosphatases: FY2-ααα09, 4-(4-[(2,5-diphenyl-oxazole-4-carbonyl)-amino]-(cyclohexyl)-(carbonyl)-2-decanoylamino butyric acid; SC-αααδ9, 4-(benzyl-(2-[2,5-diphenyl-oxazole-4-carbonyl)-amino]-ethyl)-carbamoyl)-2-decanoylamino butyric acid.

Abstract

The protein tyrosine phosphatase family controls processes such as growth, differentiation, metabolism, cell cycle regulation and cytoskeletal function. Selective inhibitors are noticeably lacking but are essential to increase our understanding of the functionality of specific protein phosphatases. Thus, we expanded a previously described library of tyrosine-specific and dual specificity phosphatase inhibitors [Rice et al., (1997) *Biochemistry*. 36, 15965-15974] by diversifying the chemical structure of one element, SC-ααδ9, which is a competitive inhibitor of Cdc25 phosphatases and a noncompetitive inhibitor of PTP1B. Because the antiphosphatase activity of SC-ααδ9 was enantiomeric-independent, we rigidified the basic antiphosphatase pharmacophore in eight core analogues. Among the modified analogs, we found several potent inhibitors of PTP1B and a cyclohexyldiamine-containing congener, FY2-αα09, which is the first selective inhibitor of VHR phosphatase known to us that lacks significant activity against the tyrosine-specific phosphatase PTP1B or the dual specificity phosphatase $Cdc25B_2$. Moreover, FY2-αα09 displayed a competitive kinetic profile against VHR phosphatase with a K_{is} of 4 ± 1 μM. We also identified compounds FY7-αα09 and FY8-αα09, which were competitive inhibitors of $Cdc25B_2$ phosphatase with a K_{is} of 4 ± 1 μM. Modification of the SC-ααδ9 pharmacophore at the R_4 position revealed the importance of a terminal hydrophobic moiety for both tyrosine and dual specificity phosphatase inhibitory activities. The exquisite and distinct sensitivities of VHR, $Cdc25B_2$ and PTP1B to modifications of our lead structure document selective inhibition of dual specificity and tyrosine phosphatases is feasible.

Protein phosphorylation is a highly regulated process that relays external information for propagation and dissemination within a cell. Phosphorylation and dephosphorylation by the coordinated actions of kinases and phosphatases are critical control mechanisms for numerous physiological functions. The tyrosine phosphatase family controls processes such as cellular growth, differentiation, metabolism, cell cycle regulation and cytoskeletal function (1-5). Phosphatases belonging to this family prefer phosphotyrosine-containing peptides, although a subset have dual specificity and also hydrolyze phosphothreonine found on phosphotyrosine peptides. Despite extremely limited sequence similarity, the tyrosine phosphatases share an active site motif consisting of a cysteine and an arginine separated by five variable residues (CX_5R) (1-7).

On the basis of the proposed biological function, structure and primary amino acid sequence, the human tyrosine phosphatase family can be grouped into at least three distinct classes of tyrosine phosphatases (1-5). The tyrosine-specific phosphatases, such as PTP1B, regulate both epidermal growth factor and insulin signaling pathways (5, 8-10). PTP1B can also reverse the transformation of cells by v-src, v-crk and v-ras when overexpressed in these cells (11). Another category is represented by the VH-1-like dual specificity phosphatases, which include the VHR dual specificity phosphatase and mitogen-activated protein (MAP) kinase phosphatase. The enzymology and structure of VHR has been carefully examined, although its endogenous function remains unknown (12). MAP kinase phosphatases regulate the phosphorylation status, and thereby the duration of MAP kinase activation, which is important in growth factor and oncogene signaling pathways. A third category represents the Cdc25 dual specificity phosphatases.

These dual specificity phosphatases coordinate the cell cycle by dephosphorylating and, thereby, activating cell cycle dependent kinases. For example, Cdc25B and Cdc25C dephosphorylate $p34^{cdc2}$ and permit entry into mitosis (13-22).

Since members of the tyrosine phosphatase family may have an important role in cell signaling, oncogenesis and cell cycle control, selective inhibitors would be highly desirable chemical probes to determine their true intracellular function. Unfortunately, selective and potent inhibitors of protein tyrosine phosphatases are not currently available. Present crystallographic data, however, suggest selective inhibitors may be obtainable as significant differences have been observed in the active site of VHR, Cdc25A and PTP1B phosphatase (12, 23-25). The shallow 6Å pocket of VHR and the even shallower pocket of Cdc25A can accommodate both phosphotyrosine as well as phosphoserine/threonine (12, 23). In contrast, PTP1B possesses a deeper 9 Å catalytic pocket where only the more extended phosphotyrosine side chain, unencumbered by any adjacent phosphoserine/threonine, can reach the nucleophilic cysteine at the base of the catalytic pocket (12, 25). The structural differences present in these phosphatases should be exploitable in the selection of targeted inhibitors. A particularly challenging objective, however, is the design of selective inhibitors of VHR and the Cdc25 family, given their closely homologous active site topography.

We have used a successful nonelectrophilic antiphosphatase pharmacophore as a lead structure to synthesize a new targeted library of small molecules, and examined each element for selective dual specificity phosphatase inhibition (26, 27). By thoughtfully

modifying both the modular substituents on the core pharmacophore as well as the core pharmacophore itself, we have defined a structure with reduced peptide properties and enhanced selectivity for the VHR phosphatase. Compound FY2-αα09 is the first competitive inhibitor of VHR with no inhibitory activity against $Cdc25B_2$ or PTP1B. The minimal structural changes in the inhibitor FY2-αα09 compared to other compounds in the library reveals the sensitivity of the active sites of these enzymes and demonstrates how target-array, small molecular libraries can facilitate active site probing of protein phosphatases.

Materials and Methods

Chemical compounds. The general synthesis of compounds SC-ααδ9 and SC-αα09 has been previously described (26). The nomenclature for the compounds previously described (26) was used throughout this manuscript. A slightly modified strategy was used for the synthesis of the new compounds SC-ααδ6III and SC-ααδ4II. Briefly, rac-glutamate was selectively side-chain esterified with trimethylsilylchloride in allyl alcohol, *N*-protected with β,β,β-trichloroethoxycarbonyl chloride, and methylated to give Troc-Glu(allyl)-OMe that was extended at the side-chain carboxyl terminus by Pd(0)-catalyzed deallylation, PyBroP-mediated coupling with $BnNHCH_2CH_2NHAlloc$, renewed Pd(0)-catalyzed deallylation and coupling with the oxazole segment. After deprotection of the N-terminus with zinc in acetic acid, EDCI-mediated coupling provided SC-ααδ6III and SC-ααδ4II in 12-16% overall yield from dl-glutamate. All intermediates and products were purified by chromatography and nuclear magnetic resonance and characterized by high resolution mass spectroscopy as described previously (26). For the synthesis of FY2-αα09, we acylated protected dl-glutamate Scheme 1, compound **1**) at the N-terminus after removal of the Troc group, then deallylated and coupled the resulting compound to a diamine (Scheme 1, compound **3**) to give the compound **4** (Scheme 1). Acidolytic cleavage of the Boc group and PyBroP-mediated coupling with the oxazole shown as compound **5** in Scheme 1 provided ester **6**, which was readily converted to the desired FY2-αα09 (Scheme 1, compound **7**). Yields for each step are indicated in Scheme 1.

Plasmids and reagents. Plasmids pGEX2T-KG containing the GST-fusion of full length human $Cdc25B_2$ were previously described (26). The substrate 3,O-methyl fluorescein monophosphate (OMFP) was purchased from Sigma (St. Louis, MO). Recombinant PTP1B was obtained from Upstate Biotechnology (Lake Placid, NY).

Subcloning of VHR phosphatase and production of recombinant proteins. The coding sequence for VHR phosphatase was removed from pT7-7-VHR, which was a gift from Dr. Jack E. Dixon (University of Michigan, Ann Arbor, MI). This plasmid was digested using NdeI and EcoRI and ligated into the pMTL 22 vector. The pMTL 22-VHR plasmid was used to transform *DHα5 E. coli*, and the plasmid DNA was purified. The VHR phosphatase sequence from pMTL 22-VHR was excised with EcoRV and XhoI and ligated into the pGEX-4T3 plasmid, which had been digested with SmaI and XhoI. The pGEX-4T3 plasmids were used to transform *DHα5 E. coli*. This clone was then used to produce the GST-VHR phosphatase protein as were all other recombinant fusion proteins by our previously published methods (26).

Tyrosine specific phosphates and dual specificity phosphatase assay. The activity of the GST- dual specificity phosphatases and tyrosine-specific phosphatase was measured in 96-well microtiter plates with OMFP (Sigma; St. Louis, MO), which was readily metabolized to the fluorescent O-methyl fluorescein. The final incubation mixture (150 μl) was optimized for enzyme activity and comprised 30 mM Tris (pH 8.5), 50 mM NaCl, 1.5 mM EDTA, 0.033% bovine serum albumin, 1 mM DTT for $Cdc25B_2$

phosphatase and 30 mM Tris (pH 7.5), 75 mM NaCl, 1 mM EDTA, 0.033% bovine serum albumin, and 1 mM DTT for VHR and PTP1B. OMFP concentrations approximating the K_m were used: $Cdc25B_2$ 40 μM; VHR, 10 μM; PTP1B, 200 μM. Inhibitors were resuspended in DMSO and all reactions including vehicle controls were performed at a final concentration of 7% DMSO. Reactions were initiated by adding ~ 0.25 μg of $Cdc25B_2$ fusion protein, ~0.05 μg VHR and 0.1 μg PTP1B phosphatase. GST-fusion proteins were prepared as previously described (26). We measured fluorescence emission from the product over a 5-min reaction period at ambient temperature with a multiwell plate reader (Perseptive Biosystems Cytofluor II; Framingham, MA; excitation filter, 485/20; emission filter, 530/30). For all enzymes the reaction was linear over 15 min of incubation and was directly proportional to both the enzyme and substrate concentration.

Steady-state kinetics. Kinetic studies were conducted with GST-VHR as previously described (26). Data were collected for 4 min at 1 min intervals. The V_0 was determined for each substrate concentration and then fit to the Michaelis-Menten equation (Equation 1):

$$V_o=V_{max}[S]/(K_m+[S]) \qquad \text{(Eq. 1)}$$

using Kinetasyst (Intellikinetics Inc., Princeton, NJ). The correlation coefficient for each experiment and substrate concentration was always >0.9. At least six substrate concentrations between 10 and 200 μM OMFP were used to determine the steady-state kinetics for VHR and $Cdc25B_2$.

Determination of inhibition constant. The inhibition constants of FY7-αα09 and FY8-αα09 were determined for the $Cdc25B_2$-mediated hydrolysis of OMFP while the inhibition constant for FY2-αα09 was determined for the VHR hydrolysis of OMFP. At various fixed concentrations of inhibitor, the initial rates with different concentrations of OMFP were measured. The data were then fit to Equation 2 to obtain the inhibition constants for the competitive model.

$$Vo=V_{max}[S]/(K_m(1+ [I]/ K_{is})+[S]) \qquad \text{(Eq. 2)}$$

At least three concentrations of FY2-αα09 ranging from 1 to 10 μM were used with VHR phosphatase. At least four concentrations of FY7-ααδ9 and FY8-ααδ9 ranging from 1 to 30 μM were used with $Cdc25B_2$.

Determination of cLog P values. Computation of cLog P, the calculated logarithm of the octanol-water partition coefficient, was performed on an Indigo2 R4400 workstation according to a previously published protocol (28). Extended conformations of compounds were fully optimized using the semiempirical method PM3. Charges and other parameters for the regression analysis were also obtained with the PM3 module on Spartan 5.0 (Wavefunction, Inc., Irvine, CA).

Results

Phosphatase inhibition by enantiomers of SC-ααδ9. Because we previously found that the racemic library member SC-ααδ9 (Figure 1) was a competitive inhibitor of Cdc25 phosphatases and a noncompetitive inhibitor of PTP1B, we examined the structural basis for the inhibition further by synthesizing and testing both the (*R*)- SC-ααδ9 and (*S*)- SC-ααδ9 enantiomers separately. Both enantiomers, however, completely inhibited VHR, PTP1B and $Cdc25B_2$ phosphatase activity at 100 μM (Table 1). At 3 μM both enantiomers had identical inhibitory profiles for each phosphatase and displayed a slight preference for PTP1B compared to Cdc25 or VHR, which was consistent with our previous observation that racemic SC-ααδ9 was a better inhibitor of PTP1B than Cdc25. The absence of stereoselectivity in protein phosphatase inhibition suggested rigidification of the pharmacophore might be desirable for more potent and selective inhibitors.

Phosphatase inhibition by modified core pharmacophore library members. A greater level of conformational rigidity can be achieved by replacing the flexible ethylenediamine portion of the original SCααδ9 pharmacophore with a series of cyclic diamines (Figures 1 and 2). Specifically, cyclohexyldiamine, piperazine and phenyldiamine substructures were used to enhance rigidity and alter overall size. Because of the absence of stereospecificity in the parental structure, all congeners were synthesized as racemic mixtures. In comparison to SC-αα09, SC-α109 was a less potent inhibitor of $Cdc25B_2$ (Table 2) revealing the importance of an aromatic moiety on the oxazole R2 position. When we examined the inhibition of $Cdc25B_2$ with 100 μM of the

αα09 series, we found enzyme inhibition was remarkably resistant to modification of the core pharmacophore structure (Table 2) with the exception of FY2-αα09 and FY10-αα09, which lost activity compared to the parent compound SC-αα09. In the α109 series all congeners were similar to SC-α109 except FY7-α109, which was a superior inhibitor compared with SC-α109. Only FY7-αα09 caused any detectable inhibition of $Cdc25B_2$ at 3 μM (Table 2), and this was limited to < 20%. In contrast to the relative inactivity of the FY series against $Cdc25B_2$, FY2-αα09 caused 50% inhibition of VHR at 3 μM. No other compounds, including even the structurally closely related library member FY2-α109, led to this level of inhibition at 3 μM. FY2-αα09 had no detectable inhibitory action against PTP1B while four of the rigidified library members produced >50% inhibition of PTP1B at 3 μM (Table 2).

Inhibition kinetics of compounds. We next determined the kinetic characteristics with dual specificity phosphatases of the three most potent compounds: FY2-αα09, FY7-αα09 and FY8-αα09. The K_m with OMFP for VHR and $Cdc25B_2$ was 36 ± 6 μM (SEM, N > 3) and 45 ± 7 μM, respectively. Kinetic studies using 0.3 to 10 μM FY2-αα09 with VHR were most consistent with a competitive inhibition model (Figure 3), although higher concentrations presented a more mixed profile. We also found that FY7-αα09 and FY8-αα09 were competitive inhibitors of $Cdc25B_2$ (Figure 4). The K_{is} of FY2-αα09 for VHR was 4 ± 1 μM. Both FY7-αα09 and FY8-αα09 had K_{is} for $Cdc25B_2$ of 4 ± 1 μM.

Modification of R_4 position of SC-ααδ9. Previous observations lead us to speculate that the hydrophobic nonyl substituent of our original SC pharmacophore was critical for inhibition. To investigate this hypothesis, we replaced the nonyl moiety (R_4) of the SC-ααδ9 core pharmacophore with hydrophobic substituents of variable length (Figure 5). The addition of a pentadecyl side chain to form SC-ααδ15 enhanced PTP1B inhibition and decreased VHR inhibition compared with either SC-ααδ9 enantiomer (Table 4). The inhibition seen with SC-ααδ15 against $Cdc25B_2$ was comparable to that seen with SC-ααδ9 (Table 4). Not surprisingly, the cLog P of SC-ααδ15 was also increased compared to that of SC-ααδ9 (Table 3). SC-ααδ17A, which had a greater cLog P than SC-ααδ15, however, had less inhibitory activity against PTP1B in comparison to (R)-SC-ααδ9 or (S)-SC-ααδ9 (Table 3 and 4). SC-ααδ17A did maintain excellent actiVHR activity and, thus, showed some selectivity for VHR, although not as conspicuous as FY2-αα09. The ether-containing SC-ααδ6III and SC-ααδ4II had no inhibitory activity against VHR, $Cdc25B_2$ or PTP1B up to a concentration of 100 μM and had the lowest cLog P of these compounds (Table 3 and 4). These results demonstrated a critical role for hydrophobic moieties on the R4 position for tyrosine phosphatase inhibition.

Discussion

Based on their crystal structure, the active sites of VHR and Cdc25A appear more open to substrates and less sterically restricted than PTP1B. The structure of the VHR catalytic site represents an even more accessible binding site for compounds than the catalytic site of Cdc25. Consequently, an opportunity exists for the development of selective inhibitors of VHR. The emerging power of molecular diversity through combinatorial chemistry and targeted array small molecule libraries is becoming increasingly obvious. We have used a targeted array approach supplemented by parallel synthesis to seek new selective inhibitors of protein phosphatases.

The basic SC pharmacophore model used to develop our initial targeted library was rigidified in an effort to improve the inhibitor profile against dual specificity phosphatases. By replacing the ethylenediamine linker with a cyclohexyldiamine scaffold, such as in FY2-αα09, FY3-αα09 and FY4-αα09, we found any inhibitory activity against PTP1B was lost. In addition, FY3-αα09 and FY4-αα09 did not inhibit Cdc25B2 or VHR at 3 μM while FY2-αα09 inhibited VHR and did not inhibit $Cdc25B_2$ (Table 2). One possible explanation for the ability of FY2-αα09 to inhibit VHR and not PTP1B could be the more permissive nature of the VHR active site toward bulky substrates compared with PTP1B (6). We speculate that the 1,4-substituted cyclohexane ring of FY2-αα09 presents a greater steric obstacle for PTP1B than the 1,2-substituted FY3-αα09 or FY4-αα09. FY2-αα09 also did not inhibit $Cdc25B_2$ suggesting the lack of an opportune binding site compared to the catalytic site of VHR. Therefore, FY2-αα09

represents an attractive lead structure for the design of compounds that selectively inhibit VHR phosphatase but not the tyrosine-specific phosphatase PTP1B or the dual specificity Cdc25 phosphatase. We also identified two members of the pharmacophore library, FY7-αα09 and FY8-αα09, that like SC-ααδ9 retained an ability to competitively inhibit $Cdc25B_2$. These compounds or future derivatives may be useful chemical reagents to probe the biological role of VHR and dual specificity phosphatases. As with the parent pharmacophore, almost all new VHR and Cdc25 inhibitors revealed a strong preference for an aromatic moiety at the oxazole C5, namely, the R_2 position (Tables 2-4). The inhibition of PTP1B was largely independent of the nature of the substituent at the R_2 position. It is interesting that despite the apparent depth of the PTP1B active site relative to Cdc25 or VHR, PTP1B was the most readily inhibited by all compounds in our library except the FY2 series (Table 2).

We modified the nonyl moiety at the R_4 position of SC-ααδ9 to investigate the hypothesis that tyrosine phosphatases prefer an extended hydrophobic moiety in inhibitors. When comparing SC-ααδ9 to SC-ααδ15, which has a more hydrophobic moiety at the R4 position (Table 3), we found a modest increased in the inhibitory activity against PTP1B but not against VHR or $Cdc25B_2$ (Table 4). Introduction of a less hydrophobic moiety at R_4, such as in the oligo-ethers in SC-ααδ4II and SC-ααδ6III, caused a complete loss of activity. Nonetheless, increased hydrophobicity alone did not ensure increased PTP1B inhibition. SC-ααδ17A and SC-ααδ17B with extended hydrophobic substituents at R_4 and cLog P values four orders of magnitudes larger than

SC-ααδ9 had a decreased activity against PTP1B in comparison to (R)-SC-ααδ9 or (S)-SC-ααδ9 (Table 4). In contrast, SC-ααδ17A maintained antiVHR activity at a level comparable to FY2-αα09. Thus these results underlined the importance of an aliphatic, strongly hydrophobic moiety at this position for tyrosine but not VHR phosphatase inhibitory activity.

In summary, with FY2-αα09 we have identified a new readily available competitive and selective inhibitor of VHR. Moreover, modification of the R_4 position of SC-ααδ9 revealed the importance of a hydrophobic substituent for tyrosine and dual specificity phosphatase inhibitory activity. SC-ααδ17A inhibited VHR at a level similar to FY2-αα09, but did not share its pronounced selectivity against PTP1B. Because the biological function of VHR is unknown, we are now attempting to determine the cellular effects of FY2-αα09. The pharmacophore used in FY2-αα09 should provide an excellent platform for future analog development. Our results illustrate the exquisite and distinct sensitivities of VHR, $Cdc25B_2$ and PTP1B to structural modifications of our lead structure, and indicate that selective inhibition of dual specificity and tyrosine phosphatases is indeed possible.

References

1. Dixon, J. E. (1996) *Recent Progress in Hormone Research 51*, 405-414.
2. Denu, J. M., Stuckey, J. A., Saper, M. A., and Dixon, J. E. (1996) *Cell 87*, 361-364.
3. Dixon, J. E. (1995) *Ann. New York Acad. Sci. 766*, 18-22.
4. Draetta, G., and Eckstein, J. (1997) *Biochim. Biophys. Acta 1332*, M53-63.
5. Li, L., Ernsting, B. R., Wishart, M. J., Lohse, D. L., and Dixon, J. E. (1997) *J. Biol. Chem. 272*, 29403-29406.
6. Chen, L., Montserat, J., Lawrence, D. S., and Zhang, Z. Y. (1996) *Biochemistry 35*, 9349-9354.
7. Montserat, J., Chen, L., Lawrence, D. S., and Zhang, Z. Y. (1996) *J. Biol. Chem. 271*, 7868-7872.
8. Brown-Shimer, S., Johnson, K. A., Hill, D. E., and Bruskin, A. M. (1992) *Cancer Res. 52*, 478-482.
9. Flint, A. J., Tiganis, T., Barford, D., and Tonks, N. K. (1997) *Proc. Natl. Acad. Sci. U. S.A. 94*, 680-1685.
10. Seely, B. L., Staubs, P. A., Reichart, D. R., Berhanu, P., Milarski, K. L., Saltiel, A. R., Kusari, J., and Olefsky, J. M. (1996) *Diabetes 45*, 1379-1385.
11. Liu, F., Hill, D. E., and Chernoff, J. (1996) *J. Biol. Chem. 271*, 31290-31295.
12. Fauman, E. B., Cogswell, J. P., Lovejoy, B., Rocque, W. J., Holmes, W., Montana, V. G., Piwnica-Worms, H., Rink, M. J., and Saper, M. A. (1998) *Cell 93*, 617-625.

13. Baldin, V., Cans, C., Superti-Furga, G., and Ducommun, B. (1997) *Oncogene 14*, 2485-2495.

14. Gabrielli, B. G., De Souza, C. P., Tonks, I. D., Clark, J. M., Hayward, N. K., and Ellem, K. A. (1996) *J. Cell Sci. 109*, 1081-1093.

15. Gabrielli, B. G., Clark, J. M., McCormack, A. K., and Ellem, K. A. (1997) *Oncogene 15*, 749-758.

16. Gabrielli, B. G., Clark, J. M., McCormack, A. K., and Ellem, K. A. O. (1997) *J. Biol. Chem. 272*, 28607-28614.

17. Galaktionov, K., and Beach, D. (1991) *Cell 67*, 1181-1194.

18. Chang, T. H., Ray, F. A., Thompson, D. A., and Schlegel, R. (1997) *Oncogene 14*, 2383-2393.

19. Peng, C., Graves, P., Thoma, R., Wu, Z., Shaw, A., and Piwnica-Worms, H. (1997) *Science 277*, 1501-1505.

20. Peng, C. Y., Graves, P. R., Thoma, R. S., Wu, Z., Shaw, A. S., and Piwnica-Worms, H. (1997) *Science 277*, 1501-1505.

21. Poon, R. Y. C., Chau, M. S., Yamashita, K., and Hunter, T. (1997) *Cancer Res. 57*, 5168-5178.

22. Sanchez, Y., Wong, C., Thoma, R. S., Richman, R., Wu, Z., Piwnica-Worms, H., and Elledge, S. J. (1997) *Science 277*, 1497-1501.

23. Yuvaniyama, J., Denu, J. M., Dixon, J. E., and Saper, M. A. (1996) *Science 272*, 1328-1331.

24. Stuckey, J. A., Schubert, H. L., Fauman, E. B., Zhang, Z. Y., Dixon, J. E., and Saper, M. A. (1994) *Nature 370*, 571-575.

25. Barford, D., Flint, A. J., and Tonks, N. K. (1994) *Science 263*, 1397-1404.

26. Rice, R. L., Rusnak, J. M., Yokokawa, F., Yokokawa, S., Messner, D. J., Boynton, A. L., Wipf, P., and Lazo, J. S. (1997) *Biochemistry 36*, 15965-15974.

27. Wipf, P., Cunningham, A., Rice R.L., and Lazo, J.S. (1997) *Bioorg. and Med. Chem. 5*, 165-177.

28. Alkorta, I., and Villar, H. O. (1992) *Int. J. Quant. Chem. 44*, 203-218.

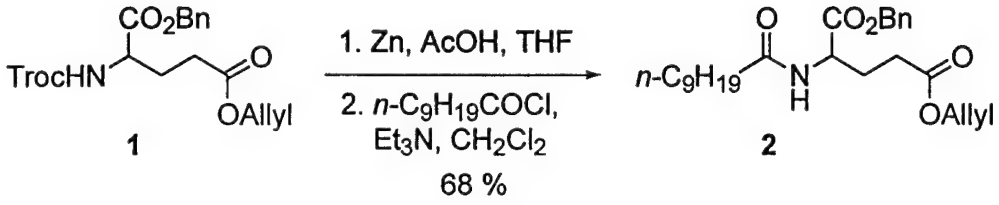
CO2Bn
TrocHN
O
OAllyl
1
1. Zn, AcOH, THF
2. n-C9H19COCl,
Et3N, CH2Cl2
68 %
O
CO2Bn
n-C9H19
N
H
O
OAllyl
2

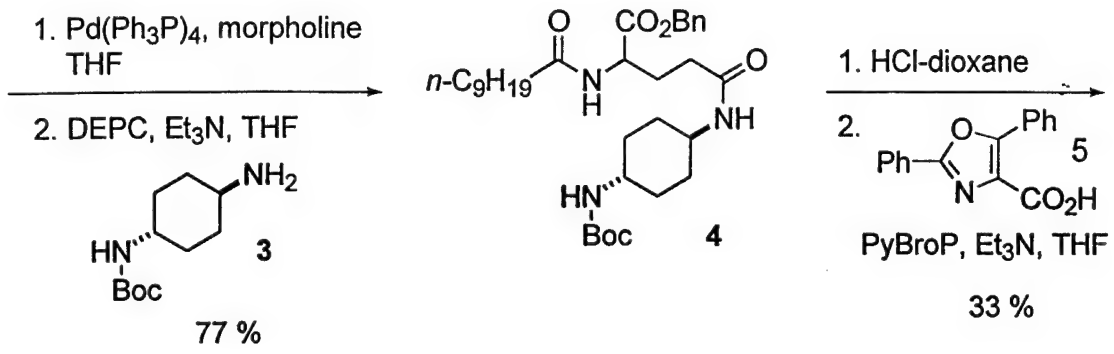
1. Pd(Ph3P)4, morpholine
THF
2. DEPC, Et3N, THF
NH2
HN
Boc
3
77 %
O
CO2Bn
n-C9H19
N
H
NH
HN
Boc
4
1. HCl-dioxane
2.
O
Ph
Ph
N
CO2H
5
PyBroP, Et3N, THF
33 %

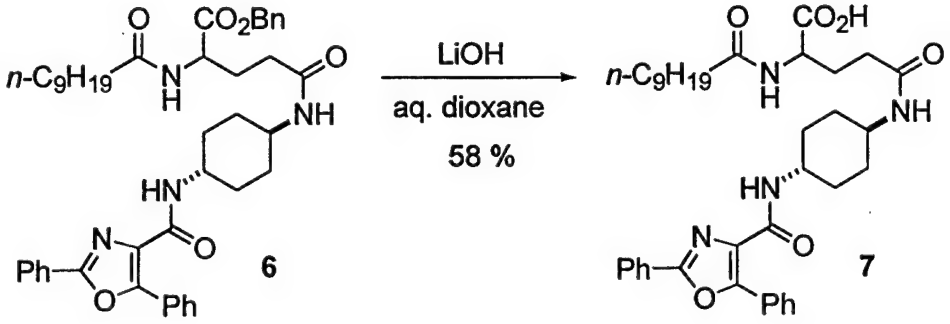
O
CO2Bn
n-C9H19
N
H
NH
HN
N
O
Ph
O
Ph
6
LiOH
aq. dioxane
58 %
O
CO2H
n-C9H19
N
H
NH
HN
N
O
Ph
O
Ph
7

Figure Legends

Figure 1. General chemical structures of SC-ααδ9 and diamine linker substitutions. R indicates the combinatorial sites on the pharmacophore. Circle indicates the variable core region for the FY series.

Figure 2. Chemical structures of pharmacophores.

Figure 3. Kinetic analyses of VHR inhibition by FY2-αα09. The symbols -■- represent 0 μM inhibitor concentration, -▲- are 0.3 μM, -▼- are 1 μM, -◆- are 3 μM, -● - are 5 μM and -□- are 10 μM. Lineweaver-Burke plot of VHR inhibition by FY2-αα09. Enzyme activities were determined as outlined in the Material and Methods Section and the data fit to Michaelis-Menten equation while all the data points were also fit simultaneously by the Kinetasyst II program. The values are reported in Table 3 for K_m and K_{is} and were calculated for competitive inhibition with log weighting using the same program.

Figure 4. Kinetic analyses of $Cdc25B_2$ inhibition by FY7-αα09 and FY8-αα09. The symbols -■- represent 0 μM inhibitor concentration, -▲- are 3 μM, -▼- are 10 μM, -●- are 30 μM and -◆- are 100 μM. Panel A. Hanes-Wolf plot of $Cdc25B_2$ inhibition by FY7-αα09 ; Panel B, Hanes-Wolf plot of Cdc25B2 inhibition by FY8-αα09. Enzyme activities were determined as outlined in the Material and Methods Section and the data fit to Michaelis-Menten equation while all the data points were also fit simultaneously by

the Kinetasyst II program. The values are reported In Table 3 for K_m and K_{is} and were calculated for competitive inhibition with log weighting using the same program.

Figure 5. General chemical structures of phosphatase inhibitor library members.

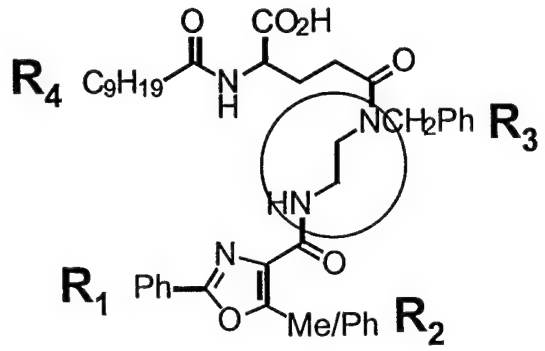

SC–α1δ9/**SC**–ααδ9

SC-αα09/SC-α109

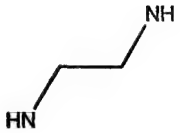

FY5-αα09/FY5-α109

FY2-αα09/FY2-α109

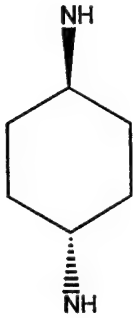

FY7-αα09/FY7-α109

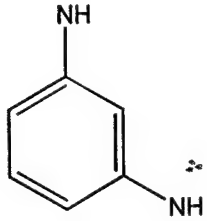

FY3-αα09/FY3-α109

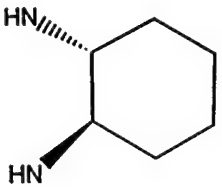

FY8-αα09/FY8-α109

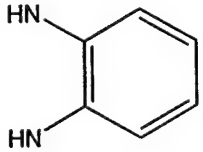

FY4-αα09/FY4-α109

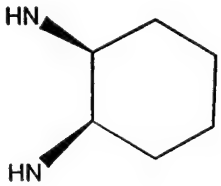

FY9-αα09/FY9-α109

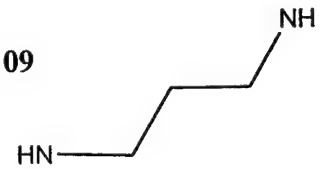

FY10-αα09/FY10-α109

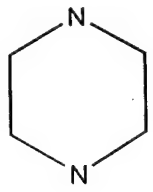

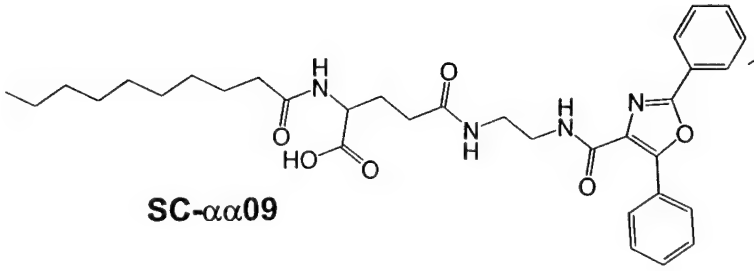

SC-αα09

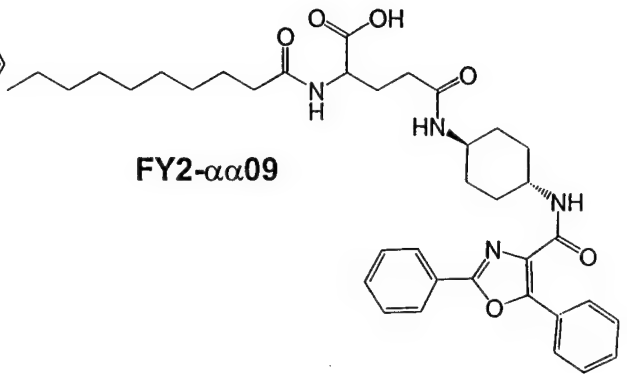

FY2-αα09

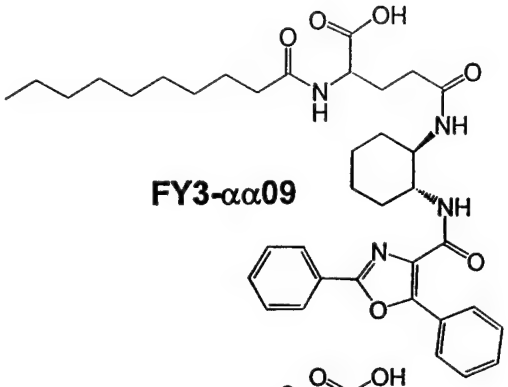

FY3-αα09

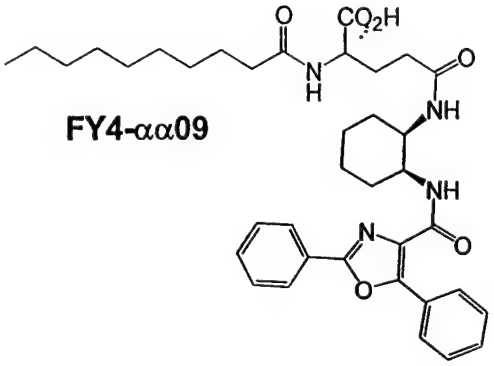

FY4-αα09

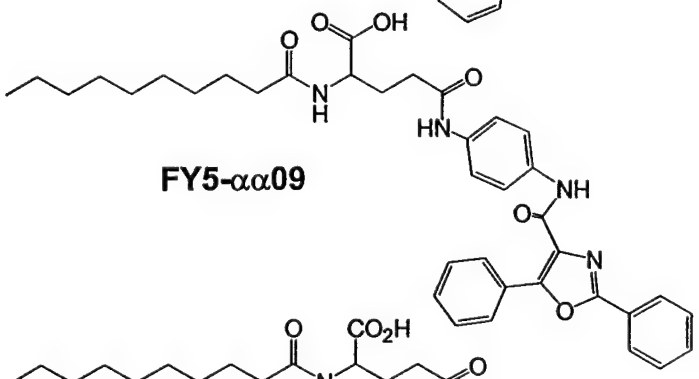

FY5-αα09

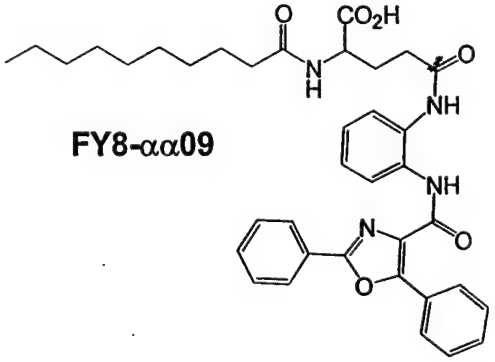

FY8-αα09

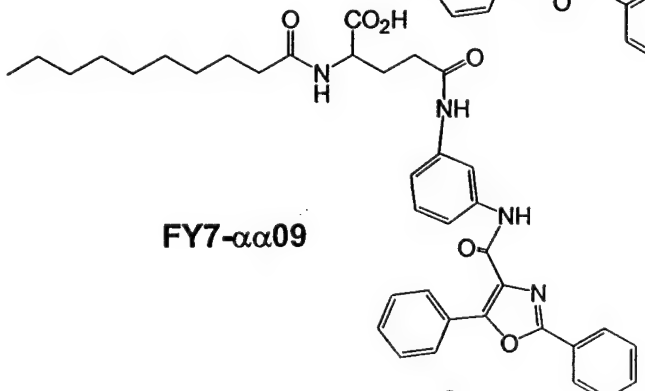

FY7-αα09

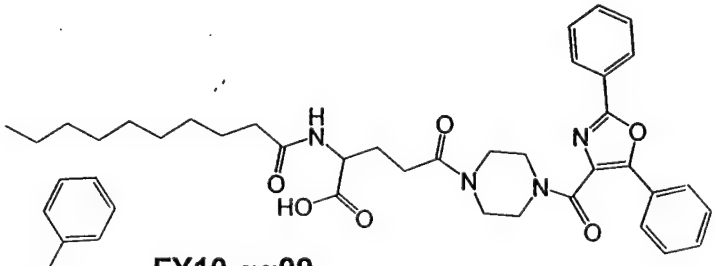

FY10-αα09

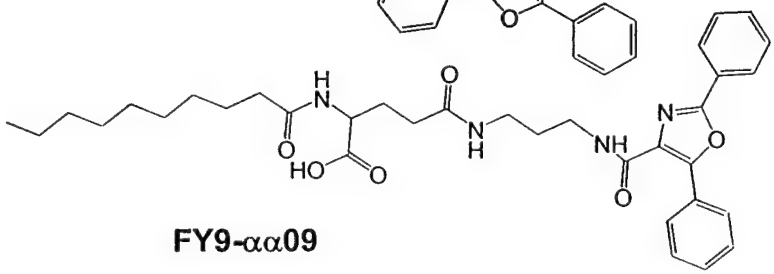

FY9-αα09

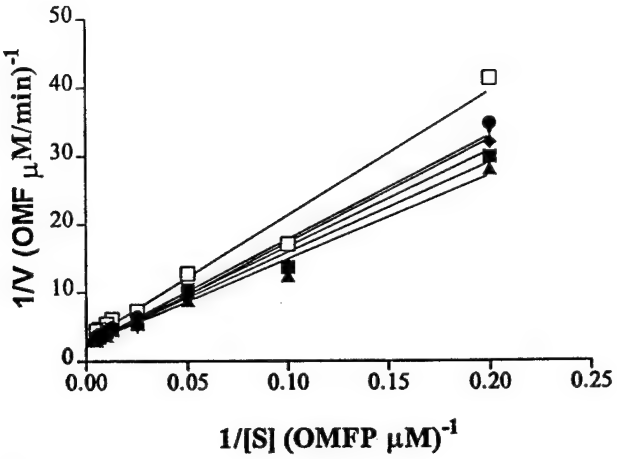
50
40
30
20
10
0
0.00
0.05
0.10
0.15
0.20
0.25
1/V (OMF μM/min)-1
1/[S] (OMFP μM)-1

A

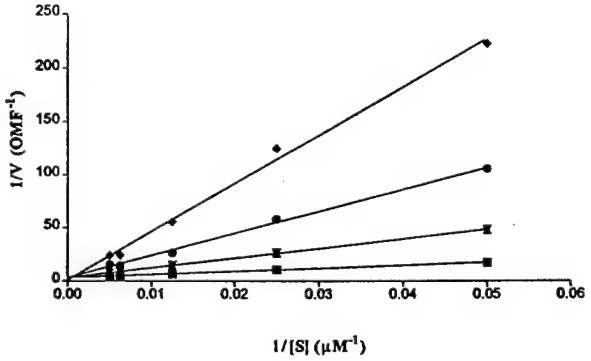
250
200
150
100
50
0
1/V (OMF-1)
0.00
0.01
0.02
0.03
0.04
0.05
0.06
1/[S] (μM-1)

B

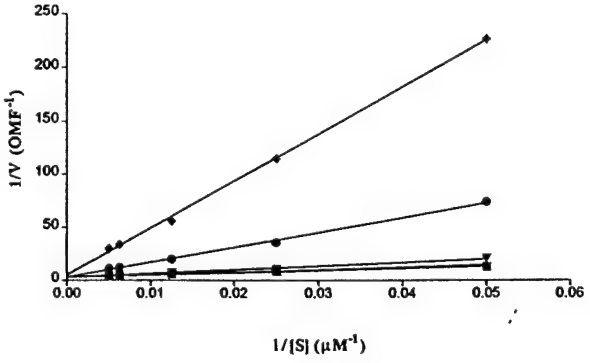
250
200
150
100
50
0
1/V (OMF-1)
0.00
0.01
0.02
0.03
0.04
0.05
0.06
1/[S] (μM-1)

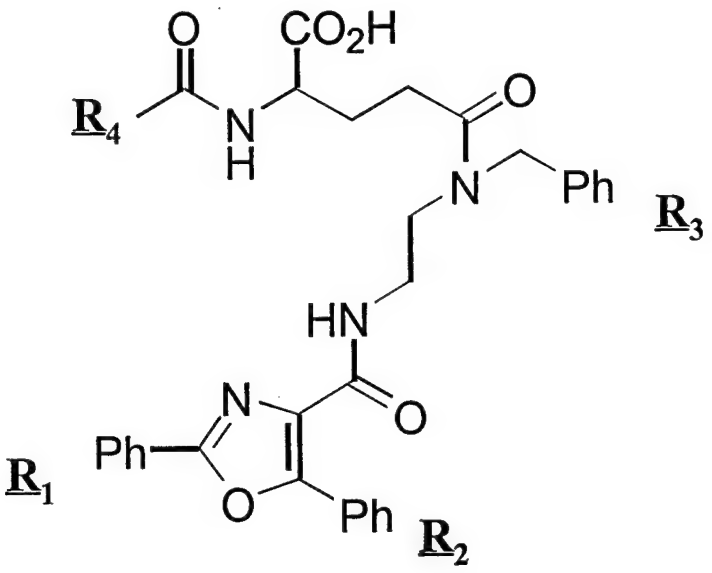

Compound	R_4
SC-ααδ9	$Me(CH_2)_8$
SC-ααδ15	$Me(CH_2)_{14}$
SC-ααδ17A	$Me(CH_2)_7CH{=}CH(CH)_{27}$
SC-ααδ17B	$Me(CH_2)_4CH{=}CH{-}CH{=}CH(CH_2)_7$
SC-ααδA	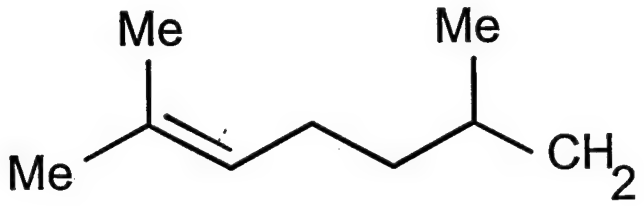
SC-ααδ4II	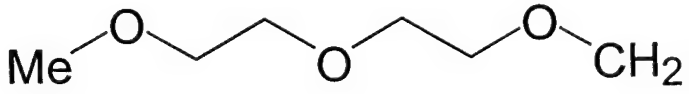
SC-ααδ6III	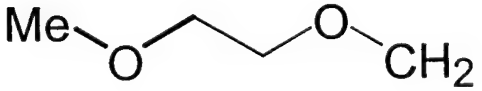

Table 1: Percent inhibition of tyrosine and dual specificity phosphatase activity with the enantiomeric forms of SC-ααδ9[a]

	$Cdc25B_2$				VHR				PTP1B			
	3 μM		100 μM		3 μM		100 μM		3 μM		100 μM	
Compound	**Mean**	**SEM**	**Mean**	**SEM**	**Mean**	**SEM**	**Mean**	**SEM**	**Mean**	**SEM**	**Mean**	**SEM**
(R)-SC-ααδ9	3	3	85	2	10	4	96	2	30	12	96	2
(S)-SC-ααδ9	2	2	83	2	10	3	74	13	36	5	74	13

[a] Each value was the percent inhibition from untreated control and the mean from three independent determinations.

Table 2: Percent inhibition of tyrosine and dual specificity phosphatase. activity with modified core library.

	$Cdc25B_2$				VHR		PTP1B	
	3 μM		100 μM		3 μM		3 μM	
Compound	Mean	SEM	Mean	SEM	Mean	SEM	Mean	SEM
SC-αα09	2	2	61	9	9	2	58	8
SC-α109	2	2	14	11	13	3	68	8
FY2-αα09	0	0	14	14	54	11	0	0
FY2-α109	0	0	23	12	16	3	16	13
FY3-αα09	2	2	68	4	23	4	29	12
FY3-α109	3	3	22	13	19	3	45	12
FY4-αα09	3	3	73	1	18	1	34	22
FY4-α109	1	1	15	9	12	3	40	21
FY5-αα09	0	0	63	6	19	5	34	12
FY5-α109	4	4	46	4	16	3	62	10
FY7-αα09	19	6	83	1	30	1	61	7
FY7-α109	2	2	70	2	10	4	62	17
FY8-αα09	4	4	86	3	15	3	51	4
FY8-α109	1	1	40	11	21	5	65	13
FY9-αα09	0	0	55	5	7	5	66	7
FY9-α109	5	5	3	3	7	2	56	11
FY10-αα09	2	2	28	12	6	3	63	5
FY10-α109	4	4	17	10	10	4	47	23

[a] Each value was the percent inhibition from untreated control and the mean from three independent determinations.

Table 3. cLog P Values[a] of Selected Compounds

	Carboxylate	Free acid
SC-ααδ9	1.2	4.9
SC-αα09	-0.3	3.5
SC-α109	-0.2	3.9
SC-ααδ6III	-2.0	1.4
SC-ααδ4II	-1.8	1.9
FY2-αα09	0.5	4.3
FY2-α109	-1.0	2.8
FY3-αα09	-1.9	4.4
SC-ααδ15	3.6	8.4
SC-ααδ17A	4.3	8.9
SC-ααδ17B	4.4	9

[a] cLog P values represent computed logarithms of the octanol-water partition coefficient and were calculated based on energy-minimized extended confirmations by the method of Alkorta and Villar (1992).

Table 4: Percent inhibition of tyrosine and dual specificity phosphatase activity with R_4 modifed compounds.

	$Cdc25B_2$				VHR				PTP1B			
	3 μM		100 μM		3 μM		100 μM		3 μM		100 μM	
Compound	**Mean**	**SEM**	**Mean**	**SEM**	**Mean**	**SEM**	**Mean**	**SEM**	**Mean**	**SEM**	**Mean**	**SEM**
(R)-SC-ααδ9	3	3	85	2	10	4	96	2	30	12	96	2
(S)-SC-ααδ9	2	2	83	2	10	3	74	13	36	5	74	13
SC-ααδA	6	6	78	2	38	17	85	7	25	25	96	3
SC-ααδ15	11	9	76	3	21	17	28	17	53	16	ND	ND
SC-ααδ17A	13	10	78	3	49	12	84	4	26	15	54	7
SC-ααδ17B	7	7	79	4	37	20	78	9	18	13	79	1
SC-ααδ6III	7	5	13	2	2	1	0	0	24	9	31	21
SC-ααδ4II	6	4	23	2	2	2	0	0	10	10	5	3

[a] Each value was the percent inhibition from untreated control and the mean from three independent determinations.

[b] ND stands for not determined.